Master's thesis

NTNU
Norwegian University of Science and Technology
Faculty of Engineering
Department of Civil and Environmental Engineering

Louis James Steigerwald

Comparison of the NGI-ADP and AUS soil models for slope stability involving anisotropic clays

Master's thesis in Geotechnics and Geohazards
Supervisor: Gudmund Eiksund
February 2021

NTNU
Norwegian University of
Science and Technology

Louis James Steigerwald

Comparison of the NGI-ADP and AUS soil models for slope stability involving anisotropic clays

Master's thesis in Geotechnics and Geohazards
Supervisor: Gudmund Eiksund
February 2021

Norwegian University of Science and Technology
Faculty of Engineering
Department of Civil and Environmental Engineering

NTNU
Norwegian University of
Science and Technology

Preface

The following is a presentation of a Project thesis carried out as part of the requirements for completing an MSc in Geotechnics and Geohazards through the department of Civil and Environmental Engineering at NTNU. This project is completed in the spring of 2021.

This thesis project focuses on the comparison of a newly released soil model against an older and more established soil model used in geotechnical engineering for clays that exhibit anisotropic strength. Modelling of such clays is extremely relevant to Norwegian conditions, as typical low plasticity clays are prone to exhibit anisotropic strength responses. Coming from the flatlands of the Great Plains in the United States, I have developed a large interest in slope stability perhaps due to the foreign nature of the problem. Coupled with the very challenging soil conditions, including destructive quick clays, this project provided valuable insight into several components of Norwegian geotechnical engineering that I find fascinating.

Before completing this project, I was recruited by Sunnfjord Geo Center to work in a part-time capacity while I continued to write. This wonderful opportunity served as both early career training and wonderful motivation to persevere to the conclusion of my master's studies.

I would like to especially thank Professor Gudmund Eiksund for volunteering to be my advisor on short notice despite difficult circumstances.

Louis Steigerwald

Acknowledgments

I would like to thank my closest friends and family for their unwavering support throughout my educational career and my pursuit of a MSc in Geotechnical Engineering through NTNU. Their support has made this continuation possible. My appreciation for my parents cannot be overstated, as they have been tremendous in helping me through many personal journeys.

I would also like to thank Even Vie, Einar Alsaker and the rest of the Sunnfjord Geo Center team for helping me to realize a very long held dream by taking a chance on me.

And I would of course like to thank my supervising professor Gudmund Eiksund for all of his patience and support. He offered a very quiet and calm encouragement that was especially helpful. Professors Gustav Grimstad and Steinar Nordal also made contributions of which I am very grateful for.

My sincere thanks.

Abstract

A new soil model capable of incorporating anisotropic shear strength has recently become available for public use. This model, called the AUS soil model, is a total stress-based model and operates based on directly inputting undrained shear strength values. In this way, the model is similar to the NGI-ADP model, which has long been used for modeling anisotropy in soils. However, the implications of differences in model design are not fully understood, and it is not known if the two models will generate similar solutions. Idealized simple slopes consisting of homogenous, undrained anisotropic clays are analyzed in a slope stability parametric study to discover under what soil conditions the models will generate similar and dissimilar solutions. It is demonstrated that for the condition that $s_{uDSS}/(s_{uE} + s_{uC}) = 0{,}5$ the two models generate statistically identical solutions. When this ratio falls below 0,5, the AUS soil model generates lower FoS solutions relative to the NGI-ADP model. The difference between model solutions increases as $s_{uDSS}/(s_{uE} + s_{uC})$ approaches $4/9$ and as the slope angle increases in steepness. When s_{uDSS} and s_{uC} are kept constant, increasing s_{uE} will result in higher FoS solutions for the NGI-ADP model, and lower solutions for the AUS model. Differences in FoS up to 35% are demonstrated in the case of the vertical slope. This magnitude coincides with the decrease in Active plane strain strength in the AUS model, which depending on anisotropic strengths and relative magnitudes can reduce Active plane strain strength as much as $s_{uA}/s_{uC} = 0{,}6$. Both models use curve-fitting simplifications and are designed for use with minimal input data, which may lead to unconservative or overly conservative estimations dependent on soil strength parameters.

Sammendrag

En ny jordmodell som kan inkorporere anisotrop skjærstyrke har nylig blitt tilgjengelig for offentlig bruk. Denne modellen, kalt AUS jordmodell, er en totalspenningsbasert modell og opererer basert på direkte innføring av udrenerte skjærstyrkeverdier. På denne måten ligner modellen NGI-ADP-modellen, som lenge har vært brukt til modellering av anisotropi i jord. Implikasjonene av forskjeller i modelldesign er imidlertid ikke helt forstått, og det er ikke kjent om de to modellene vil gi lignende løsninger. Idealiserte enkle skråninger bestående av homogene udrenerte anisotropisk leire blir analysert i en parametrisk studie av skråningsstabilitet for å oppdage under hvilke jordforhold modellene vil gi lignende og forskjellige løsninger. Det er vist at for tilstanden $s_{uDSS}/(s_{uE} + s_{uC}) = 0{,}5$ gir de to modellene statistisk identiske løsninger. Når dette forholdet faller under 0,5 gir AUS jordmodellen lavere sikkerhetsfaktor enn NGI-ADP modellen. Forskjellen mellom løsningene øker når $s_{uDSS}/(s_{uE} + s_{uC})$ nærmer seg $4/9$ og når hellingsvinkelen øker i bratthet. Når s_{uDSS} og s_{uC} holdes konstant, vil økende s_{uE} resultere i høyere sikkerhetsfaktorer for NGI-ADP modellen og laver sikkerhetsfaktorer for AUS-modellen. Forskjeller i sikkerhetsfaktor opptil 35% er vist i tilfelle vertikal skråning. Denne størrelsen sammenfaller med reduksjonen i aktivt styrke i AUS modellen, som avhengig av anisotrope styrker og relative størrelser kan redusere aktivt styrke opptil $s_{uA}/s_{uC} = 0{,}6$. Begge modellene bruker kurvetilpassede forenklinger og er designet for bruk med minimale inngangsdata, noe som kan føre til ukonservative eller altfor konservative beregninger avhengig av jordstyrkeparametere.

Contents

List of Figures

List of Tables

Chapter 1

Introduction

1.1 Background

The anisotropic shear strength response of low plasticity clays is a well-known and documented behavior. Many engineering projects in Norway encounter such soils, and engineers require modelling programs that can accurately predict the behavior of such soils under different stress scenarios. Understanding and properly modelling the stress-strain response of anisotropic clays has remained challenging. Additionally, not every aspect of soil behavior is able to be incorporated into the soil models. A good example of this is strain softening behavior, which is a common characteristic of quick clays, and can have very serious consequences.

Accurate modelling of anisotropic undrained clay slopes is extremely relevant for Norwegian geotechnical practice. Many projects are constructed on or in normally consolidated clay slopes that typically exhibit anisotropic behaviors. Certain areas of Norway are also prone to large clay slope failures. These landslides are especially destructive when they occur in quick clays, which often fail retrogressively and result in large volumes of liquified soils. Near the time of writing, the nation was shocked in wake of the Gjerdrum slide in eastern Norway, which claimed the lives of ten people and destroyed at least 31 houses. As a result, the dangers of building on and around quick clay have come under public focus. Currently, one of the most widely used programs for modelling anisotropic clays is the commercially available NGI-ADP model, which is featured in both PLAXIS and GeoSuite. While the creators have stipulated that this model is only appropriate for horizontally deposited clays, the model has been employed by engineers for use with natural clay slopes. This model by Grimstad et al. (2012) is a total stress-based model which employs a shift in the classical Tresca criterion to incorporate anisotropic strength.

A new soil model has recently been released for commercial use. The Anisotropic Undrained Soil (AUS) model by Krabbenhøft et. al. (2019) is available in the FE program Optum CE.

This model uses a modified Tresca criterion termed the Generalized Tresca which is then shifted.

One of the major challenges for geotechnical engineers is choosing the most appropriate soil model for a situation while still being mindful of that soil model's limitations.

This thesis seeks to illuminate some of the ramifications of using either the NGI-ADP model or the AUS model for similar situations involving slope stability analysis for idealized simple slopes consisting of homogenous undrained anisotropic clays.

1.2 Problem Formulation and limitations of the project

The main focus of this thesis is determining if using one of the afore-mentioned soil models will result in a similar or dissimilar factor of safety solution for a given slope, and under what soil conditions this will occur.

Objectives

This study is meant to provide insight into the importance of choosing an appropriate model when encountering anisotropic clay. The main goal to compare results generated by the NGI-ADP and AUS models to explore if the two models give similar results in all situations for slope stability analysis in idealized simple slopes. Along with considering the allowed ranges of admissible parameters for each model, it is the goal to give the reader an understanding into the implications of choosing between these two models. It may also help the reader to understand the fundamental differences between the two models, and to have some idea as to which model may be more appropriate to use for a given situation.

Limitations

This study was limited to idealized simple clay slopes with homogenous soil layers. No tension cracks, external ground water, shallow foundations, piles, anchors or other supports were included in the model design. Planar slides were not considered. The simulations featured solely undrained conditions without the consideration for long-term partial drainage. When calculating FoS solutions, a strength reduction analysis was performed.

Preconsolidation stress was not considered. Neither model is able to incorporate strain-softening behavior. As both soil models are designed for horizontally deposited soils, this project does not include results pertaining to natural slopes.

1.3 Approach

A brief literature review on basic soil modelling principles, soil anisotropy and the two different models are first presented. The PLAXIS 2D and Optum G2 softwares are then directly compared to first ensure that solutions from the two programs can be compared directly without some necessary degree of normalizing due to a difference in program mechanics, such as mesh effects. Then idealized simple slopes consisting of homogenous undrained anisotropic soils are created and analyzed in a parametric study for FoS solution using both AUS and NGI-ADP soil models.

1.4 Structure of the Report

A brief introduction into the basic principles of soil modeling is given in Chapter 2. Chapter 3 continues with a brief literature review outlining important concepts and studies regarding soil anisotropy and soil modeling development for anisotropic soils. The fundamental aspects of the NGI-ADP soil model are presented in Chapter 4, and the fundamental aspects of the AUS model are discussed in Chapter 5. In Chapter 6, a parametric study exploring the agreement of the PLAXIS 2D and Optum G2 soil modeling programs using similar, simple soil models is presented. The main results of this thesis are presented in Chapter 7, which shows results from the NGI-ADP vs. AUS soil models for idealized simple slopes, and in the discussion of results in Chapter 8. Findings are summarized and suggestions for future work are made in Chapter 9.

Chapter 2

Background Theory

Soil Behavior and Soil Modelling in Geotechnical Engineering

Geotechnical engineers encounter many complex geotechnical situations quite regularly. In addition to the many challenges presented by the complex scenarios, geotechnical engineers often work without complete, comprehensive data. A degree of uncertainty, especially in the soil parameters, is always present due to the limitations of modern sampling techniques. Other environmental factors, such as rainfall, ground water level, and erosion, are impossible to accurately predict and must be designed around reasonable estimations. Because of these uncertainties, geotechnical engineers are often asked to design projects based on numerous variations of design parameters. As such, there has existed serious interest in reducing the time spent on complex calculations in order to improve the efficiency of engineers, which has in part lead to the development and improvement of soil modelling software. A soil model is simply "a mathematical relationship between stress and strain or rather stress and strain increments" (Nordal, 2019). Soil models, also referred to as material laws, are designed to illustrate the most important aspects of real soil behavior and to predict reasonable responses to given stress or strain conditions. However, due to the complex relationships that govern soil behavior, these soil models often use approximations or incorrect assumptions that do not completely capture real soil behavior (Nordal, 2019). This is illustrated in **Error! Reference source not found.**, as the Mohr-Coulomb model accurately describes the real soil strength for a relevant stress interval but does not accurately describe soil strength for all stress intervals.

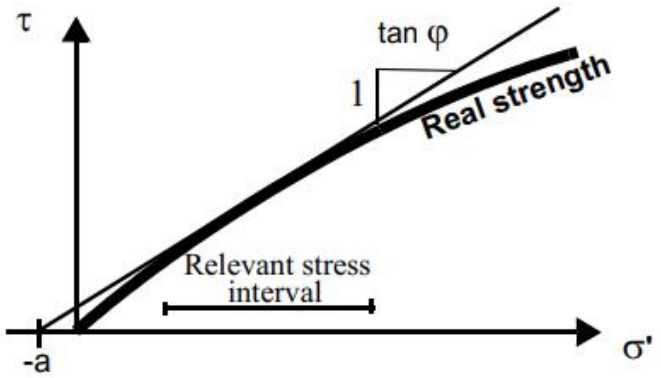

Figure 1. Prediction of shear strength by Mohr-Coulomb criteria vs real soil behavior. Retrieved from Nordal (2019).

As computing power has improved and software engineering has greatly advanced, so too has soil modelling experienced very meaningful improvements in recent decades. Modelling programs have not only improved in their computing power and complexity but have become significantly more user-friendly and expedient (e.g. Nordal, 2019). Several different types of modelling programs are employed today. The soil models explored by this thesis are classified as Finite Element (FEM) modelling programs.

In order to make models usable, and as limited by current model development, soil models often omit rather significant aspects of real soil behavior. More advanced soil models often feature more realistic aspects of soil behavior, but require more input data. While it may seem that the omission of real soil phenomenon is an unwise oversimplification, there are actually some well-founded motivations for choosing to do this. Simple models may give reasonable estimations of the ultimate limit states of a soil: at what stress condition the soil will fail. In modern geotechnical practice, this limit may be adequate for many types of problems, including slope stability (e.g. Nordal, 2019). The simplicity of the model also allows for the generation of a reasonable solution with limited data and can be used to verify the solutions generated by more advanced models. More complex problems require more accurate understanding of the real soil behavior that can be expected. A major challenge for geotechnical engineers is to understand the limitations and appropriateness of the various soil models, and choosing the optimal soil model can definitely improve the accuracy of soil behaviors, such as settlement (Nordal, 2019). However, a certain amount of ‘close enough’ is necessary due to the current limitations of the available soil models. Certain soil behaviors, such as strain softening, still

prove very difficult to be integrated into soil programs. A brief overview of the major concepts of soil modelling is provided.

FEM

The Finite Element Method (FEM) is one of the most popular and widely used numerical methods used for soil modelling in geotechnical engineering (e.g. Nordal, 2019). It was first developed in the 1950's and has been continuously improved upon to improve modelling capability and ease of use.

This type of modelling program operates using the displacement method, a theoretical method that involves the calculation of displacement or deformation in response to applied loads or forces (Nordal, 2019). Exact solutions are not able to be calculated, and instead, FEM generate approximate solutions. The accuracy of the solution is influenced by numerous factors. These factors may include chosen model aspects, such as mesh refinement, or soil parameters such as soil model, layering simplicity and boundary conditions. Additionally, choosing to model in two dimensions or three dimensions may have a significant impact. Geotechnical engineers commonly model three-dimensional problems in two dimensions, despite that fact that this can reduce accuracy (i.e. Gens et al., 1988, Zhang et al., 2013, Nordal, 2019).

The Finite Element Method uses a mesh of defined elements containing nodes, as seen in **Error! Reference source not found.**. These elements are subjected to a force or displacement in extremely small steps, called increments. The elements then must respond to the incremental force or displacement according to a defined stiffness matrix. This process results in the approximation of displacement in the x and y directions for the element. By repeating this process over and over, an estimation of the response of an entire soil body can be generated (Nordal, 2019).

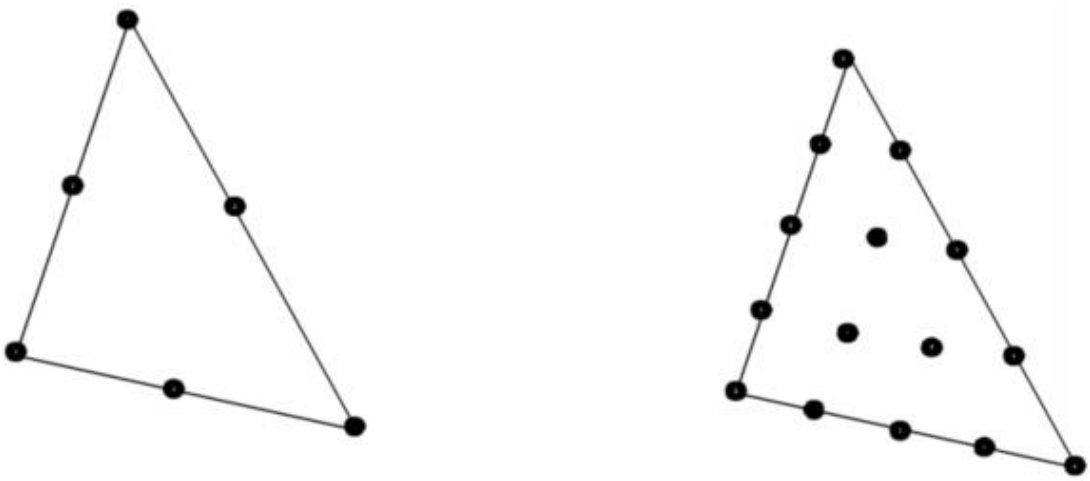

Figure 2. Triangular elements with 6 nodes (left) and 15 nodes (right). Retrieved from Nordal (2019).

Triangular elements are commonly encountered in FEM programs. Both PLAXIS and Optum incorporate 6- and 15-noded triangular elements. Different types of elements exist, such as the Gaussian and Lagrange elements (Krabbenhøft et. al., 2016). Gaussian elements are featured in both PLAXIS and Optum and are commonly used.

Modelling principles for soil behavior

Continuum Mechanics

Soil can be thought of in basic terms as a mixture of solid particles, air and water (Nordal, 2019). When describing the basic ingredients of soil, the individual components of soil may seem rather simple. However, soil behaves as a very complex material with significantly varying characteristics that change in response to soil makeup. When trying to understand and model soil behavior, it can then be very useful to imagine soil as a continuum. The theoretical framework of continuum mechanics can then be applied to illustrate the most important aspects of soil behavior.

To apply continuum mechanics to soil behavior, the following basic principles must be applied (Grimstad and Benz, 2018, Aamodt, 2019):

- Conservation of mass
- Linear momentum
- Moment of momentum
- Conservation of energy

The soil model, also referred to as the constitutive model or material law, also must adhere to the framework of continuum mechanics (Aamodt, 2019). It should be noted that while compression stresses are usually treated as positive in soil mechanics, more general material mechanics usually defines these stresses as negative. This should be kept in mind as both PLAXIS and Optum soil modeling programs define compressive stresses as negative.

Principal stresses and directions

The concept of principal planes and principal stresses are vital in understanding soil behavior. According to Cook and Young (1999) there will always exist three principal planes that do not experience any shear forces along those planes, regardless of the stress state (Aamodt, 2019). These principal planes can also be described by their normal vectors, termed principal directions. The principal stresses in a point can be classified as invariant properties, meaning that they are independent of the reference coordinate system that is used. Because of this, the principal stresses are extremely useful for describing the actual state of stress in a point (e.g. Nordal, 2018, Aamodt, 2019).

In common geotechnical notation, it is commonly assumed that $\sigma_1' \geq \sigma_2' \geq \sigma_3'$, where σ_1' is the major principal stress and σ_3' is the minor principal stress. The intermediate principal stress, σ_2', is often disregarded in soil behavior. Though it has been shown that the intermediate principal stress may have significant effects (e.g. Lade, 1978), due to the configuration of many laboratory tests and the common use of 2D plane strain soil modelling software, the intermediate principal stress is seldom taken into account.

A convenient way to illustrate the stress state for a soil is to plot the principal stress space in three dimensions, using a coordinate system the three principal stresses acting as the axes (Nordal, 2018). In doing so, the pi plane can be utilized. Understanding that the hydrostatic axis is defined as $\sigma_1 = \sigma_2 = \sigma_3$, the pi plane exists normal to the hydrostatic axis and the triaxial plane defined by $\sigma_2 = \sigma_3$ (Nordal, 2018). The pi plane can be seen in **Error! Reference source not found.**. The pi plane is very useful as yield criterion can be easily illustrated in this view. For example, the Tresca yield criterion forms a hexagon in the pi plane.

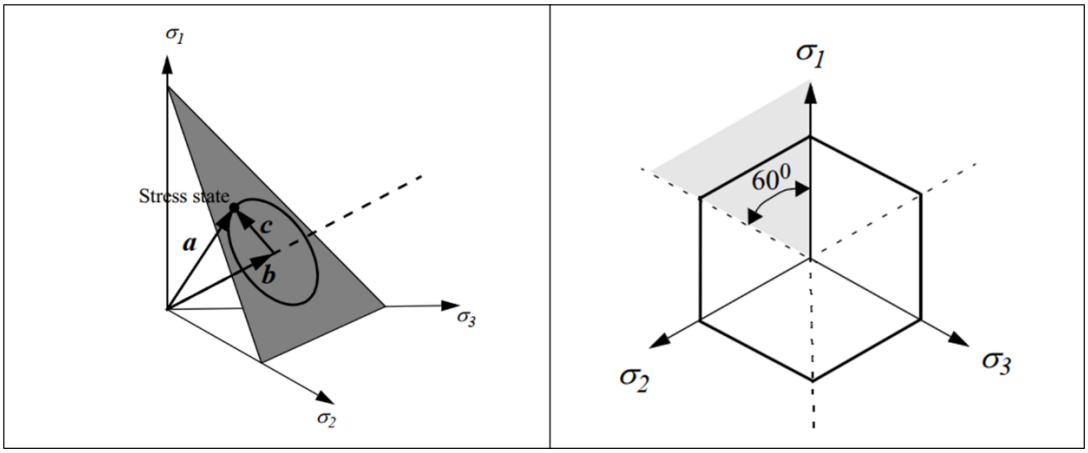

Figure 3. 3D principal stress space (left) with the hydrostatic axis shown as the dashed line, and gray triangle represents the pi-plane. The Tresca yield criterion (right) forms a hexagon when viewed in the pi-plane. Figures from Nordal (2018).

The stress state can further be described by mean and deviatoric stresses, where deviatoric stresses s_{ij} express the deviation from the isotropic mean stress, and are defined in continuum mechanics as (Nordal, 2018):

$$\boldsymbol{s} = \boldsymbol{\sigma} - \boldsymbol{p} \tag{2.1}$$

$$\boldsymbol{p} = p * \boldsymbol{I} \tag{2.2}$$

Where $\boldsymbol{I}$ is the identity matrix and the scalar p is:

$$p = (\sigma_1 + \sigma_2 + \sigma_3)/3 \tag{2.3}$$

For a more in-depth illustration of the manipulations of mean stresses and deviatoric stresses in soil modelling, the reader is referred to Nordal (2018).

Elasticity

While soil is not technically an elastic material, under certain stress conditions soil is known to behave elastically or near-elastically. As such, it can be useful to treat some aspects of soil behavior as exhibiting elasticity (e.g. Nordal, 2019). If a soil is designated as an elastic material,

there must exist some proportionality between stress and strain, as defined by Hooke's law (Nordal, 2019).

$$\Delta\varepsilon_1 = \frac{1}{E}(\Delta\sigma_1' - \nu\Delta\sigma_2' - \nu\Delta\sigma_3') \tag{2.4}$$

$$\Delta\varepsilon_2 = \frac{1}{E}(-\nu\Delta\sigma_1' + \Delta\sigma_2' - \nu\Delta\sigma_3') \tag{2.5}$$

$$\Delta\varepsilon_3 = \frac{1}{E}(\nu\Delta\sigma_1' - \nu\Delta\sigma_2' + \Delta\sigma_3') \tag{2.6}$$

Elastic deformations are reversible, and following the removal of an added force, the soil returns to its original form. While soils do not behave in this way, this simplification has proven to be useful and is incorporated and built upon in several important soil models.

Elasticity can be modelled as an isotropic property. When modelled in this way, it can be defined using only two parameters, though there are two different sets of parameters most commonly used. E and ν from Hooke's law are commonly used, though an alternative is to use the volumetric modulus K and the shear modulus G (Nordal, 2019).

The volumetric modulus K, also called the bulk modulus, can be defined as:

$$K = \frac{E}{3(1-2\nu)} \tag{2.7}$$

It can be observed that as ν approaches 0,5, the bulk modulus will increase towards infinity. This is describing an infinite stiffness, which can be thought of as incompressibility. A Poisson's ratio greater than 0,5 will result in a negative stiffness, which cannot occur (Nordal, 2019).

The relation between volumetric stress and volumetric strain can be written as:

$$\Delta p' = K\Delta\varepsilon_v \tag{2.8}$$

Where:

$$\Delta\varepsilon_v \approx \Delta\varepsilon_1 + \Delta\varepsilon_2 + \Delta\varepsilon_3 \tag{2.9}$$

This equation shows that for isotropic elasticity, a change in volume is uniquely determined by a change in mean stress (Nordal, 2019).

The shear modulus G can be written as:

$$G = \frac{E}{2(1+\nu)} \tag{2.10}$$

The shear modulus G is advantageous as it can be used to describe the relation between shear stress and shear strain, when:

$$\Delta\tau = G\Delta\gamma \tag{2.11}$$

Where

$$\Delta\gamma = \Delta\varepsilon_1 - \Delta\varepsilon_3 \tag{2.12}$$

Plasticity and Elastoplasticity

Plastic strains by definition are permanent changes in the soil structure and can occur as volumetric strain or shear strain (Nordal, 2019). Soils can be more accurately modelled by combining elastic and plastic theories together to illustrate stress-dependent behaviors. These elastoplastic models then imagine that a soil will deform elastically until its maximum strength is breached, upon which it deforms plastically. The concept of elastoplasticity is based on the concept that elastic strains and plastic strains can be distinguished from one another (Nordal, 2019).

In order to more accurately mimic real soil behavior, these models can be modified to show some amounts of plastic deformation before breaching the failure surface. The concept of elastoplasticity is implemented using three new soil behavior concepts: a yield criterion, plastic flow, and hardening (Nordal, 2019; Aamodt, 2019).

Yield criterion

A yield criterion describes the maximum state of stress a soil may be subjected to before developing strain. Applying additional stress to a point already on the yield criterion will not

change the stress state of that point. Instead, as the soil cannot maintain its matrix shape, the soil will deform and strain will develop (Nordal, 2019).

The principal stresses and stress invariants can be used to uniquely describe the yield surface of isotropic materials (Nordal, 2019). This allows for the illustration of the yield surface in three-dimensional principal stress space. The von Mises, Extended von Mises, Mohr-Coulomb and Tresca yield criteria are illustrated in **Error! Reference source not found.**. The major principal stress σ_1, minor principal stress σ_3, first stress invariant I_1 and second deviatoric stress invariant J_2 define the stress state (Nordal, 2018).

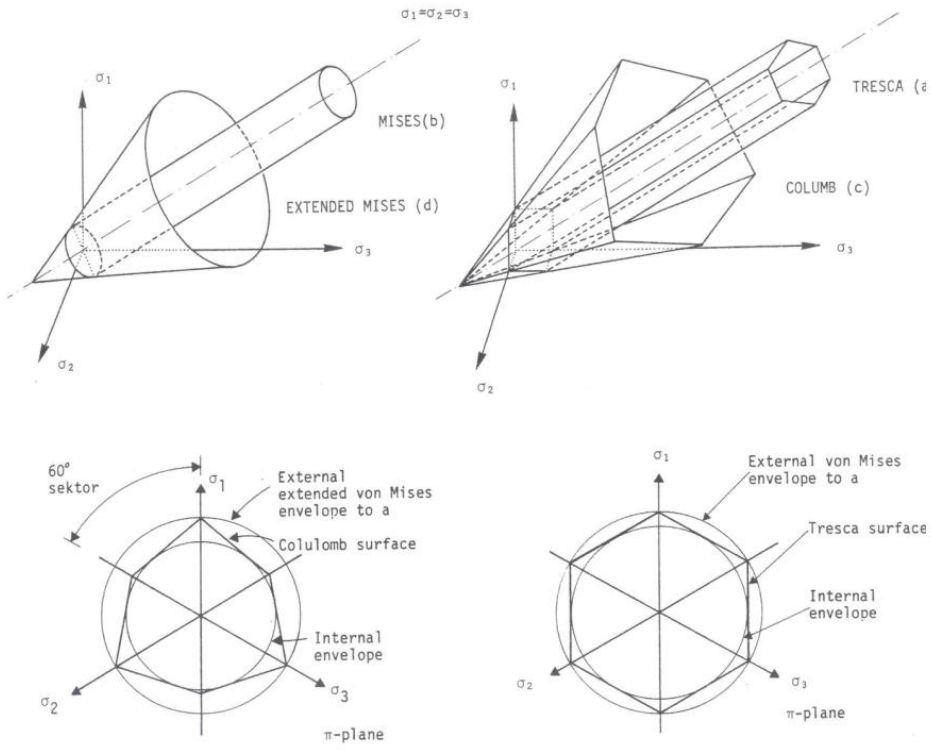

Figure 4. Common yield criterion in 3D principal stress space and pi-planes. von Mises, Extended von Mises, Tresca and Coulomb criterion are shown. Figure from Nordal (2018).

Flow rule

The development of plastic strains at failure can be described using a flow rule. These plastic strains develop when soil stress increases beyond a failure limit. The soil is not strong enough to bear the stress, and the soil skeleton develops strain in response (Nordal, 2019).

It is possible to separate a stress increment into two components. One component can be called the plastifying stress increment $d\vec{\sigma}'^{p}$. This increment can be drawn as normal to the failure surface and is the component that causes plastic strain. The second component will be tangential to the failure surface. As this component would then be in the direction of the elastic domain, this stress component would generate an elastic strain response (Nordal, 2019).

A simple elastoplastic soil model dictates that when the failure surface is breeched by a plastifying stress increment $d\vec{\sigma}'^{p}$, the plastic stiffness is zero. This results in the formation of unlimited plastic strain. However, because the soil has no stiffness to resist the stress increment, the stress cannot be sustained and the plastifying stress $d\vec{\sigma}'^{p}$ becomes zero. At the same time, plastic strain is continuously developed (Nordal, 2019).

More advanced soil models may try to address this behavior by simulating the development of plastic strains below the ultimate yield surface. This then allows some amount of plastifying stress increment to be sustained in the soil body. If the amount of plastic strain that occurs develops proportionally to the plastifying stress increment, this can be said to be described as associated flow (Nordal, 2019).

A flow rule mathematically describes the normality of the plastic strain increment to the failure surface (Nordal, 2019). The failure surface gradient, determined by partial-derivatives of the yield criteria, define the surface normal. The flow rule for associated flow is written:

$$d\overrightarrow{\varepsilon^{p}} = \begin{bmatrix} d\varepsilon_1^p \\ d\varepsilon_3^p \end{bmatrix} = d\lambda \begin{bmatrix} 1 \\ -N \end{bmatrix} = d\lambda \begin{bmatrix} \dfrac{\partial F}{\partial \sigma_1'} \\ \dfrac{\partial F}{\partial \sigma_3'} \end{bmatrix} \tag{2.13}$$

Experimental data shows that plastic strain development is often less than what is predicted using the associated flow rule. This led to the development of the non-associated flow rule which includes the concept of dilatancy, represented by the dilation angle ψ (Nordal, 2019).

$$d\overrightarrow{\varepsilon^{p}} = \begin{bmatrix} d\varepsilon_1^p \\ d\varepsilon_3^p \end{bmatrix} = d\lambda \begin{bmatrix} 1 \\ -N_\psi \end{bmatrix} = d\lambda \begin{bmatrix} \dfrac{\partial Q}{\partial \sigma_1'} \\ \dfrac{\partial Q}{\partial \sigma_3'} \end{bmatrix} \tag{2.14}$$

Dilatancy describes the change in volume during plastic yielding. Soils may be dilatant, meaning that they expand during shearing, or contractant, meaning that they contract during shearing. Some soil types, including sensitive and quick clays, exhibit negative dilatancy. In undrained conditions, the change of pore pressure is controlled by the dilatancy angle. In most cases, the angle of dilatancy is much smaller than the friction angle, and as a consequence, non-associated flow better captures real soil behavior (Nordal, 2019). Because the angle of dilatancy is normally only a few degrees, in many cases it is assumed to equal to zero when there is a lack of precise data.

Hardening

In the linearly elastic-perfectly plastic soil models, once the yield criterion is surpassed, an unlimited amount of shear strain may develop. While this concept has its uses, particularly in instances where the ultimate limit state is vitally important, this will not truly illustrate the behavior of the soil after failure (Nordal, 2019). Soil models can be modified to include a hardening behavior in response to a stress change. This is done by the introduction of a hardening rule. By incorporating some development of plastic strain before an ultimate failure, the yield criterion will change dependent on the stress conditions of the soil body. The hardening rule governs the behavior of the resultant yield surface until an ultimate failure surface is reached (Nordal, 2019; Aamodt, 2019). Several of the more advanced models define their yield criterion in part by the preconsolidation stress state. The way in the which the geometry of the yield criterion is altered can be described by the classification of the hardening rule. An isotropic hardening rule will cause a yield surface to expand equally in all directions, while a kinematic hardening rule will cause a translation of the existing yield surface. A mixed hardening rule incorporates both an expansion and translation of the yield surface (Nordal, 2019).

Mohr-Coulomb Model

While the Mohr-Coulomb model is not directly used in this thesis, it can be very useful to describe this model as it forms the foundations for some of the more advanced soil models. This soil model is classified as linearly elastic-perfectly plastic. According to Nordal (2019) “the Mohr Coulomb criterion is by far the most important criterion for the strength of soils”.

Laboratory experiments show that the effective stresses, the total stress minus the pore pressure, largely control the strength of soils (Terzaghi, 1942; Nordal, 2019).

Coulombs law (Coulomb, 1773) defines a failure line illustrating the maximum shear strength:

$$\tau_f = c + \sigma' \tan\varphi = (\sigma' + a)\tan\varphi \tag{2.15}$$

Where $\tan\varphi$ is the friction coefficient, a is attraction and $c = a * \tan\varphi$ is the cohesion. This model requires very few input parameters and is simple to use but may not accurately reflect all aspects of soil behavior. An illustration of the Mohr-Coulomb model is shown in Figure 5. Certain soil behaviors, such as dilatancy and hardening, are not included in this model.

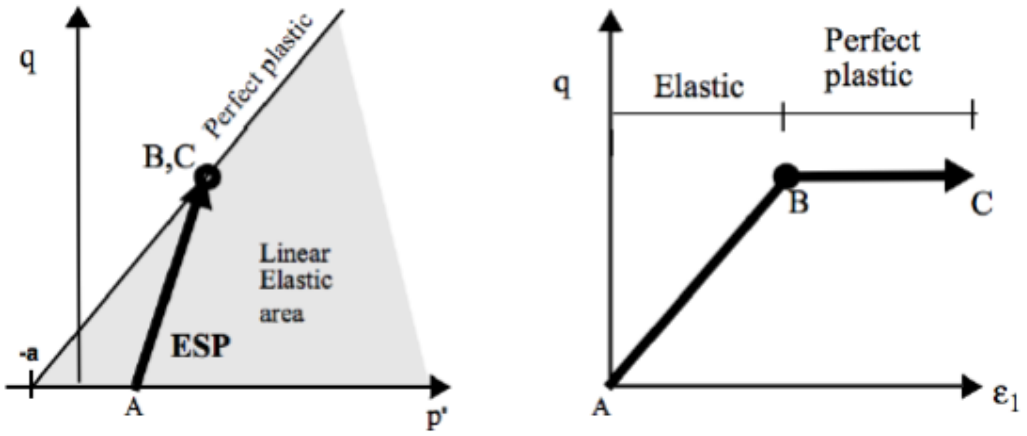

Figure 5. Linearly elastic-perfectly plastic Mohr-Coulomb model. Soil behaves either elastically or completely plastically. Figure from Nordal (2019).

Tresca Model

Geotechnical engineers are typically more interested in effective stress-based analysis of soils. However, there are certain situations in which a total stress analysis is more appropriate. When clays experience rapid load application, the undrained shear strength becomes relevant (Nordal, 2019). Gravels and sands, characterized by high permeability, must be loaded extremely rapidly to exhibit undrained behavior, as the pore fluid is able to dissipate rather freely. On the other hand, clays are characterized by very low permeabilities and entrap pore water for a much greater time. Because of this, clays are characterized by undrained soil behavior for significant amounts of time. The undrained shear strength is independent of the effective stress conditions

and is relevant in undrained scenarios. In these situations, pore pressure cannot be released. The entrapment of pore fluid prevents any significant change of soil volume.

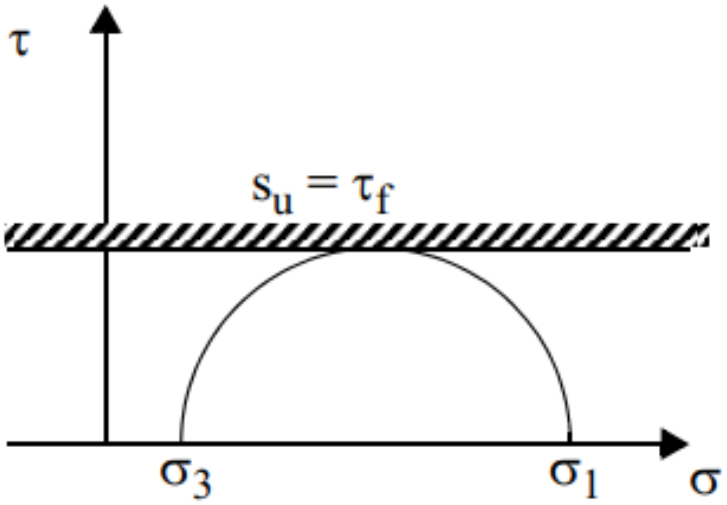

Figure 6. Tresca criterion. Notice that the intermediate stress is not considered to affect the maximum shear strength. From Nordal (2019).

It can be seen from Figure 6 that the shear strength s_u is given by:

$$s_u = \frac{1}{2}(\sigma_1 - \sigma_3) \tag{2.16}$$

The undrained shear strength can be determined using laboratory testing and is commonly determined using the undrained triaxial tests (Nordal, 2019). Field tests also exist for determining the undrained shear strength, such as the vane test.

The pore pressure was traditionally not measured when testing for the undrained shear strength. While the Tresca criterion is usually expressed in terms of the total stress, the soil still obeys the Mohr-Coulomb criterion. This can be seen if the pore pressure is measured, as it is then possible to draw the effective stress path (Nordal, 2019). The effective stress path will be identical regardless of the inclination of the total stress path, as seen in Figure 7.

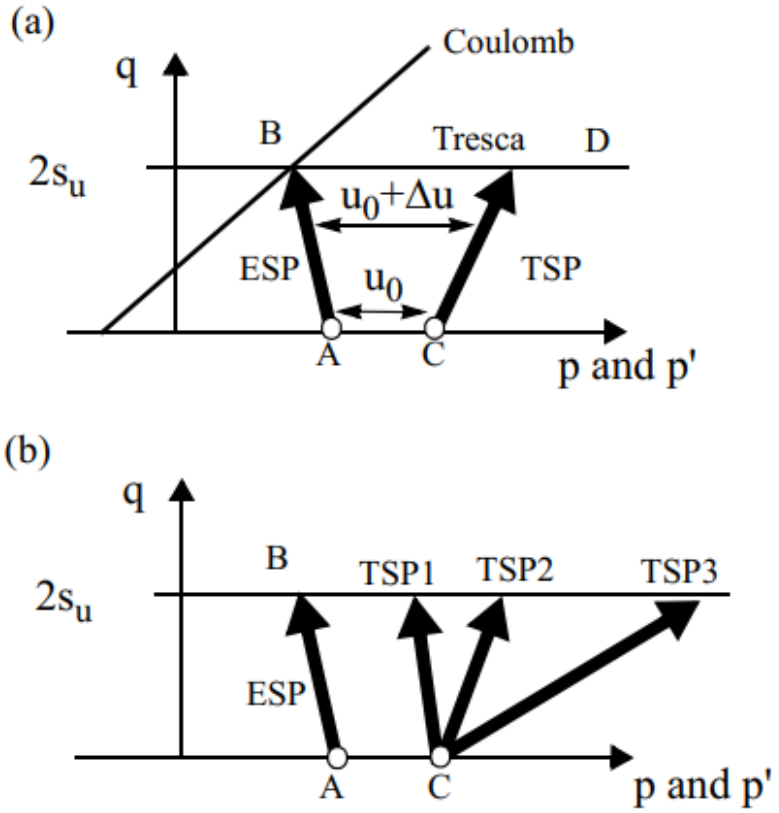

Figure 7. Figures (a) and (b) show that the undrained shear strength is actually controlled by the Mohr-Coulomb criterion. The Total stress path has no influence on the undrained shear strength. From Nordal (2019).

It can then be determined that undrained shear strength is actually controlled by the:

- Initial effective stress state
- Coulomb criterion
- Shape and inclination of the effective stress path (Nordal, 2019).

As previously discussed, the Tresca criterion can be visualized in the π-plane as a hexagon.

Undrained behavior of clays

An important characteristic of undrained behavior is that volume is assumed to remain unchanged in response to a given stress load. This is the result of the entrapment of pore fluid, which can be thought of as incompressible. This assumption forms the basis of the total stress approach, which can be applied to undrained conditions (Nordal, 2019).

$$\Delta\varepsilon_{vol} = 0 \tag{2.17}$$

Knowing that from Hooke's law the change in volume is governed by change in effective stress, it can then be reasoned that the effective stress must remain unchanged. This means that the added load only influences the pore pressure. Hooke's law states:

$$\Delta\varepsilon_v = \frac{\Delta p'}{K} \tag{2.18}$$

The change in total stress is given by the change in effective stress plus the change in pore pressure:

$$\Delta p = \Delta p' + \Delta p_w \tag{2.19}$$

No change in effective stress means that the change in pore pressure is equivalent to the change in total stress. However, these assumptions based on Hooke's law are only valid for elastic, isotropic soils, which are oversimplified assumptions and do not accurately describe real soil behavior. Volume change can also occur due to shearing (Nordal, 2019). A dilatant material will experience a change in volume in undrained conditions, which will result in a change in the effective mean stress. The concept of dilatancy is previously described in the context of elastoplasticity, and it is clear that integrating the theory of elastoplasticity with the linearly elastic-perfectly plastic Tresca model will better reflect real soil behavior.

Because undrained conditions will gradually transition into drained conditions, an effective stress approach must be incorporated when determining final soil responses, such as the eventual settlements (Nordal, 2019). First the time to consolidation must be determined, which is dependent on the length of drainage path H, permeability k, and stiffness of the soil skeleton E_{oed}:

$$t_p = \frac{H^2}{c_v} \tag{2.20}$$

Where

$$c_v = \frac{E_{oed} * k}{\gamma_w} \tag{2.21}$$

According to Nordal (2019) the scenario will usually transition from undrained conditions to drained conditions at approximately $t = 0{,}1 * t_p$.

Though it has been shown that the effective stress-based Mohr-Coulomb criterion ultimately controls the undrained shear strength, thinking of clays in terms of their total stress characteristics is still useful. Norwegian practice classifies clays based on undrained shear strength, typically (Nordal, 2019):

Soft clays: $s_u < 25kN/m^2$

Stiff clays: $s_u > 50kN/m^2$

Strain softening

In the same manner as some soils may harden in response to added stress, there are also soils that become weaker in response to added stress. This is known as strain softening and occurs in negatively dilatant soils such as sensitive and quick clays (e.g. Nordal, 2019). In simplistic terms this can be imagined as resulting from a decrease in effective mean stress as the volume decreases during shearing, causing pore pressure to increase. Strain softening is especially relevant for sensitive and quick clays, which typically exhibit anisotropic strength behavior. However, incorporating strain softening behavior in soil modelling has proven numerically difficult and is hampered by mesh effects. Most common methods employ some sort of measurement of incremental strain as part of an iterative process. However, element size greatly influences incremental strains and instead the modelling of strain softening becomes an exercise in determining optimum mesh density.

Plane strain conditions

Many geotechnical problems are analyzed in plane strain. Plane strain conditions exist when loading and structure geometry are unchanging in the longitudinal direction (e.g. El-Nasrallah, 1976). In this manner, by assuming that behavior is constant along the entirety of an axis, a three-dimensional problem can be analyzed in two dimensions. In plane strain conditions, $\tau_{zx} = 0$ and the influence of the intermediate principal stress is not taken into account.

Soil models can be illustrated in two dimensions for plane strain conditions. The yield criterion when illustrated in plane strain often take the shape of a circle (e.g. the Mohr Circle) or an ellipse. However, when describing stress-strain relationships with more advanced soil models, it becomes necessary to describe the yield criterion in 3D stress space. This will be described in more detail in a later subsection.

Triaxial test

The triaxial test is often used to test for soil parameters. Some of the more relevant parameters include the shear strength parameters in compression and extension. For clays this is an effective method for determining the anisotropic undrained shear strength. A triaxial test device is a contraption that houses a cylindrical soil sample and applies force along a vertical axis and horizontally along the length of the sample (Sandven et. al., 2015). In a triaxial compression test, the axial stress is the major principal stress σ_1 and the radial stress is the minor principal stress which is equal to the intermediate principal stress $\sigma_2 = \sigma_3$. In an extension test, the radial test is the major principal stress and $\sigma_1 = \sigma_2$. The axial stress is then σ_3.

It should be noted that geotechnical problems are commonly analyzed in plane strain. While triaxial testing simulations conditions that are very similar to plane strain, the two are not completely equivalent. Multiple studies using various designs of plane strain apparatus show that the soil strength in these plane strain devices is slightly higher than when tested in a triaxial test (e.g. El-Nasrallah, 1976, Whittle et al., 1994). Results from Ladd et. al. (1977) show a ratio of $s_u^{TXC}/s_u^{PSA} = 0{,}92 \pm 0{,}05$ and $s_u^{TXE}/s_u^{PSE} = 0{,}82 \pm 0{,}05$ where s_u^{TXC} is undrained strength in triaxial compression and s_u^{PSA} is undrained strength in active plane strain, and s_u^{TXE} is strength in triaxial extension and s_u^{PSE} is undrained strength in passive plane strength (Grimstad et. al., 2012). However, triaxial strength parameters are often input directly into plane strain analysis.

Thus it becomes very important to distinguish triaxial strength from strain in plane strain where the intermediate principal stress is often greater than the minor principal stress, though in engineering practice, use of the more conservative strength from the triaxial test offers a greater margin of safety.

Direct Simple Shear Test

In addition to the two configurations of triaxial tests, shear strength can also be determined by use of a shear-box to determine the direct simple shear. This contraption holds a soil sample, and restricts the development of horizontal strain. A gap between two metal plates allows for the development of shear strain. Normal stress is applied in a consolidation phase, and then shear stress is applied until the soil fails (Bjerre & Landva, 1966). While this testing method is generally straightforward and simple, it should be noted that in many cases this test is not conducted in Norwegian practice, as the triaxial extension and compression may be believed to adequately provide the necessary data.

PLAXIS

PLAXIS 2D is a two-dimensional geotechnical software that operates using finite elements. This program uses triangular elements of either 6 or 15 nodes, 15-noded elements being the default setting (Brinkgreve, 2017). The program arrives at solutions by performing a number of iterations until a solution satisfies the convergence parameters of an equilibrium state. The program is simple to use and provides a graphic visualization of the soil body and the expected deformations in response to stress. After establishing a soil body, the program generates a soil mesh, which is an interconnected matrix of elements. The use of a mesh of adequate element density is vital to the accuracy of the solution that the program is able to provide (Nordal, 2019). However, it is equally important that the user have adequate knowledge of the various soil models available, including their limitations.

Optum CE

Optum CE is a much newer geotechnical software provider, and the first commercially available package was released in 2014 (Optum CE). There are at present four programs for design use: Optum G2 and G3 for geotechnical design, Optum CS for concrete structures, and Optum MP for design of reinforced concrete slabs. This thesis will focus on the two-dimensional G2 software. A major selling point of the company is the development of software that requires no previous knowledge of FE programs in order for the user to operate.

Both the two-dimensional G2 and three-dimensional G3 programs are FEM programs. G2 shares many similarities with PLAXIS 2D, including a built-in array of soil models, various

analysis types and numerous geotechnical features. For a more complete overview of the programs, the reader is referred to the user manuals available at https://optumce.com/products/brochure-and-datasheet/.

Chapter 3

Literature Review

Anisotropy in Soils

A material that is isotropic exhibits identical properties regardless of direction or orientation. An anisotropic material then shows some property that is influenced by direction or orientation. Anisotropy in geotechnical engineering is usually referring to the phenomenon of anisotropic shear strength response in certain soils; the occurrence of difference shear strengths in a soil under different orientations of stress (e.g. Berre and Bjerrum, 1973). Perhaps the most commonly cited occurrence of this behavior is the response of clays to triaxial extension and compression tests. These tests regularly show that the shear strength in the compression test is higher than the shear strength in the extension test (e.g. Berre and Bjerrum, 1973, Nordal, 2019). An illustration of a typical example of this phenomenon is shown in Figure 8. However, soil anisotropy is slightly more nuanced than just this phenomenon alone. This phenomenon has sometimes been referred to in the literature as Lode angle dependency or Lode angle anisotropy (e.g. Krabbenhøft et. al., 2019). There exists also the concept of physical anisotropy, in which the natural layering of the soil makes the soil stronger in certain directions. Due to the current standard sampling methods and the prevailing concept that most soils are deposited horizontally, these two effects are often difficult to distinguish from each other, especially since the vertical axis of cross-anisotropy for horizontally deposited soils coincides with the direction of principal stresses in the triaxial tests.

While there do exist some clays that have no physical anisotropy, meaning that the physical orientation of the soil does not impact shear strength, Lode angle anisotropic response is still an expected phenomenon. This leads to some confusion in the literature, as ‘isotropic’ materials are still sometimes expected to show some kinds of anisotropic behaviors (e.g. Krabbenhøft, 2019).

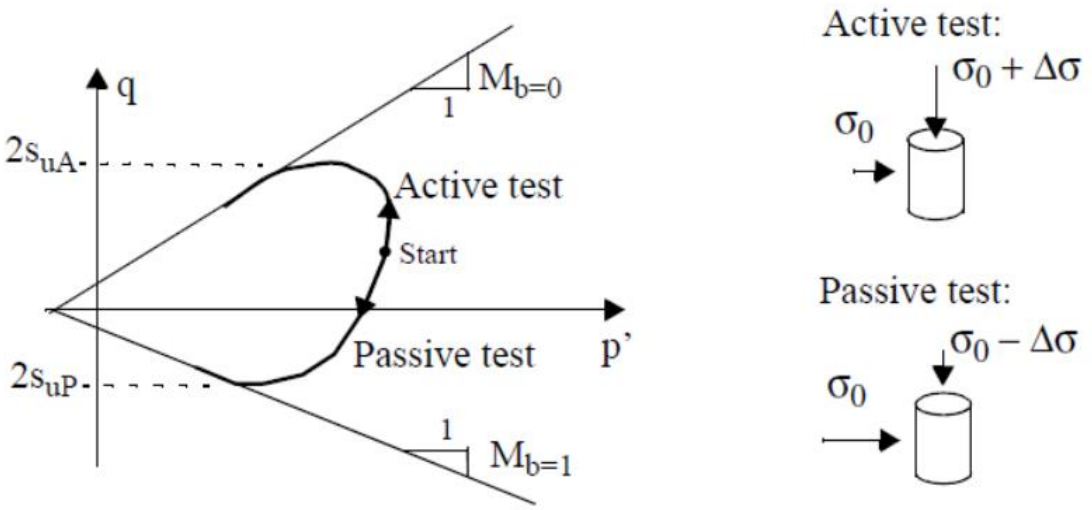

Figure 8. Typical shear strength anisotropy from triaxial compression (active) and extension (passive) tests. Figure from Nordal (2019).

Laboratory testing using the direct simple shear tests has revealed that the shear strength in this regime is often somewhere between the shear strength in the compressive and extension regimes (e.g. Nordal, 2019).

If a classical bearing capacity problem is visualized, as seen in Figure 9, the failure surface can be drawn by dividing it into an Active Rankine zone, a Prandtl zone, and a Passive Rankine zone (Grimstad et al., 2012). The stress conditions and shear strengths in these zones can best be approximated by a triaxial compression, direct simple shear, and triaxial extension test, respectively.

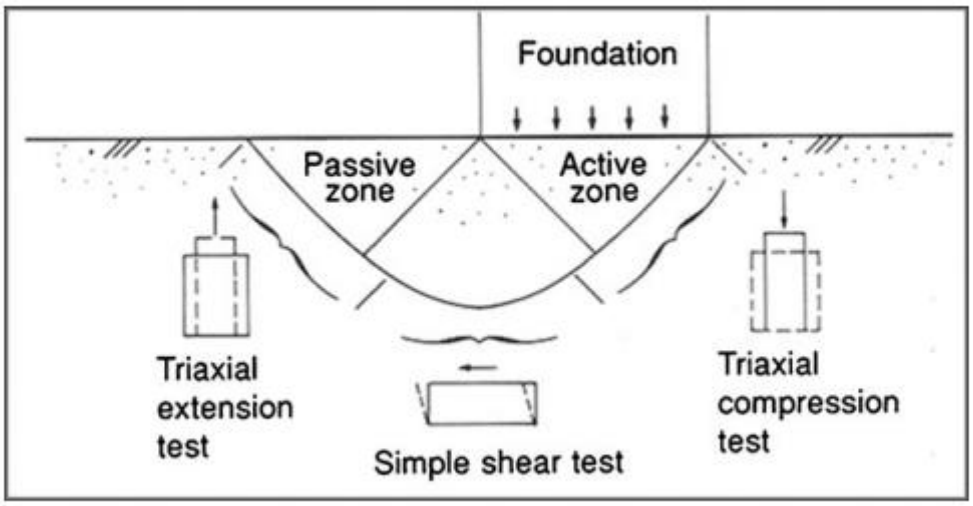

Figure 9. Relation of triaxial and direct simple shear test conditions to classically imagined failure zones for a bearing capacity problem. Figure from Grimstad et. al. (2012).

Researchers such as Berre and Bjerrum (1973) have demonstrated that soil anisotropy can be correlated to plasticity. Clays that have lower plasticity typically exhibit higher degrees of strength anisotropy. However, analysis of tests conducted on clays across 14 countries disputes the generality of this relationship, and correlating anisotropy solely on the basis of plasticity may not be appropriate for all types of clays (Won, 2013). According to Nordal (2019), typical clay anisotropic shear strength in active, direct shear, and passive regimes can be estimated by:

$$s_{uA} \approx 0{,}3 * \sigma_v' \tag{3.1}$$

$$s_{uD} \approx 0{,}2 * \sigma_v' \tag{3.2}$$

$$s_{uP} \approx 0{,}1 * \sigma_v' \tag{3.3}$$

Meaning that:

$$s_{uD} \approx \frac{2}{3} * s_{uA} \tag{3.4}$$

$$s_{uP} \approx \frac{1}{3} * s_{uA} \quad (3.5)$$

However, these are merely approximations to be used in the absence of laboratory measurements. Studies have shown that soils range widely in anisotropic strength, and accurate testing is needed whenever possible (e.g. Karlsrud & Hernandez-Martinez, 2013).

An isotropic material can be said as exhibiting coaxiality, meaning that the direction of principal stress coincides with the direction of strain (Nordal, 2019). An anisotropic material, however, may not demonstrate this behavior.

Normally consolidated clays

Clays are classified as soils consisting of more than 30% of particles smaller than 2 um (Sandven et. al., 2015). Soils with between 15%-30% makeup of particles smaller than 2 um are classified as clays, with an adjective describing the other particle fractions, for example, a 'sandy clay'. While it may seem counterintuitive that a soil that has a minority component of clay could still be considered a clay, this classification system is due to the fact that clay particles have a disproportional impact on soil behavior. A rougher definition of clay capable of being tested in the field is to chew the soil and examine the texture. Clay particles are too small to crush between the teeth. A person will feel larger particles crushing between the teeth (Sandven et. al., 2015).

In Norwegian conditions, marine clays are typically encountered, though there are some examples of clays deposited in freshwater. The chemistry of the water the clay is deposited in causes substantial differences in the soil structure, and as a result, freshwater clays are quite different than marine clays (Sandven et. al., 2015). The relative neutral ionic charge of freshwater creates an environment that leads to the parallel deposition of clay particles stacked on top of each other. Marine clays (in deglaciated northern areas) form quite differently. The flat clay particles tend to join in an 'end versus face' orientation, forming a so-called 'house of cards' structure (Sandven et. al., 2015). This structure results in the entrapment of larger volumes of pore water. Significant washing of the salt from the pore fluid, known as leeching, can lead to the development of quick behavior (Sandven et. al., 2015). This results in the liquification of the soil once the soil structure fails, as the house of cards structure collapses and quickly releases large amounts of pore fluids. Quick clays, in their liquified state, have

almost no shear strength. Experiments have shown that adding salt to a liquified quick clay can reverse the liquification and significantly increase the remolded shear strength (Sandven et. al., 2015).

It is often thought that deposition may play a key role in the formation of anisotropy in clays. Depositional environment, particle size and orientation, and stress history are key factors in the development of strength anisotropy (Lambe, 1958; Nordal, 2019).

Boston Blue Clay

Perhaps some of the most relevant studies illustrating the influence of physical anisotropy have been conducted on Boston Blue Clay (e.g. Whittle et al., 1994). Boston Blue Clay can be classified as an illitic marine clay with low plasticity, with typical I_p values between 19%-23%. This soil was studied extensively at MIT, which in part lead to the development of the MIT-E3 soil model. This model is an effective stress-based soil model capable of simulating anisotropic strength and strain-softening behavior and was developed in the later 1980s and early 1990s.

The development of a Directional Shear Cell allowed for testing of physical anisotropy. This plane strain device is stress-controlled and constructed so that both normal and shear forces can be applied to four faces of a cubicle soil sample (Arthur et al., 1977). If it is imagined that a soil develops due to a one-dimensional consolidation history, i.e. that gravity is the prominent acting force throughout the soil's history, then it can be imagined that a horizontal plane would form the normal to the major principal stress, or direction of gravity δ. The DSC device allowed for testing at principal stress increments with major principal stress at an angle δ relative to this original direction of deposition. As shown in Figure 10, the maximum shear strength occurs at $\delta = 0°$ with a maximum value of $s_u/\sigma_p' = 0.25$ for clays of OCR values of 4.0. Maximum shear strength for normally consolidated clay (OCR=1) also occur at $\delta = 0°$ and shear strength decreases as δ approaches 90°. The effect of anisotropy is greater in the normally consolidated soil, with a maximum and minimum strengths of approximately $s_u/\sigma_p' = 0.33$ and $s_u/\sigma_p' = 0.16$ respectively (Whittle et. al., 1994).

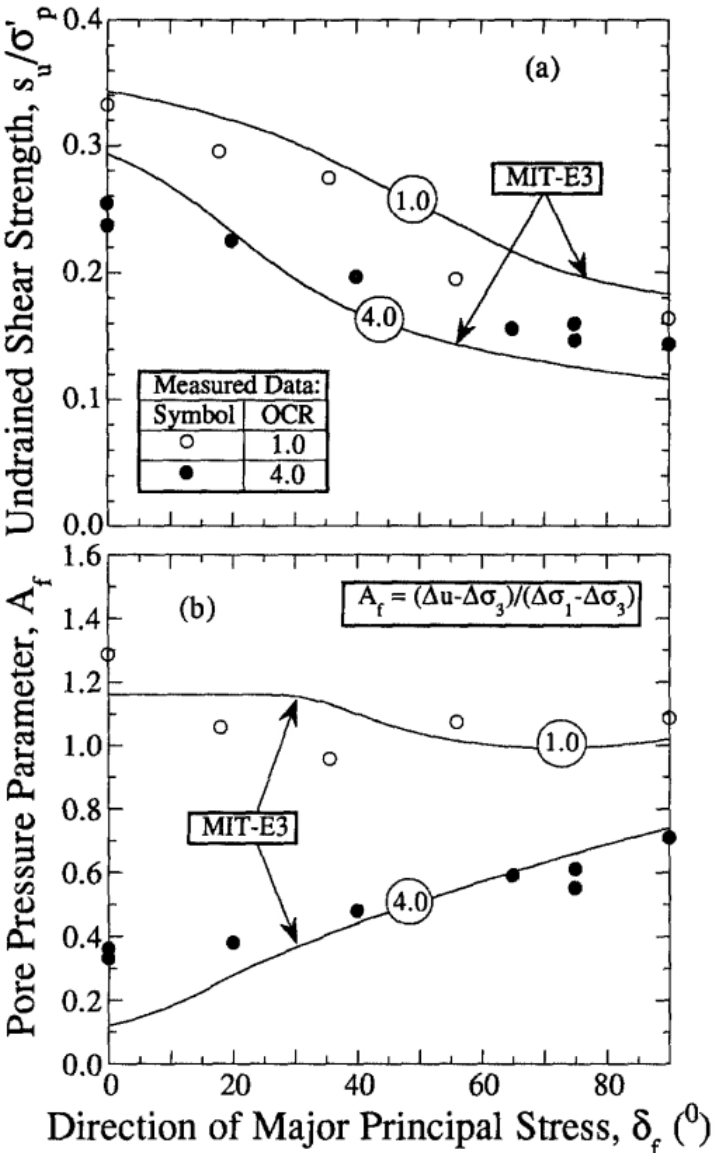

Figure 10. Measurements of undrained shear strength due to the rotation of the major principal stress. Note the more pronounced effect for normally consolidated clays. Figure from Whittle et. al. (1994).

Effect of shear stress during consolidation

Andersen (2009) demonstrates that consolidating a clay sample in a DSS test with an additional shear stress will result in an increased undrained shear strength. Andersen (2009) notes that this effect is likely more pronounced in normally consolidated clays and is likely influenced by the plasticity of the clay. This phenomenon may cause the underestimation of slope stability for slopes under additional undrained loading if this effect is overlooked. Figure 11 illustrates the normalized increase in maximum direct simple shear strength with increases consolidation shear strength. However, it must also be taken into account that standard laboratory tests reach failure in about 2 hours while an actual slope under loading would remain in undrained

conditions for much longer than this. Lunne and Andersen (2007) show that increasing the time to failure results in the decrease of static shear strength of clays by as much as 20% after 10 000 minutes. Andersen (2009) also explores the role of shear stress in pre-consolidation as it affects the cyclic bearing capacity of undrained clays.

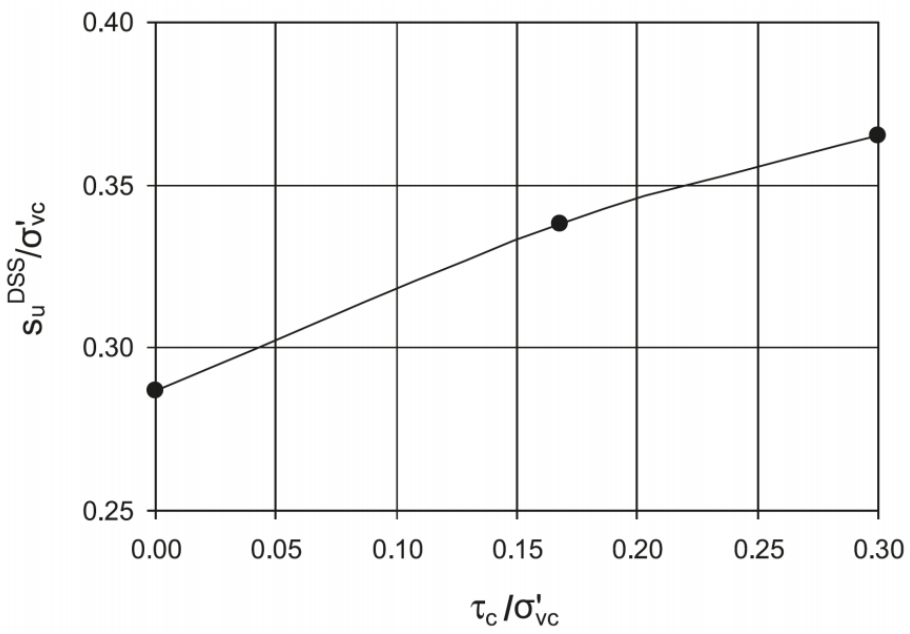

Figure 11. Undrained shear strength of quick clays in direct simple shear tests as a function of consolidation shear stress. From Andersen (2009).

Influence of intermediate stress on anisotropy

The influence of intermediate stress is largely ignored by standard triaxial tests. In a standard triaxial apparatus, the intermediate stress is either equal to the minor principal stress (compression test) or the major principal stress (extension test). Varying the intermediate principal stress requires a cubical triaxial apparatus. These have been used to study the effects of intermediate principal stress by for example Lade and Duncan (1973). These tests are often called ‘true’ triaxial tests.

True triaxial test data can be plotted in 3D stress space, and when shown in the pi plane, it is possible to compare to the fit of soil model yield criteria.

Various studies have been undertaken using undrained true triaxial tests. Results from Shibata and Karube (1965) suggested that a lower limit of shear strength could be described by the Mohr-Coulomb failure criterion. Data points from the actual failure surface of normally consolidated clays tended to form a curved failure surface that encompassed the Mohr-Coulomb hexagon. This can be seen in Figure 12. Similar results have been demonstrated by Lade and Musante (1978) on Grundite Clay and Kirkgard and Lade (1993) on San Francisco Bay Mud.

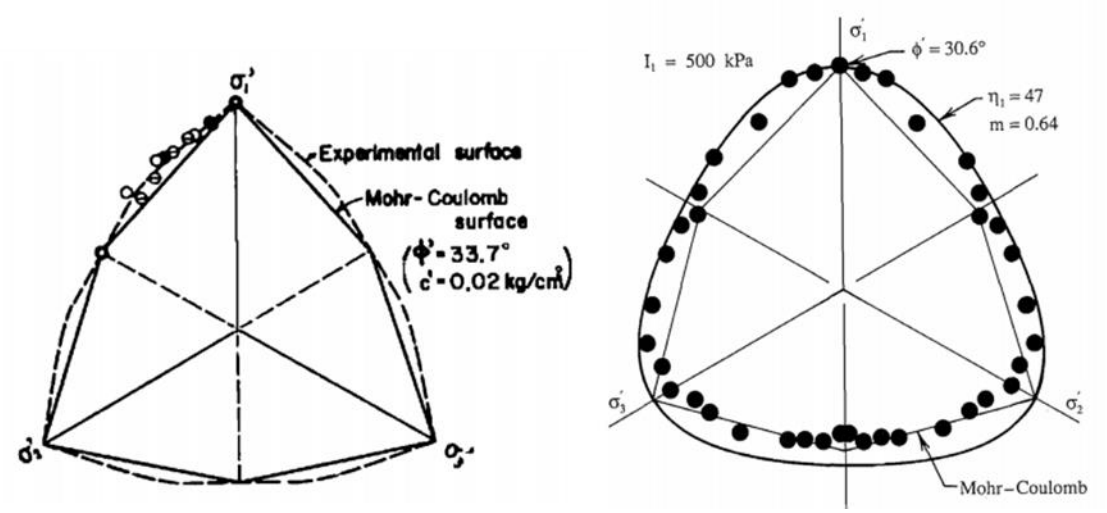

Figure 12. Failure surface from triaxial test data fit to Mohr-Coulomb criterion in pi plane (left) from Shibata and Karube (1965) and (right) failure surface for San Francisco Bay Mud from Kirkgard & Lade (1993).

Results from Prashant and Penumadu (2005) exploring Kaolin Clay also show similar behaviors, as seen in Figure 13. As part of their analysis, the authors superimposed the principal strain increment axes onto the principal stress axes. A circular plastic potential surface similar to a von Mises surface appears to fit the data quite well, appearing to coincide perpendicular to the strain increment vectors (Aamodt, 2019).

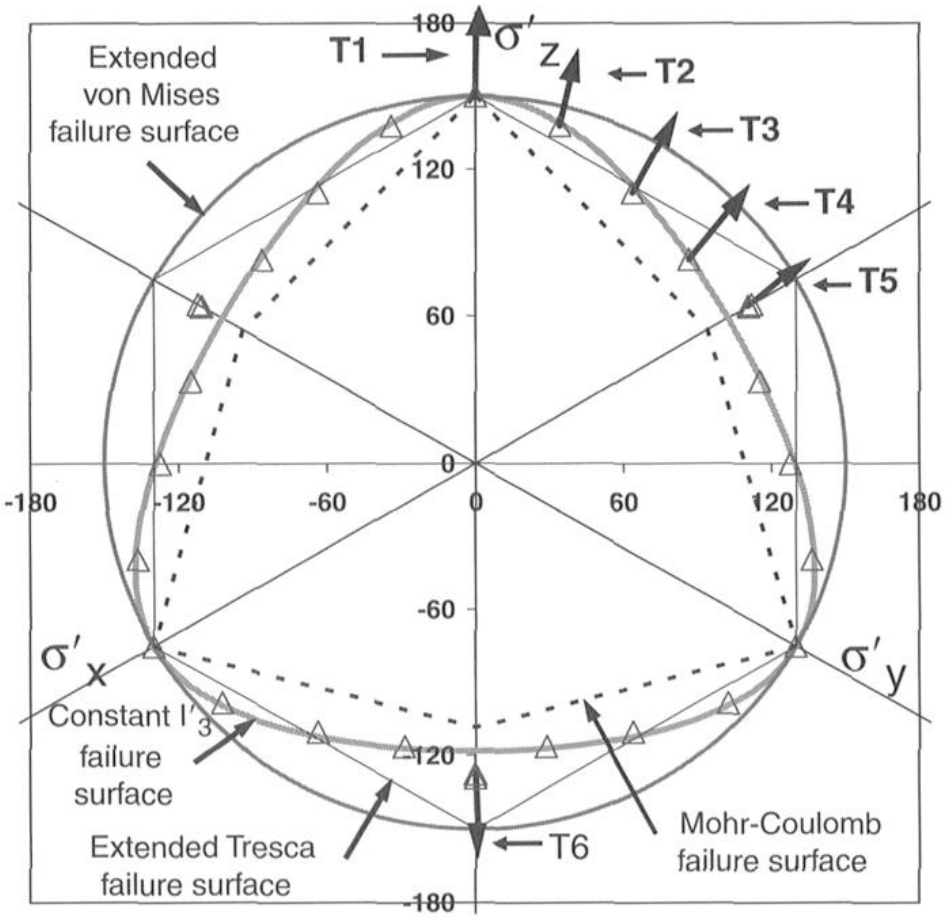

Figure 13. Experiment results of Kaolin clay vs. Tresca and Mohr-Coulomb criterion in octahedral plane. Figure from Prashant and Penumadu (2005).

Lade and Duncan (1973) suggested a failure criterion that is similar to the failure criterion presented by Matsuoka and Nakai (1974), who argued that the 'spatial mobilized plane' (SPM) could be used to uniquely express the stress-strain relationship of soil under three different principal stresses (Aamodt, 2019).

Figure 14 shows the closeness of the proposed failure criterions to the Mohr-Coulomb criterion. The Lade-Duncan and Matsuoka-Nakai criteria both coincide with the Mohr-Coulomb criterion in triaxial compression, however, only the Matsuoka-Nakai criterion coincides with the Mohr-Coulomb in triaxial extension. The Lade-Duncan overestimates the maximum stress for this stress state.

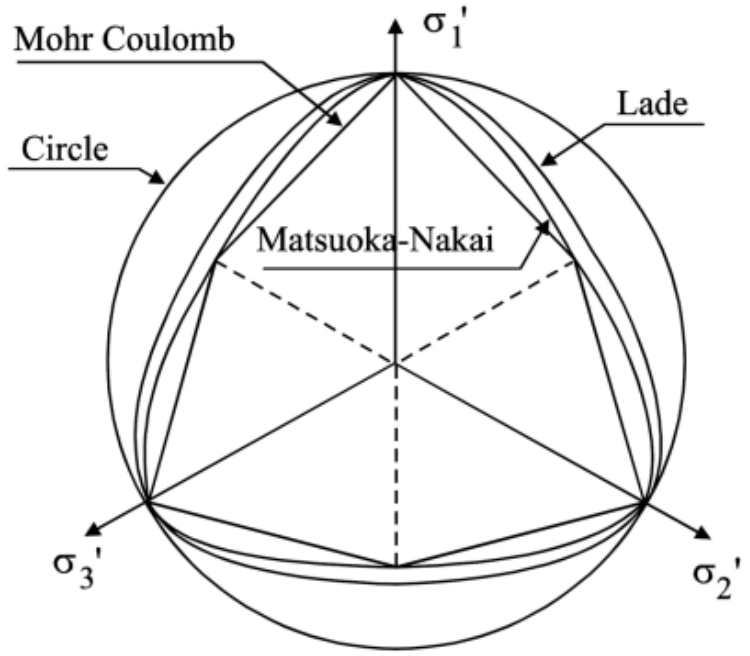

Figure 14. From Potts and Zdaravkovic (1999).

Grimstad et al. (2018) formulated a generalized yield criterion that smoothly transitions between the previously described yield criteria to eliminate false solutions. This yield criterion can be differentiated at any point in stress space. The intermediate principal stress is included in the yield criteria formulation and is controlled by the Lode angle θ:

$$F = \sqrt{3J_2} - \frac{\sin\varphi_0\,(I_1 + 3a)}{\sqrt{3} * c_\theta + s_\theta * \frac{\sin\varphi_0}{a_2}} \tag{3.6}$$

Where

$$c_\theta = \cos\left(\tfrac{1}{3}\arcsin\left(a_1 * \sin 3\theta\right)\right) \tag{3.7}$$

$$s_\theta = \sin\left(\tfrac{1}{3}\arcsin\left(a_1 * \sin 3\theta\right)\right) \tag{3.8}$$

Where the friction angle from a Lode angle of zero is φ_0. It is possible to vary the shape of the yield criterion to match those previously proposed by altering a_1, a_2 and $\sin\varphi_\theta$ (Aamodt, 2019).

Typical Anisotropic strengths in Norwegian clays

Typical shear strength anisotropy of Norwegian NC clays is very well summarized by Karlsrud and Hernandez-Martinez (2013). This article is effectively a summary of data collected from high-quality block samples from 22 sites in Norway. While these data are very useful, attention must also be drawn to the significant effects of sampling technique that this study illuminates. Since the 1950's it has been standard practice in Norway to collect samples using piston samplers. The original 54mm piston samples are still used in practice today, though there have been developments such as the 75mm and 95 mm piston samplers that have been shown to give samples of higher quality (Karlsrud & Hernandez-Martinez, 2013). One of the significant challenges with the 54mm piston sampler is that it can be challenging to recover undisturbed clay samples, particularly in low-plasticity clays which are expected to exhibit the highest degrees of strength anisotropy. Perhaps also due to the high-sensitivity nature of these clays, a different sampling method was necessary to obtain undisturbed samples.

While other steel piston samples offered marked improvement in sample quality, none has matched the performance of high-quality block sampling. Testing has shown that samples collected in this manner show different behavior than those collected by traditional methods. For example, the samples tested using the block samples exhibited very small strain at failure and brittle collapse compared to samples from piston samples (Karlsrud & Hernandez-Martinez, 2013). Figure 15 shows that soils from block samples showed higher peak shear strength. Lean silty clays also showed a change in dilatancy behavior due to sample disturbance. Samples taken from high-quality block samples showed contraction and strain-softening, while more disturbed samples from piston samples showed dilation and strain-hardening (Karlsrud & Hernandez-Martinez, 2013). It has also been demonstrated that the impacts of sample disturbance are more pronounced in triaxial compression tests compared to triaxial extension tests.

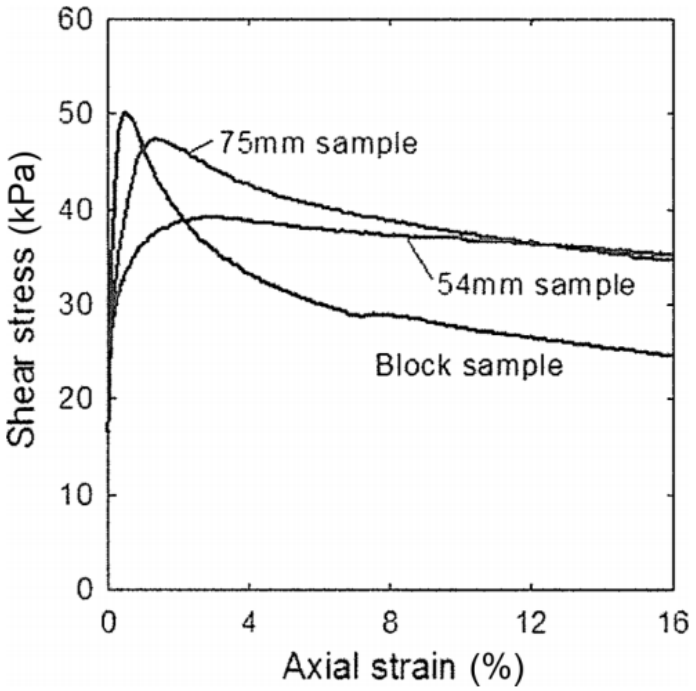

Figure 15. Shear stress vs axial strain for similar clay samples in Block samples, 54mm and 75mm piston samples. From Karlsrud & Hernandez-Martinez (2013).

Other factors in the sampling and testing process may have undesirable effects on the quality of the sample. The transportation, handling, and storage of the samples can result in significant sample disturbance and must be carefully monitored to ensure high sample quality. Additionally, trimming and handling of the sample during test preparation must be undertaken with care to minimize any sample disturbance (Karlsrud & Hernandez-Martinez, 2013).

The summaries by Karlsrud & Hernandez-Martinez (2013) developed mathematical relationships for Norwegian clays based on data from index testing. One of the results of this study was the development of mathematical relationships for anisotropic strength in clays based on the water content. This also showed some correlations in grouping when classifying clays by sensitivity. However, as seen in Figure 16, these relationships are approximations and there must be other factors that affect the anisotropic strength of soils. In the absence of anisotropic strength data, however, this approximation may be appropriate.

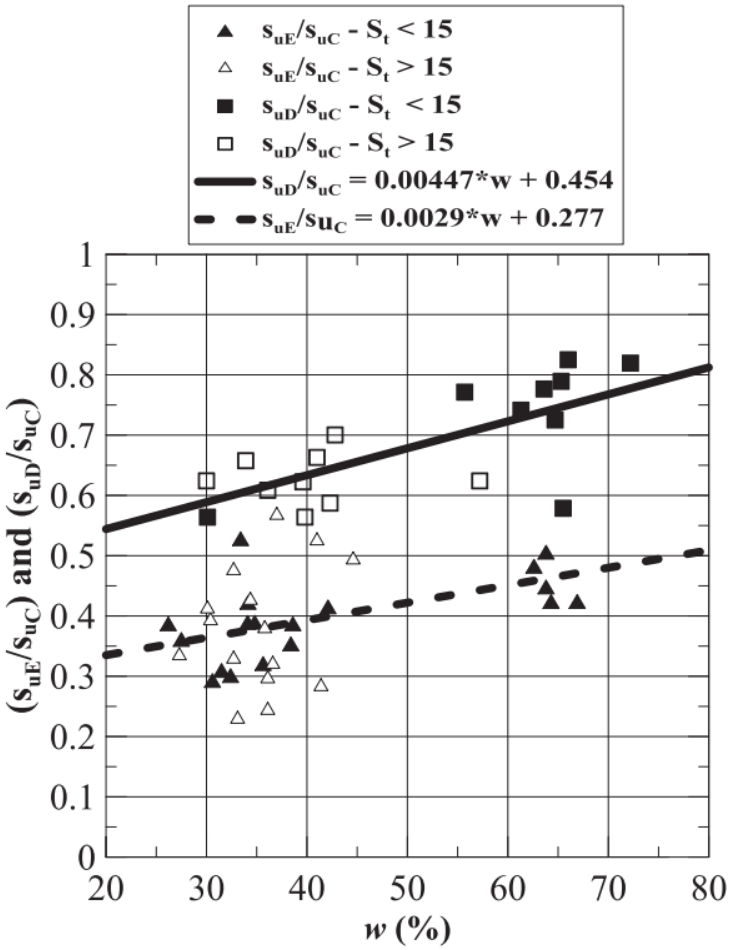

Figure 16. Anisotropic shear strength ratios vs water content for Norwegian clays taken with block sampler. From Karlsrud & Hernandez-Martinez (2013).

However, it must also be noted that the type of sampling had a significant impact on the anisotropic strength ratios. Table 1 clearly shows that samples from the block samples had lower ratios of strength in simple shear and extension. This is most likely due to the lower compression strength measured in the piston samples, as this behavior was more pronounced in the compression tests compared to the other types of tests (Karlsrud & Hernandez-Martinez, 2013).

Table 1. Type of sample collection method shows clear impact on anisotropic strength ratios. From Karlsrud & Hernandez-Martinez (2013).

	Block samples			54/95 mm samples		
Anisotropy ratio	Mean	n	r^2	Mean	n	r^2
s_u^{DSS}/s_u^{CAUC}	0.69	20	0.989	0.74	16	0.987
s_u^{CAUE}/s_u^{CAUC}	0.42	19	0.984	0.50	12	0.974

The summary of the many complications involving the sampling, testing, and modelling of anisotropic clays serves as a stark reminder of the difficulties geotechnical engineers face when encountering these situations. The process of accurately modelling soil behavior in these conditions is not straightforward, and the engineer must be aware of a number of assumptions and potential impacts due to the limitations of sampling and modelling practices that can significantly affect the accuracy of the final calculations.

Other model development

Soil models are constantly being developed and modified in attempts to more accurately model real soil behavior. Several masters theses at NTNU have dealt with the development of a soil model designed for the analysis of anisotropic soils based on the lessons learned from the development of the NGI-ADP model. Before these models can be released for commercial use, they are implemented and tested as user defined models. Many of the models will likely never be released, and the development of a new commercial model can in fact be seen as the cumulation of all the knowledge acquired in partially successful attempts that built upon each other. Rabstad (2011) presented the ADPXX model, a total stress-based anisotropic model restricted to plane strain. This model has since been modified by Isachsen (2012) and Jordbakke (2017) and Aamodt (2019). Each author has contributed their own modifications to the model, and the model has developed in complexity. The most recent model adaptation by Aamodt (2019), called the ADPX3, is an effect stress-based model that is capable of modelling anisotropic strength in soils for natural slopes where the direction of major principal stress is not necessarily fixed as vertical, allowing for physical cross-anisotropy with a non-vertical axis of symmetry.

PhD candidate Jon Rønningen of NTNU has also made significant developments in an effective stress-based model specialized for the analysis of weak Scandinavian clays. This model, called the eADP model (formerly the Geofuture Soft Clay Model) is capable of modelling anisotropy and builds upon many of the principles utilized in the NGI-ADP model. Currently this model is implemented in PLAXIS 2D as a user defined soil model. Grendahl (2019) explores the use of this model for a sizeable construction project in Oslo in which a large excavation takes place.

Additionally, the developers of Optum CE have developed an Anisotropic Generalized Tresca model that is planned for general release near the time of writing. This model would offer a different approach to modelling soil anisotropy and does not involve a shift of the yield criterion to accommodate anisotropy (Krabbenhøft, personal communication).

Chapter 4

The NGI-ADP Model

The NGI-ADP soil model is a total-stress based model that is capable of incorporating anisotropic shear strength by directly inputting measured shear strength values (Grimstad et. al., 2012). This soil model is commercially available in PLAXIS and GeoSuite geotechnical modelling programs. This model is commonly used in Norwegian engineering practice. Many geotechnical problems in Norway encounter normally consolidated anisotropic clays, and as such, this program has become well-established in the engineering community since its introduction.

While this soil model is only intended for use on horizontally clays, the model has frequently been used in engineering practice on natural slopes due to a lack of a better alternative (Aamodt, 2019). The NGI-ADP model is designed to use both the undrained failure shear strengths and strains.

The NGI-ADP model was designed to be easy to use, and able to accurately illustrate soil behavior from data collected from triaxial testing. Hardening is incorporated into the model, while strain softening behavior is not.

This soil model uses a Tresca yield criterion which can be visualized as a hexagon in the pi plane in 3D stress space. The yield criterion is then shifted to accommodate for the differences in shear strength in the compression vs extension. Due to some mathematical complications arising from the corners, the corners are slightly rounded using the Tresca approximation as described by Billington (1988) and a modified von Mises plastic potential function (Grimstad et. al., 2012). Neither the yield function nor the plastic potential function are influenced by mean stress. This then implies that plastic volume strain is not generated. Specifying a Poisson ratio of approximately 0.5 will limit elastic volume strain to near zero.

The Tresca yield criterion can be written as:

$$F = \sqrt{J_2}\cos\theta - \kappa * s_u = 0 \tag{4.1}$$

Where J_2 is the second deviatoric stress invariant, θ is the Lode angle, κ is the hardening parameter and s_u is the isotropic undrained shear strength.

The yield criterion for the NGI-ADP model in plane strain can be written:

$$F = \sqrt{\left(\frac{\sigma_{yy} - \sigma_{xx}}{2} - (1-\kappa) * \tau_0 - \kappa * \frac{s_u^A + s_u^P}{2}\right)^2 + \left(\tau_{xy} * \frac{s_u^A + s_u^P}{2 * s_u^{DSS}}\right)^2} - \kappa * \frac{s_u^A + s_u^P}{2} = 0 \tag{4.2}$$

Where s_u^A, s_u^P, and s_u^{DSS} are the undrained shear strengths obtained in plane strain active, plane strain passive and in direct simple shear tests, respectively. In order to simplify the model, the model is restricted to clays with horizontal surfaces and y is treated as the vertical direction (Grimstad et. al., 2012).

Hardening is treated as isotropic. This results in an elliptical shaped yield criterion when plotting in a plane strain deviatoric stress plot. When hardening is taking place, this can be illustrated as a distortion of the elliptical yield curves, as seen in Figure 17. The shape of the yield curves is controlled by the magnitude of strain at failure, as well as the interpolation function that is used. The NGI-ADP model uses elliptical interpolation between failure strain in the different failure modes. Certain inputs are restricted in order to keep the yield surface convex. s_u^{DSS} must be greater than or equal to s_u^P (Grimstad et. al., 2012).

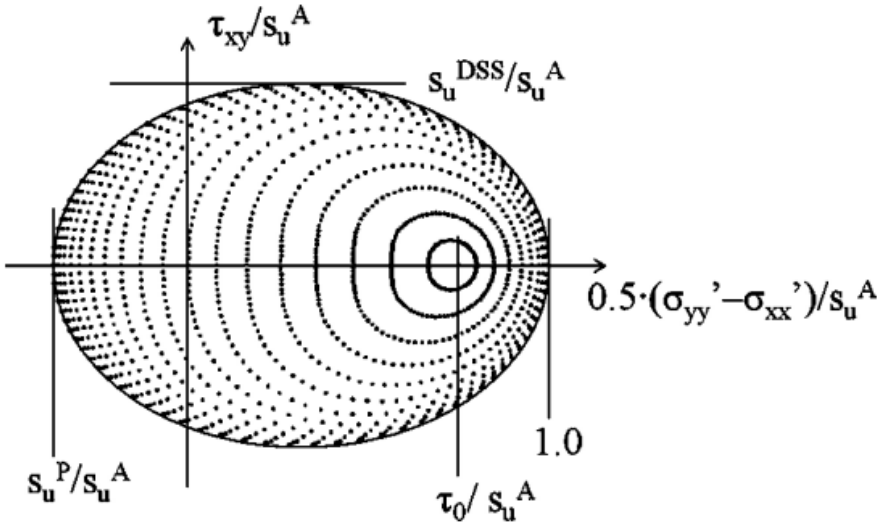

Figure 17. Shear strain contours in a deviatoric plane strain plot. From Grimstad et. al. (2012).

The yield criterion in 3D stress space is defined as:

$$F = \sqrt{H(\omega) * \hat{J}_2} - \kappa * \frac{s_u^A + s_u^P}{2} = 0 \tag{4.3}$$

The term $H(\omega)$ is used to approximate the Tresca criterion and is defined as:

$$H(\omega) = cos^2(\frac{1}{6}\arccos(1 - 2a_1\omega)) \tag{4.4}$$

With:

$$\omega = \frac{27}{4}\frac{\hat{J}_3^2}{\hat{J}_2^3} \tag{4.5}$$

The model is written by using the undrained shear strength in the Active and Passive regimes. However, undrained triaxial tests generate results for shear strength in compression and extension. While generally the triaxial compression tests correspond to the active regime and extension test correspond to the passive regime, it is possible that some adjustment is necessary to properly calibrate the data to the model. A rounding ratio s_u^C/s_u^A is used, and is set at default to a value of 0.97 (Grimstad et. al., 2012).

Figure 18 shows how undrained strength in passive plane strain is related to undrained strength in triaxial extension due to the influence of the anisotropy ratio s_u^P/s_u^A and the rounding ratio s_u^C/s_u^A.

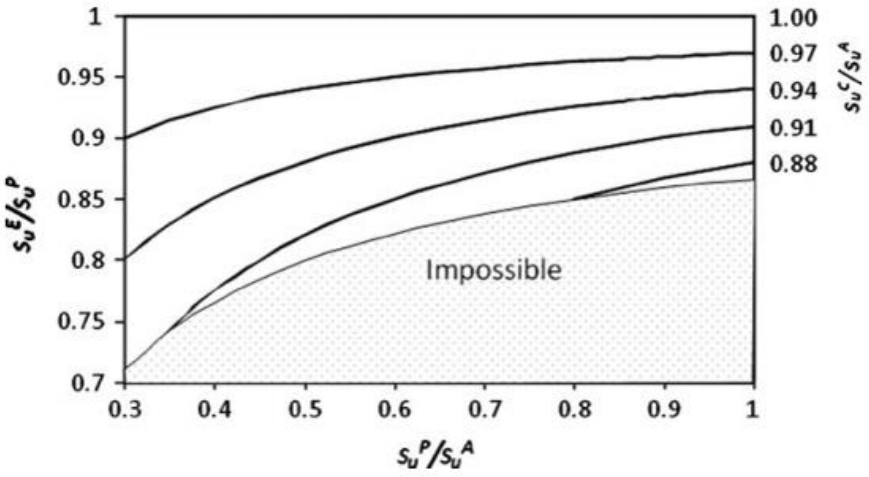

Figure 18. Impact of the rounding ratio and anisotropic strength ratio on the ratio of strength in extension to plane strain passive s_u^E/s_u^P. Figure from Grimstad et. al. (2012).

Figure 19 and Figure 20 show an example from the verification of the model in the publication for a bearing capacity problem. From the figures it can be seen how the stress path influences the shear strength. Of note in this example is that only point F is modelled to be in direct simple shear. In other words, the shear strength across the shearing region or Prandtl zone is variable as the stress regime transitions from Active to Passive.

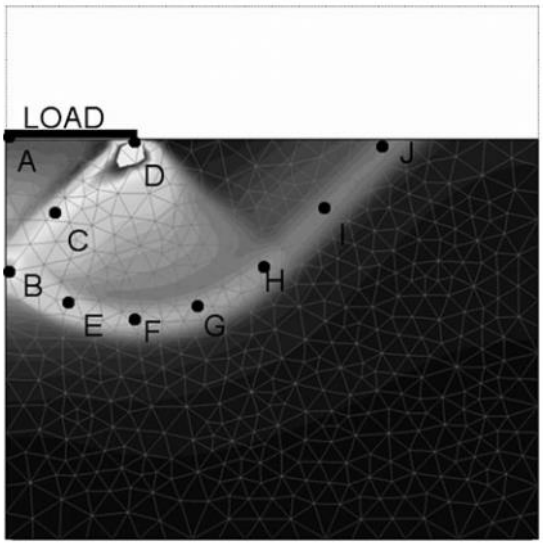

Figure 19. Shear strains at failure. Points are selected to plot the stress path as part of the model verification. From Grimstad et. al. (2012).

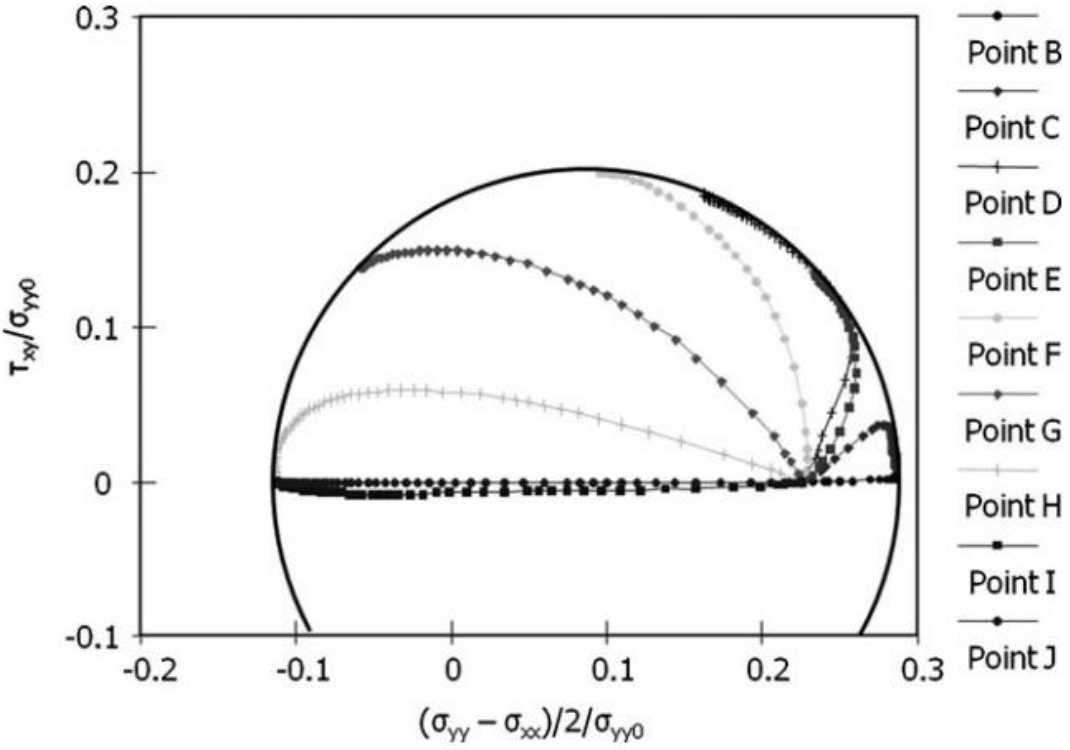

Figure 20. Stress path in plane strain of the selected points. Note that while there are several points within the Prandtl shear zone, final stress in this zone is variable. From Grimstad et. al. (2012).

Chapter 5

The Anisotropic Undrained Shear strength model

The Anisotropic Undrained Shear strength model (AUS) is a total-stress based soil model based on elastoplasticity (Krabbenhøft et. al. 2019). The model is featured in the newly commercially available software Optum CE, in both G2 and G3 versions. This soil model was developed in order to provide a user-friendly platform for modelling the effects of anisotropic soil strength in undrained loading and unloading conditions. As such, one of the key features of the model is the direct input of shear strength parameters from triaxial testing data, as also featured in the NGI-ADP soil model. While the model shares some other notable similarities to the NGI-ADP model, there are some significant differences.

The AUS soil model built as a continuation of the Generalized Tresca Model, also available through Optum (Krabbenhøft et. al. 2019). Or rather, the Generalized Tresca Model describes soil behavior for specific anisotropic soil conditions. The creators of the soil models point out clear distinctions between anisotropy effects due to Lode angle dependency vs physical anisotropy. As previously discussed, an isotropic clay is still expected to have a lower shear strength in a triaxial extension test vs a triaxial compression test. The Generalized Tresca soil model describes this Lode angle dependency for isotropic materials. The yield criterion is utilized in the AUS model, which incorporates physical anisotropy.

The yield criterion for the Generalized Tresca model is as follows. The linearly elastic-perfectly plastic Generalized Tresca model is formulated based on the input of shear strength in triaxial compression s_{uc} and extension s_{ue} (Krabbenhøft et. al. 2019). No shear strength in simple shear is included.

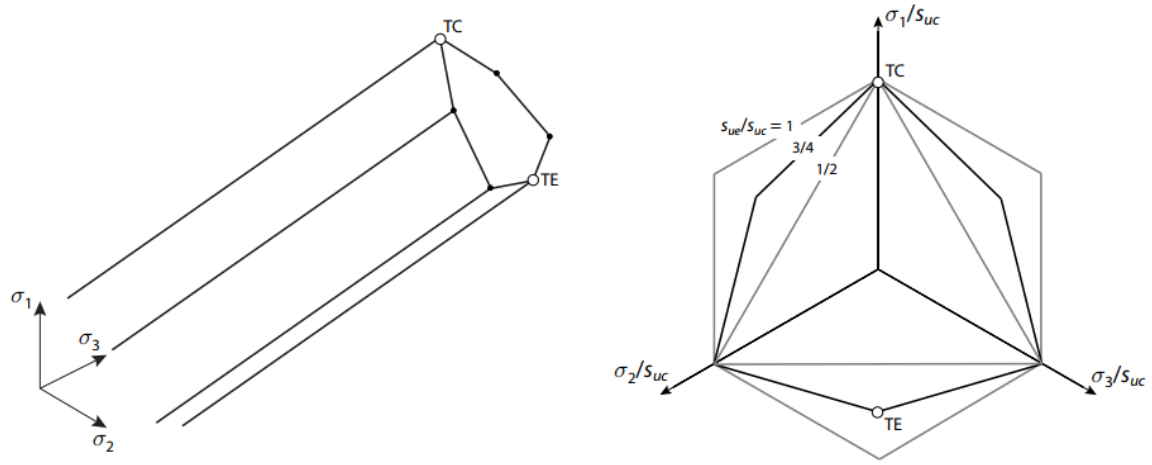

Figure 21. The Generalized Tresca failure surface. TC corresponds to triaxial compression and TE corresponds to triaxial extension. From Krabbenhøft et. al. (2019).

As see in Figure 21, the shape of the failure criterion changes based on the ratio of $^{s_{ue}}/_{s_{uc}}$. When this ratio = 1, this gives a Tresca hexagonal criterion. At $^{s_{ue}}/_{s_{uc}}$ = ¾, the failure criterion closely resembles the Mohr-Coulomb criterion. A ratio of $^{s_{ue}}/_{s_{uc}}$ = ½ gives a triangular criterion. A ratio lower than this results in a non-valid, non-convex failure criterion (Krabbenhøft et. al. 2019).

The AUS soil model differs from the Generalized Tresca model in some distinct manners.

The AUS soil model employs three shear strength parameters:

- s_{uc}: undrained shear strength in triaxial compression test
- s_{ue}: undrained shear strength in triaxial extension test
- s_{us}: undrained shear strength in simple shear test

While the Generalized Tresca model is linearly elastic-perfectly plastic, the AUS model incorporates a hardening yield surface to stipulate the formation of plastic strain before failure (Krabbenhøft et. al. 2019). The AUS model also delineates the effects of Lode angle dependency and physical anisotropy by introducing a shift of the yield surface in a similar manner to that employed by the NGI-ADP model. As with the NGI-ADP model, the AUS model as currently developed assumes cross anisotropy generated by vertical major principal stress only, i.e. the direction of gravity for horizontally deposited clays (Krabbenhøft et. al.

2019). Thus, for natural clay slopes in which the major principal stress is no longer vertical, the use of this soil model is not entirely appropriate.

Failure criterion

With the added parameter of s_{us}, the AUS soil model can be written as (Krabbenhøft et. al. 2019):

$$F_u = \hat{q} - \frac{6k}{\sqrt{3}\left(1 + {}^{1}/_{\rho}\right)\cos\hat{\theta} - 3\left(1 - {}^{1}/_{\rho}\right)\sin\hat{\theta}} \tag{5.1}$$

Where

$$\hat{q} = \sqrt{3\hat{J}_2} \tag{5.2}$$

$$\hat{J}_2 = \frac{1}{2}\hat{\boldsymbol{s}}^{\top}\boldsymbol{D}\hat{\boldsymbol{s}} \tag{5.3}$$

$$\hat{\boldsymbol{s}} = \boldsymbol{\sigma} - \boldsymbol{m}p - ak\boldsymbol{r} \tag{5.4}$$

$$\boldsymbol{m} = (1,1,1,0,0,0)^{\top} \tag{5.5}$$

$$\boldsymbol{D} = \mathrm{diag}(1,1,1,2,2,2) \tag{5.6}$$

$$p = \frac{1}{3}\boldsymbol{m}^{\top}\boldsymbol{\sigma} \tag{5.7}$$

$$r = \left(\tfrac{1}{3}, \tfrac{1}{3}, -\tfrac{2}{3}, 0,0,0\right)^{\top} \tag{5.8}$$

$$\hat{\theta} = \frac{1}{3}\arcsin\left(\frac{3\sqrt{3}}{2}\frac{\hat{J}_3}{\hat{J}_2^{3/2}}\right) \tag{5.9}$$

$$\hat{J}_3 = \hat{s}_{xx}\hat{s}_{yy}\hat{s}_{zz} + 2\hat{s}_{xy}\hat{s}_{yz}\hat{s}_{zx} - \hat{s}_{xy}^2\hat{s}_{zz} - \hat{s}_{yz}^2\hat{s}_{xx} - \hat{s}_{zx}^2\hat{s}_{yy} \tag{5.10}$$

And k, ρ, and a are material parameters that are related to the geometry of the yield criterion. The size of the yield surface is related to k, the shape is controlled by ρ and the shift is related to a. The original Generalized Tresca yield surface for an isotropic material occurs when $k = s_{uc}$, $\rho = s_{ue}/s_{uc}$, and $a = 0$ (Krabbenhøft et. al. 2019). The material parameters k, ρ, and a can be written in terms of the anisotropic undrained shear strengths s_{uc}, s_{ue}, and s_{us} by:

$$k = \frac{1 + s_{ue}/s_{uc}}{1 + \rho}s_{uc} \tag{5.11}$$

$$a = 2\frac{\rho - s_{ue}/s_{uc}}{1 + s_{ue}/s_{uc}} \tag{5.12}$$

$$\rho = \frac{s_{ue} + s_{uc} - s_{us} - \sqrt{(s_{ue} + s_{uc})(s_{ue} + s_{uc} - 2s_{us})}}{s_{us}} \tag{5.13}$$

The influence of the parameter ρ on the shape of the yield function can be seen in Figure 22.

A von Mises flow rule is used, and stipulates that:

$$\dot{\varepsilon}^p = \dot{\lambda}\frac{\partial G}{\partial \boldsymbol{\sigma}} \tag{5.14}$$

Where G is a von Mises type potential given by:

$$G = \hat{q} \tag{5.15}$$

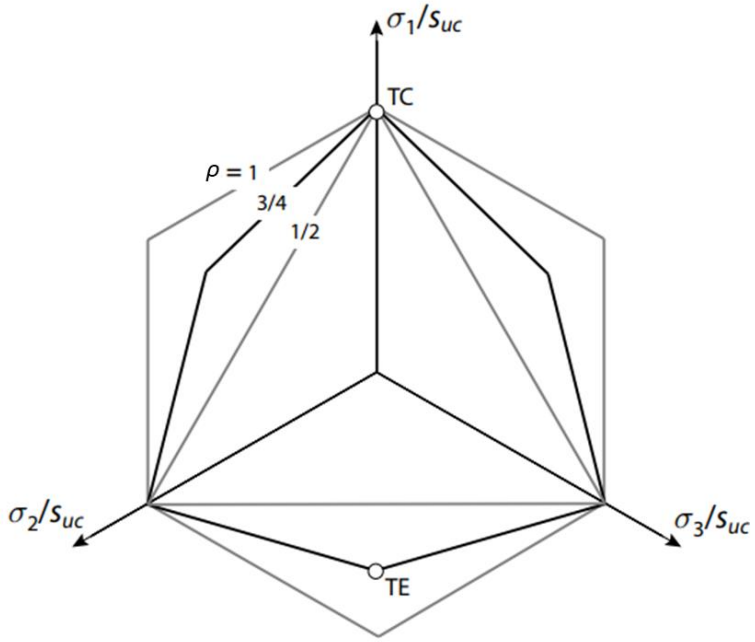

Figure 22. AUS yield criterion in 3D deviatoric stress space where the geometry is controlled by ρ. From Krabbenhøft et. al. (2019).

In other words, a Mises cylinder that is shifted together with the failure surface. This flow potential was chosen by the authors, citing good agreement with observations from true triaxial experiments and previous use in modelling of clays, including Roscoe and Burland (1968) with the Modified Cam Clay model (Krabbenhøft et. al. 2019).

As written, the AUS model has a failure criterion of the same variable shape as the Generalized Tresca model. However, whereas the shape of the Generalized Tresca failure criterion is controlled by s_{ue}/s_{uc}, the AUS model failure criterion shape is controlled by the parameter ρ that is influenced by all three shear strengths (Krabbenhøft et. al. 2019).

In order to keep the yield criterion convex requires that $\frac{1}{2} \leq \rho \leq 1$, meaning that:

$$\frac{4}{9}\left(1+\frac{s_{ue}}{s_{uc}}\right) \leq \frac{s_{us}}{s_{uc}} \leq \frac{1}{2}\left(1+\frac{s_{ue}}{s_{uc}}\right) \tag{5.16}$$

This means that the yield surface is a Tresca criterion when s_{us} is the average of s_{ue} and s_{uc}, and is a triangular (Rankine) criterion when:

$$s_{us} = \frac{4}{9} * (s_{uc} + s_{ue}) \tag{5.17}$$

The admissible parameter range is shown in Figure 23 along with experimental data from Ladd (1991) and Karlsrud and Hernandez-Martinez (2013) which shows Norwegian clays. Note that the ranges seen in experimental results for Norwegian clays extend beyond the limits of admissible anisotropic strength.

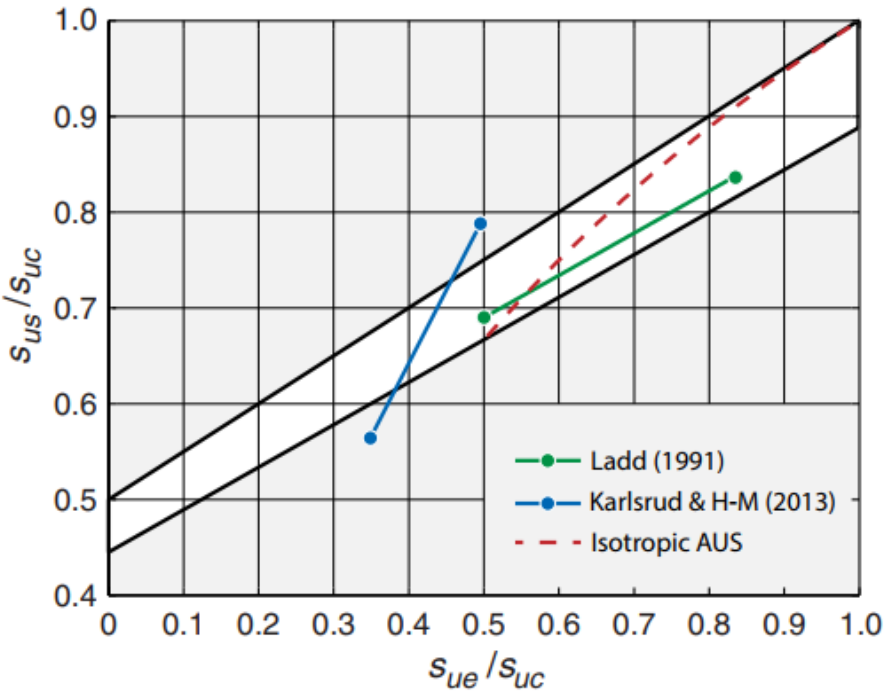

Figure 23. Admissible anisotropic strength ratios for AUS model (white area). The dashed red line shows the anisotropy ratio of the isotropic AUS model. Included are results from Karlsrud & Hernandez-Martinez (2013) and Ladd (1991). From Krabbenhøft et al. (2019).

Plane strain

The yield criterion may be written as the following for the special case of plane strain:

$$F = \sqrt{(\sigma_z - \sigma_x + ak)^2 + 4\tau_{zx}^2} - \frac{4\rho}{1+\rho}k \tag{5.18}$$

When $s_{ue} = s_{uc} = s_{us} = s_u$ the soil is isotropic and exhibits no Lode angle dependency, this results in a standard Tresca yield function (Krabbenhøft et. al. 2019). This set of conditions would correspond to $a = 0\ (no\ shift),\ \rho = 1\ (Tresca\ shape),\ k = s_u\ (size\ deterimined\ by\ shear\ strength)$.

When the soil parameters are assumed to represent isotropic soils that exhibit Lode angle dependency $[s_{us} = 2s_{ue}s_{uc}/(s_{ue} + s_{uc})]$, this gives $a = 0,\ \rho = s_{ue}/s_{uc},\ k = s_{uc}$, allowing the yield function to be written as:

$$F = \sqrt{(\sigma_z - \sigma_x)^2 + 4\tau_{zx}^2} - 2s_{us} \tag{5.19}$$

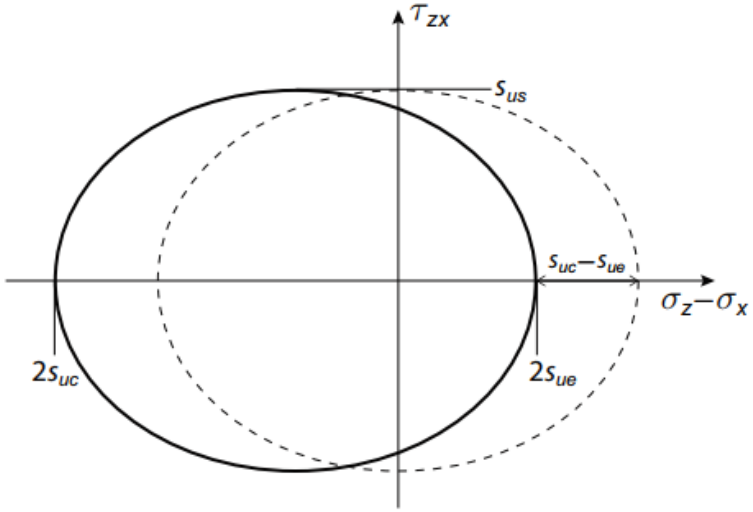

Figure 24. Plane strain illustration of the AUS yield surface for $s_{us} = \frac{1}{2}(s_{uE} + s_{uC})$ with compression giving negative stress. From Krabbenhøft et. al. (2019).

In the special case that $s_{us} = \frac{1}{2}(s_{ue} + s_{uc})$ corresponding to the upper limit of strength ratios along which the yield surface is a Tresca criterion, the yield function in plane strain can be written:

$$F = \sqrt{(\sigma_z - \sigma_x + s_{uc} - s_{ue})^2 + 4\tau_{zx}^2} - 2s_{us} \tag{5.20}$$

This yield surface in plane strain can be visualized in Figure 24 by an ellipse of magnitude with axes $s_{ue} + s_{uc}$ and s_{us} shifted by an amount $s_{uc} - s_{ue}$ along the $(\sigma_z - \sigma_x)$-axis (Krabbenhøft et. al. 2019).

Hardening Rule

The AUS soil model employs a hardening rule to allow for some deformation before failure. A hardening variable κ is introduced:

$$F_u = \hat{q} - \frac{6\kappa}{\sqrt{3}\left(1 + {}^{1}/_{\rho}\right)\cos\hat{\theta} - 3\left(1 - {}^{1}/_{\rho}\right)\sin\hat{\theta}} \tag{5.21}$$

The hardening variable κ varies from some initial value κ_0 such that the initial stress state $\boldsymbol{\sigma}_0$ satisfies $F(\boldsymbol{\sigma}_0, \kappa_0) = 0$ to an ultimate value of $\kappa = k$. This results in the generation of a family of affine surfaces for each value of κ between $\kappa = \kappa_0$ and $\kappa = k$, meaning that the soil undergoes isotropic hardening, as shown in Figure 25. For monotonic loading the type of hardening does not create significant impacts. However, when modelling cyclic loading, it is much more important to carefully consider the type of hardening. A more complete description of the hardening law is presented in Krabbenhøft et al. (2019).

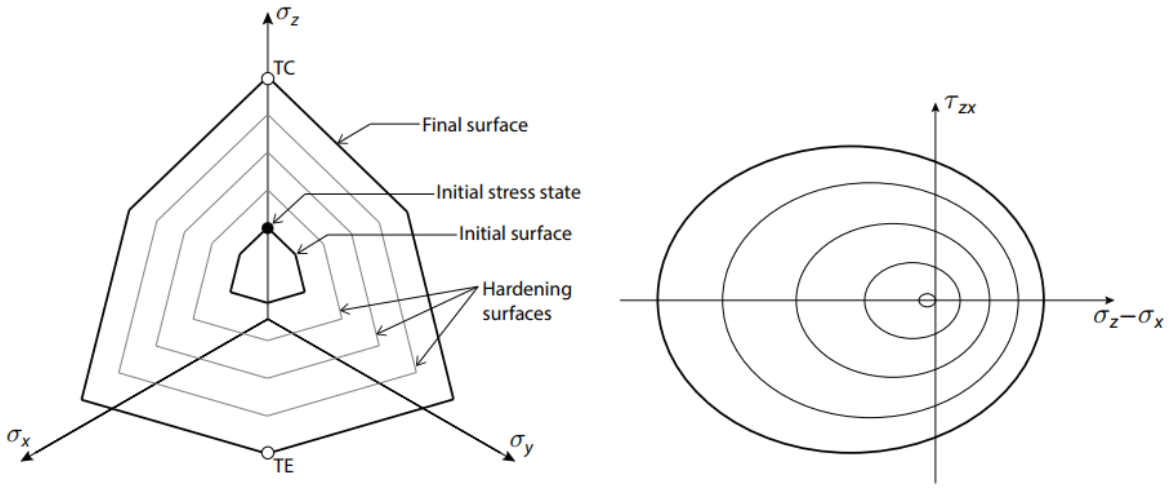

Figure 25. Hardening surface for the AUS model in the pi-plane (left) and plane strain (right). Taken from Krabbenhøft et. al. (2019).

Two parameters related to the axial strain at half the failure stress, in both triaxial compression and extension tests, are used in describing the behavior of the yield surface. Like the undrained shear strengths, these parameters can be inferred directly from laboratory data, allowing for straightforward calibration of the model.

Elasticity

Isotropic elasticity is employed to relate elastic strains to total stresses. Assuming linear elasticity:

$$\varepsilon^e = \mathbb{C}_u \boldsymbol{\sigma} \tag{5.22}$$

where the undrained elastic compliance modulus is given by:

$$\mathbb{C}_u = \frac{1}{3G_0}\begin{bmatrix} 1 & -\frac{1}{2} & -\frac{1}{2} & & & \\ -\frac{1}{2} & 1 & & & & \\ -\frac{1}{2} & -\frac{1}{2} & 1 & & & \\ & & & 3 & & \\ & & & & 3 & \\ & & & & & 3 \end{bmatrix} \tag{5.23}$$

With G_0 = shear modulus and $3G_0 = E_u$ undrained Young's modulus (Krabbenhøft et. al., 2019).

While the use of isotropic elasticity for modelling materials that behave anisotropically may be inappropriate, the authors point out that elasticity is not expected to play a prominent role in most problems of practical interest. Using isotropic elasticity is much simpler and is another reason that this method was chosen (Krabbenhøft et. al. 2019).

Chapter 6

Direct comparison of PLAXIS to Optum

Before the NGI-ADP soil model can be compared to the AUS soil model, it must first be determined if the two geotechnical FEM programs give identical solutions when using identical soil models. It is possible that differences in the two operating programs, such as meshing effects or similar program mechanics, may systemically influence generated solutions that would need to be adjusted for when comparing the AUS and NGI-ADP soil models. By directly comparing the two FEM programs, it is then possible to distinguish between program differences and soil model differences. As such, a parametric study was undertaken to test for significant differences in solution from the two programs. This was done by running FoS analyses of idealized simple slopes for undrained conditions in both programs using strength reduction. A Tresca soil model was chosen in Optum, while Undrained (C)- corresponding to the Tresca soil model- was used in PLAXIS.

Analysis shows that PLAXIS and Optum can be directly compared with the need for relative adjustment of the solutions. It is demonstrated that provided adequate mesh density, the two programs generate solutions with less than 1% difference in value.

Factors included in the parametric study include:

- Slope height
- Slope angle
- Shear strength
- Shear strength profile
- Unit weight
- Number of elements
- Type of element solution

A base case scenario was created. The base case was a clay slope with height 15 m, s_u = 30 kPa, unit weight $\gamma = 18\,kN/m^2$. A full table of parameters is available in the Appendix.

Optum has the option for Adaptive Meshing, which results in the mesh around the failure surface to become finer through iterations. It has been previously shown (Steigerwald, 2020) that the employment of Adaptive Meshing can have significant effect on the generated FoS, more so than number of elements or number of iterations. This is considered to be a mesh effect, as the meshing mechanism has an effect on the solution independent of the soil model. The solver presets were left on their default settings for both programs. For Optum, this included the Maximum Iterations which is set to a default setting of 200 iterations, though in an analysis a solution satisfying the tolerance criteria is typically generated after roughly 10 iterations. It has previously been shown (Steigerwald, 2020) that effects of Adaptive Meshing become less severe as the (non-adaptive) mesh becomes increasingly dense. In other words, adequate mesh density is necessary for solution robustness.

While the Optum software allows the number of mesh elements to be input directly, PLAXIS generates mesh based on choosing from options ranging from Very Coarse to Very Fine. There are also options to refine or coarsen broad or distinct regions of the mesh. This quickly allows for the generation of a mesh for what may be considered appropriate based on the PLAXIS coding, though for direct comparisons of two different programs, may not be very convenient. In the direct comparison, five mesh refinements were tested to explore the effects of mesh refinement between the two programs. Mesh densities ranging from Medium to refined Very Fine meshes were created and tested first in PLAXIS. The number of elements was recorded and directly input into Optum to directly compare the two programs.

Optum features several types of element solutions to choose from. The default element solutions in Optum G2 are Upper and Lower solutions, which generate solutions based on the classical theory of rigid plasticity, with the upper boundary corresponding to the kinematic solution and the lower boundary corresponding to the static equilibrium solution (Krabbenhøft et al., 2016). In the initial analysis, an average value was computed by running an analysis with both Upper and Lower solutions and taking the average value. This method is shown to generate less than 1% difference to the analysis by PLAXIS, in which 15 noded Gaussian elements were utilized, when sufficient mesh density is applied. Later the 15 noded Gaussian solution was analyzed in Optum, as it allows for a more direct comparison between PLAXIS

and Optum. It is shown that this method allows for the direct comparison between the two programs.

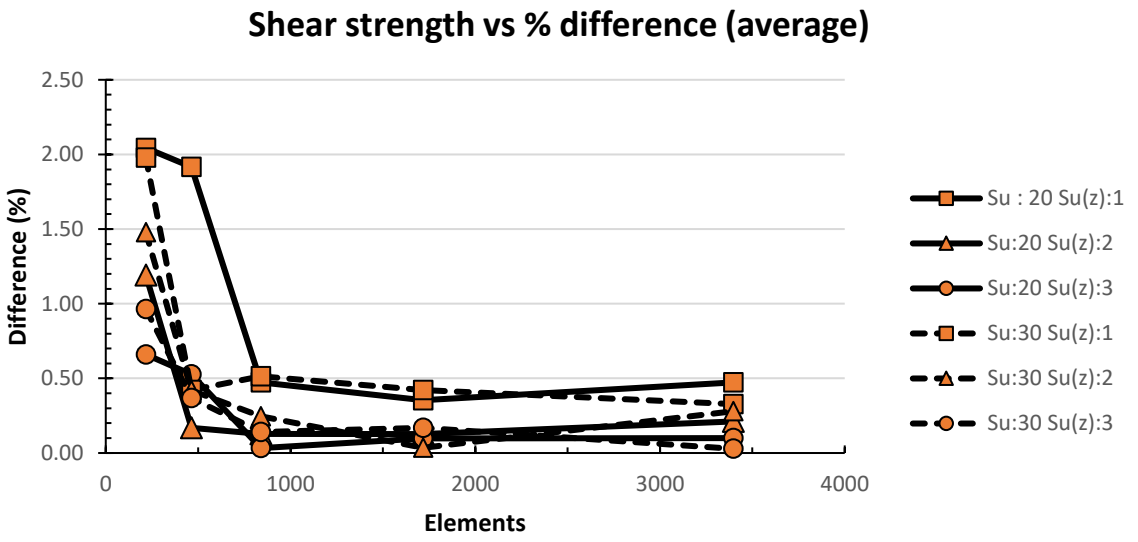

Figure 26. Shear strength profile vs model agreement. Taken from the average of Upper and Lower bound solutions from Optum.

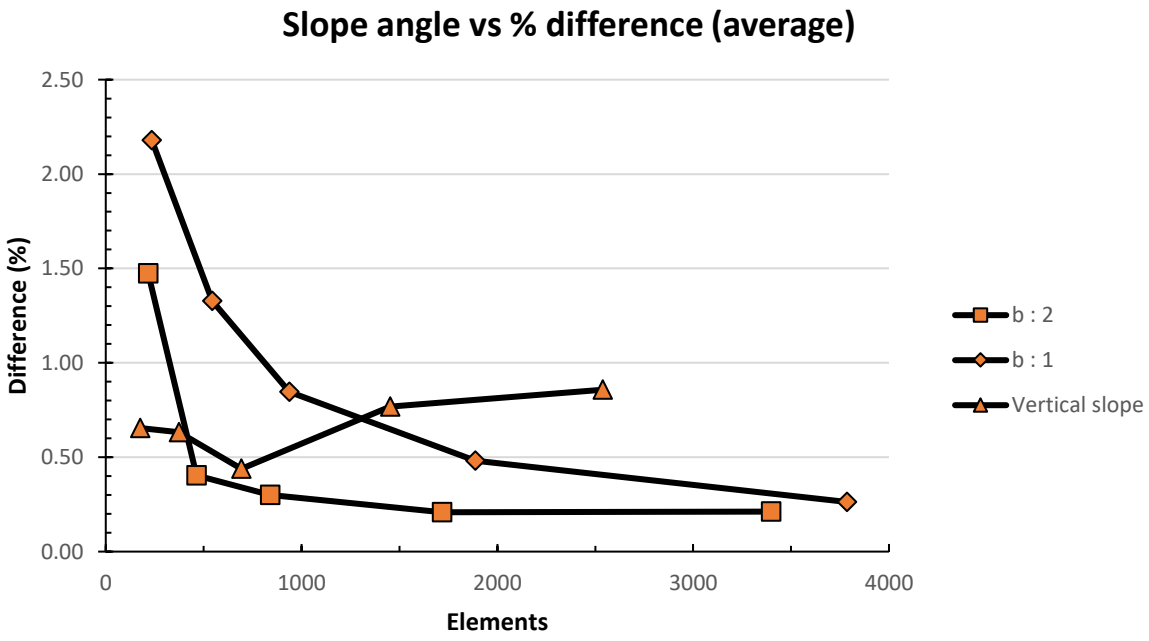

Figure 27. Effect of slope angle on model agreement. Taken for the averages of Upper and Lower bound solutions from Optum.

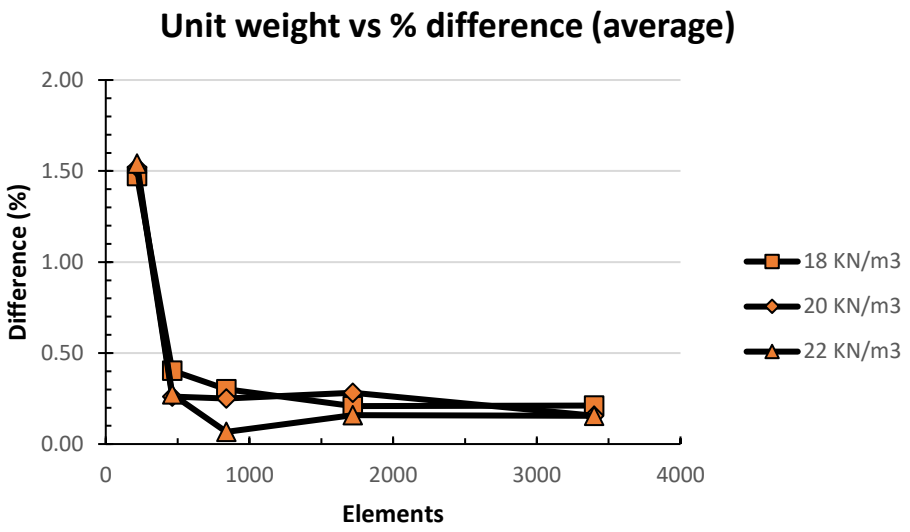

Figure 28. Effect of unit weigth on model agreement. Taken from the average of Upper and Lower bound solutions for Optum.

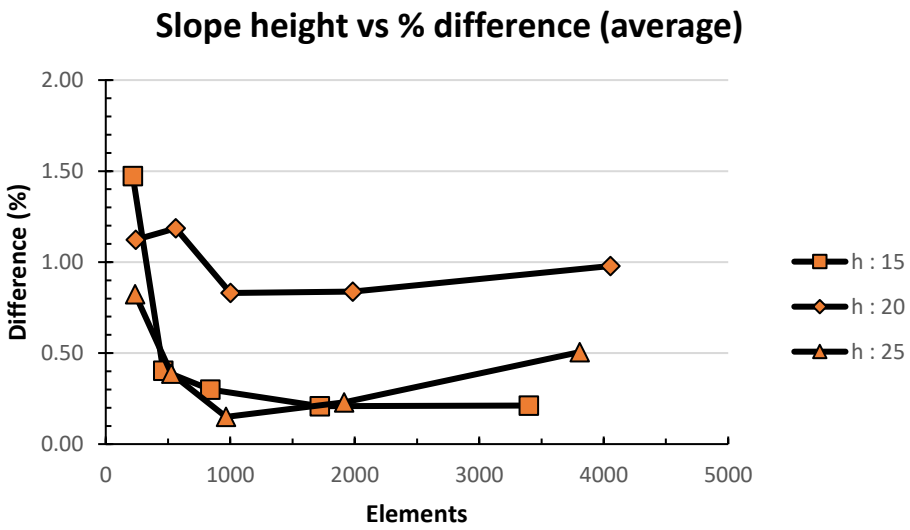

Figure 29. Effect of slope height on model agreement. Taken from the average of Upper and Lower bound solutions for Optum.

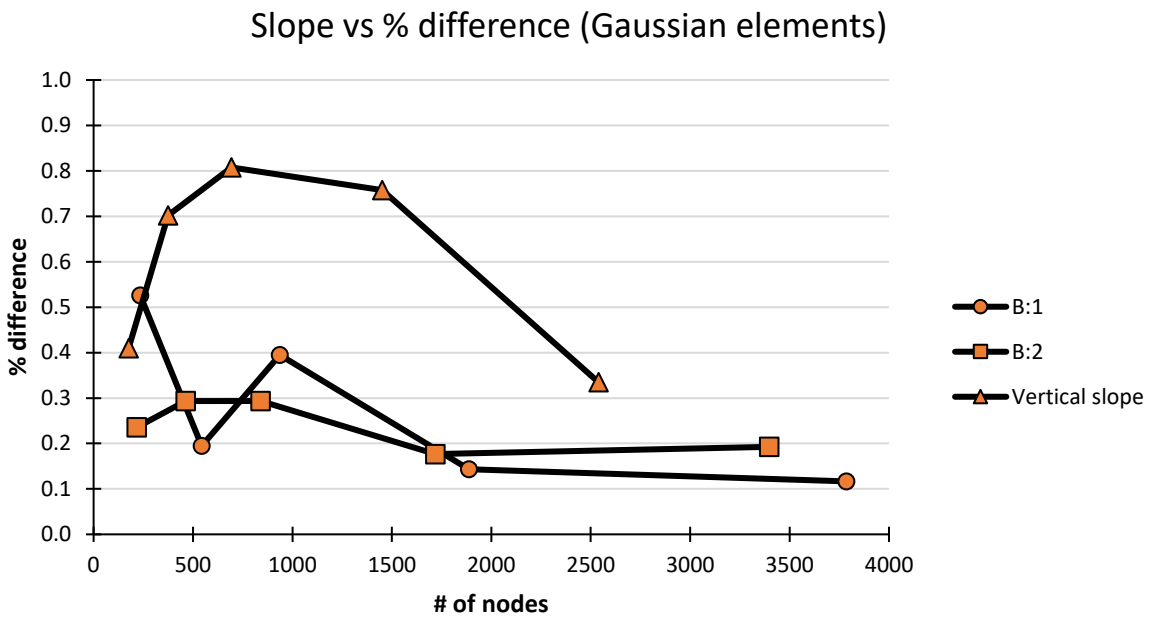

Figure 30. Effect of slope angle on model agreement using Gaussian elements in both models.

As seen in Figure 26-30, utilizing adequate mesh density results in solutions of less than 1% difference. Use of Gaussian nodes in the Optum program generated especially good agreement with PLAXIS. After analysis it was determined that sufficient mesh density for Optum was set to a standard 1000 mesh elements, while PLAXIS required Fine mesh density as it was seen that the FoS solution generated by PLAXIS was not significantly affected by denser mesh refinement above this setting.

Chapter 7

Results

The NGI-ADP and AUS soil models were directly compared using idealized simple slopes consisting of homogenous undrained anisotropic clays. Several parameters were tested to explore if they significantly impacted model agreement. These parameters included: Shear strength profile, slope angle, and the anisotropy factors s_{uDSS} and s_{uE}. A FoS was calculated using a strength reduction analysis.

The NGI-ADP and AUS soil models require anisotropic strengths to be directly input. However, there is a slight difference between the two programs regarding the relationship between triaxial shear strength and plane strain shear strength. AUS uses the parameters s_{uc} and s_{ue} for the shear strengths in triaxial compression and extension tests, respectively. The NGI-ADP model is formulated using the shear strength in plane strain, s_{uA} and s_{uP}, and these values are directly input into the model. To convert the measured shear strength in triaxial tests to plain strain, the NGI-ADP model uses a conversion ratio that can be specified by the user, as triaxial conditions are approximate to, but not precisely equal to plane strain conditions. The current default setting $\frac{s_u^C}{s_u^A} = 0.99$ was used.

Given that the NGI-ADP model uses plain strain anisotropic strengths that are nearly equivalent to triaxial strengths, which are kept constant by a fixed ratio input parameter, and in consideration that the AUS model only features the option for the input of the triaxial anisotropic strengths, it is then decided to focus on the impact of the variation of the triaxial anisotropic strengths. Parameters are denoted as such:

- s_{uC} – shear strength in triaxial compression
- s_{uE} – shear strength in triaxial extension

- s_{uDSS} – shear strength in direct simple shear test

Range of admissible anisotropic strengths

The AUS and NGI-ADP soil models have different stipulations for acceptable values of s_{uDSS} and s_{uE}. The NGI-ADP model incorporates a wider range of values and is limited by $s_{uDSS} \geq s_{uE}$ with the default s_{uC}/s_{uA} rounding ratio. The AUS model has a more restricted range of admissible of s_{uDSS} and s_{uE} values. This is in part due to the definition of the failure criterion, which has the same variable shape in 3D stress space as the Generalized Tresca failure criterion. The model is valid when:

$$\frac{1}{2} \leq \rho \leq 1 \tag{7.1}$$

The admissible range for anisotropic strength parameters in the AUS model, as previously discussed, is then:

$$\frac{4}{9}\left(1 + \frac{s_{ue}}{s_{uc}}\right) \leq \frac{s_{uDSS}}{s_{uc}} \leq \frac{1}{2}\left(1 + \frac{s_{ue}}{s_{uc}}\right) \tag{7.2}$$

Or, when rewritten can be expressed as:

$$\frac{4}{9}(s_{uE} + s_{uC}) \leq s_{uDSS} \leq \frac{1}{2}(s_{uE} + s_{uC}) \tag{7.3}$$

Figure 31 shows the admissible ranges for the two models. A set of anisotropy parameters that satisfy the admissible ranges for both models was selected. Data points can be roughly divided along three trend lines that describe where they fall relative to the AUS range of admissibility as a function of s_{uE} and s_{uDSS}: Top, middle, and bottom boundary lines. Note that 2 data points lie along the NGI-ADP admissible boundary and do not truly lie along the same function of s_{uDSS}/s_{uE} as the other data points of the Middle or Bottom data lines, but are likewise included. Test parameters are shown in Table 2. Over 550 simulations were performed.

Table 2. Test parameters.

Parameters	
Slope Height H	10 m
Undrained shear strength s_{uC}	40 kPa
Shear strength increase with depth s_u^{inc}	1, 2, 3 kPa/m
Unit weight γ	20 kN/m^3
Slope angle β	15°, 30°, 45°, 60°, 75°, 90°
s_{uDSS}/s_{uC}	s_{uE}/s_{uC}
0.45	0
0.55	0.1
0.55	0.1647
0.55	0.2375
0.65	0.3
0.65	0.3765
0.65	0.4625
0.75	0.5
0.75	0.5882
0.75	0.6875
0.85	0.7
0.85	0.8
0.85	0.85
0.95	0.9
0.95	0.95

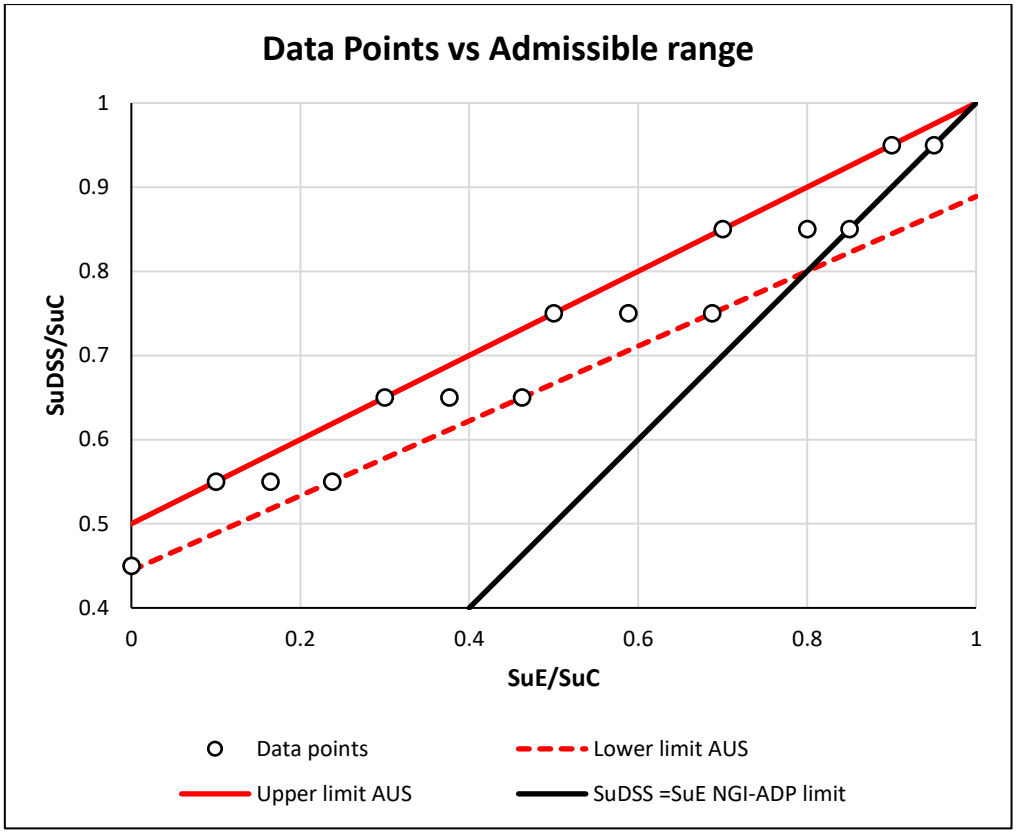

Figure 31. Data points and admissible anisotropic strength ratios of both models. Strength ratios on and to the left of the black line are valid for the NGI-ADP model, while the boundaries of the AUS model are shown in red.

Results

Figure 32 qualitatively shows that for one case tested, agreement between the two models is highest along the upper limits of AUS anisotropy admissibility. As the s_{uDSS} and s_{uE} values approach the lower limit of AUS admissibility, the difference in solution generated by the two programs becomes greater. This figure shows the results for one example that is consistent with all other findings. The bubble chart shows the percent difference relative to the NGI-ADP solution by the size of the bubbles (negative difference illustrated by colorless bubbles). This is a convenient way to show this result as it allows for a qualitative illustration of model agreement while plotting directly along the admissible range of strength anisotropy factors in order to clearly illustrate important trends.

In the analysis that follows, the percent difference of the AUS FoS solution relative to the NGI-ADP solution is presented. This is not to imply that the NGI-ADP soil model necessarily generates the most accurate solution, but was chosen with consideration that the NGI-ADP soil model is well established and is used in standard Norwegian practice. Examining the newer

AUS soil model with respect to the more well-known model may serve as a more optimal context for those familiar with NGI-ADP. This method, rather than calculating the absolute percent difference between the two models, also serves to show if the AUS model consistently gives higher or lower solutions than the NGI-ADP model.

As shown in Figure 32, the AUS soil model generated lower FoS solutions than the NGI-ADP model.

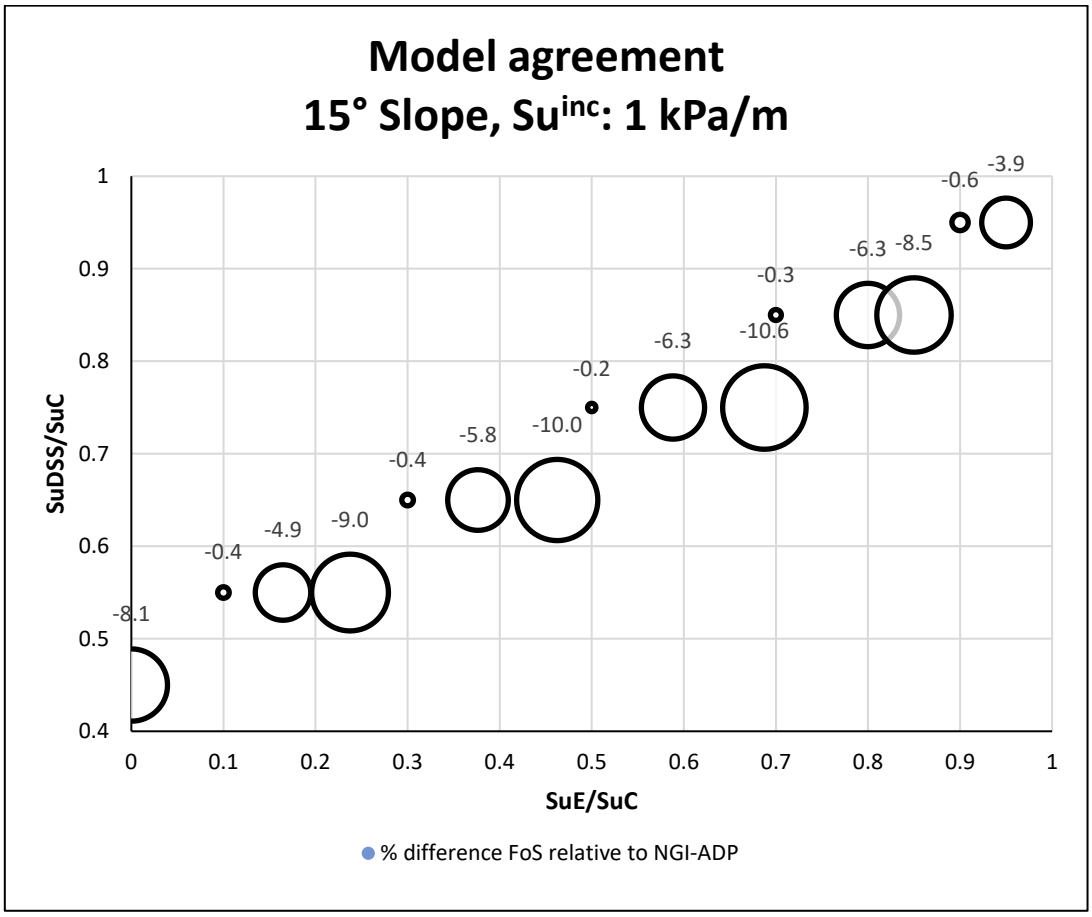

Figure 32. Bubble chart showing FoS percent difference relative to NGI-ADP for slope angle 15° vs anisotropic strength parameters. Values are listed above corresponding bubbles.

From the figure above it is clear that data points along the upper anisotropy boundary give the highest agreement between the two models. It is also quickly seen that the data can be roughly grouped in three distinctions based on the relationship of the anisotropic strength ratios. Data points are grouped according to the Top, Middle (Mid), and Bottom boundary lines of the AUS range of admissibility, as seen in Figure 33. This allows for the results to be shown in a

meaningful way to display trends while simultaneously roughly describing the relationship of the anisotropic strength ratios.

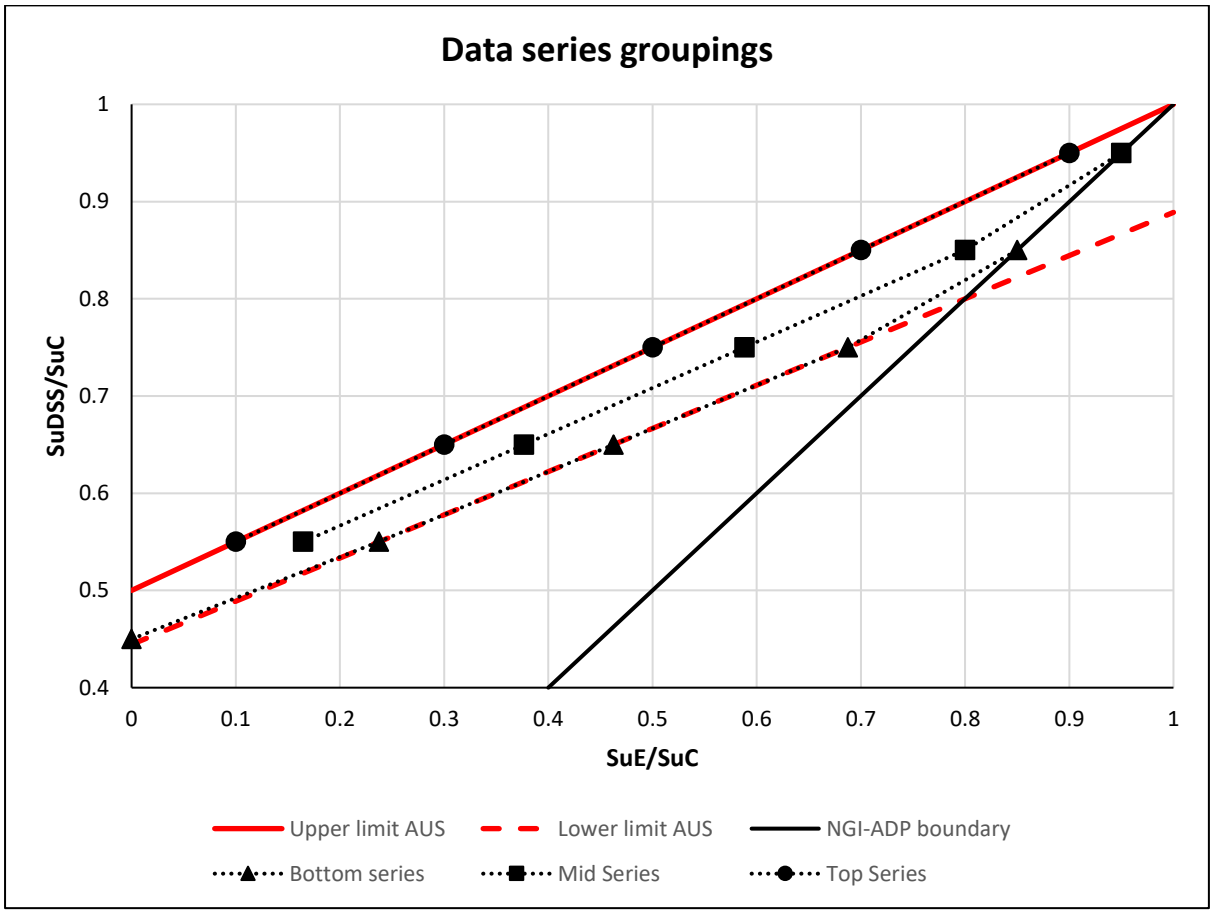

Figure 33. Grouping of data series after initial analysis based on direct simple shear strength to extension strength ratio.

Analysis reveals slope angle also had significant effects on the agreement of the solution generated by the two programs. Steeper slopes resulted in greater divergence between AUS and NGI-ADP. More specifically, steeper slopes resulted in a lower FoS predicted by AUS relative to NGI-ADP. However, the effect of slope angle is not independent of the strength anisotropy parameters. That is to say, along the upper limit of AUS admissibility, there is no influence of slope angle as all models along this range generated FoS solutions separated by less than 1% difference. Results are shown in the following figures.

Figure 34 again shows three distinct groupings: Top, Mid and Bottom. Note the apparent upward trend at the upper limits of the Mid and Bottom trend lines. It must here be noted the shifted position of these points in order to accommodate the restrictions of the NGI-ADP

model; these points do not truly sit along the Middle and Bottom boundaries. Shear strength profile had no apparent effect on the agreement between the two models.

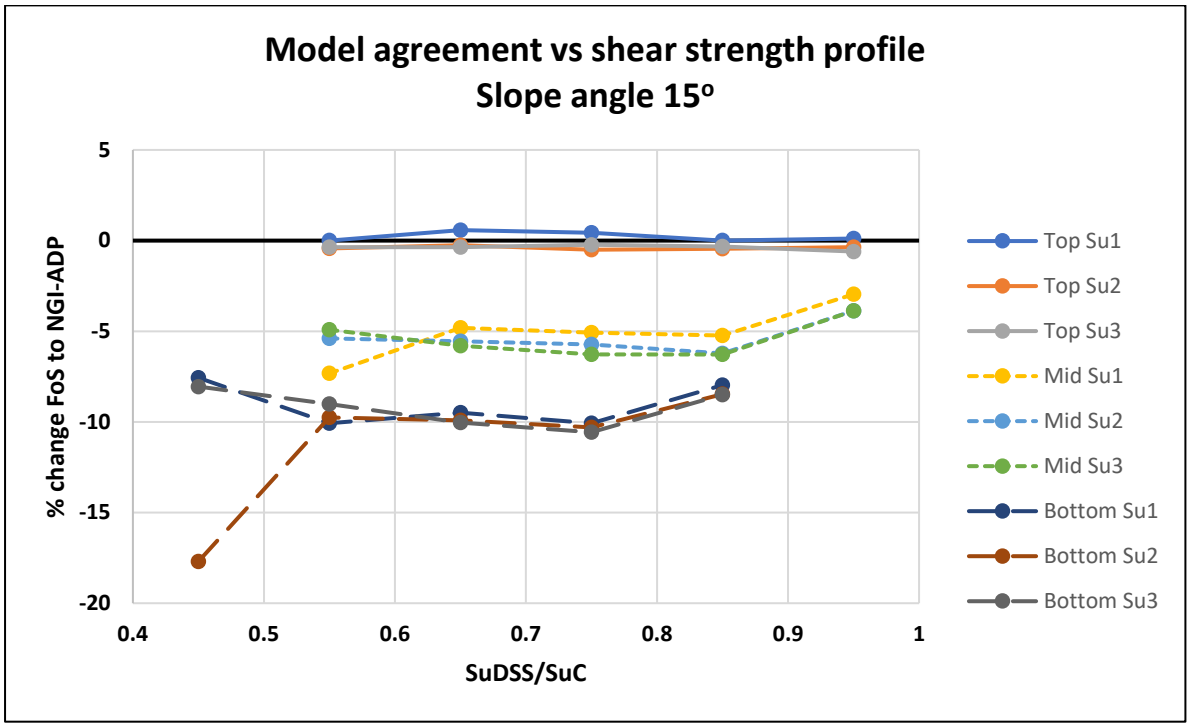

Figure 34. Model agreement for 15° slope for different profiles of increasing shear strength with depth. Data series are labled with shear strength increase with depth. Su1 corresponds to an increase of 1 kPa/m.

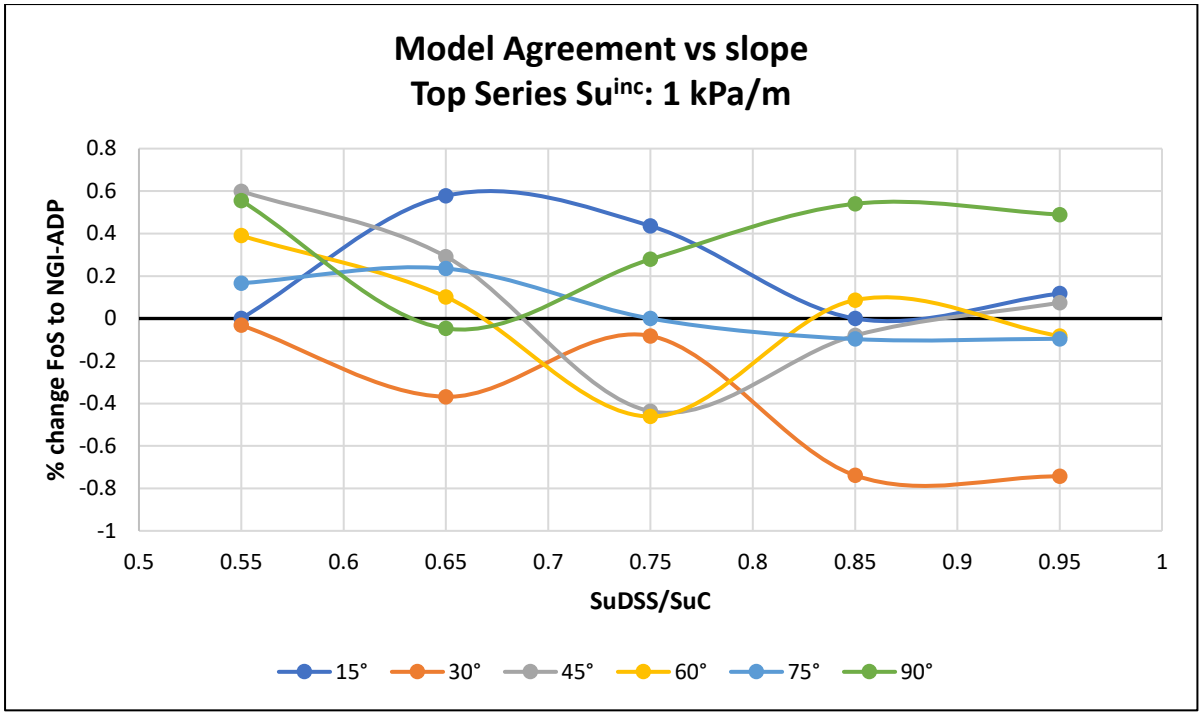

Figure 35. Model agreement versus slope angle for ρ=0,5.

Figure 35 shows model agreement versus slope angle for the Top range of strength anisotropy. It clearly illustrates that along this boundary, the two models give statistically identical solutions (percent difference less than 1% relative to NGI-ADP). No clear trends resulting from slope angle are visible. No clear trends resulting from the magnitude of anisotropic strength parameters are visible.

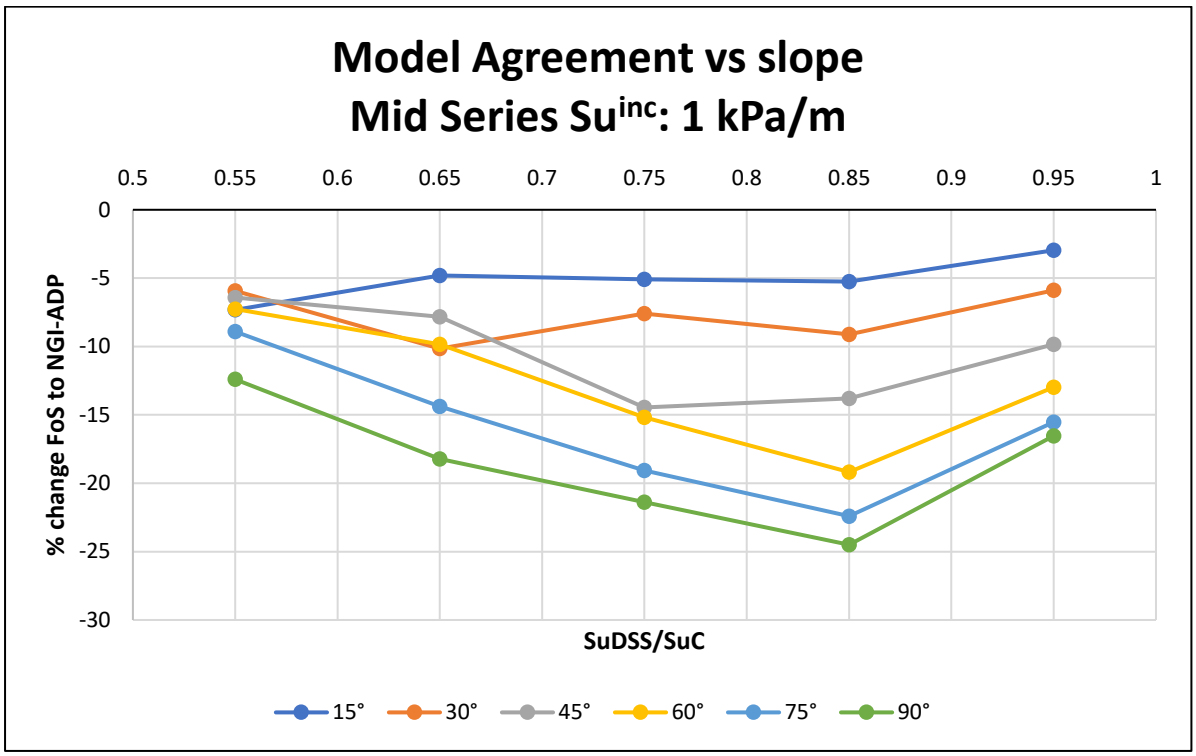

Figure 36. Model agreement vs slope angle for the 'Middle' anisotropy data grouping.

Figure 36 shows the effect of slope angle on the calculated FoS for the Middle range of anisotropy. Several interesting trends are clearly visible. The first observation is that the calculated FoS generated by the AUS soil model is lower than the NGI-ADP solution. Secondly, there is an obvious influence of slope angle. The figure clearly shows that increasing slope angle results in greater differences between the two programs. In other words, slope steepness is directly related to underestimation of the FoS by the AUS soil model relative to the NGI-ADP model. Thirdly, remembering that the point at $s_{uDSS}/s_{uC} = 0{,}95$ is skewed, for slopes 45° and steeper, the increasing magnitude of the s_{uDSS} and s_{ue} anisotropy factors results in greater difference, or greater underestimation of the FoS by the AUS model. Additional figures are available in the Appendix.

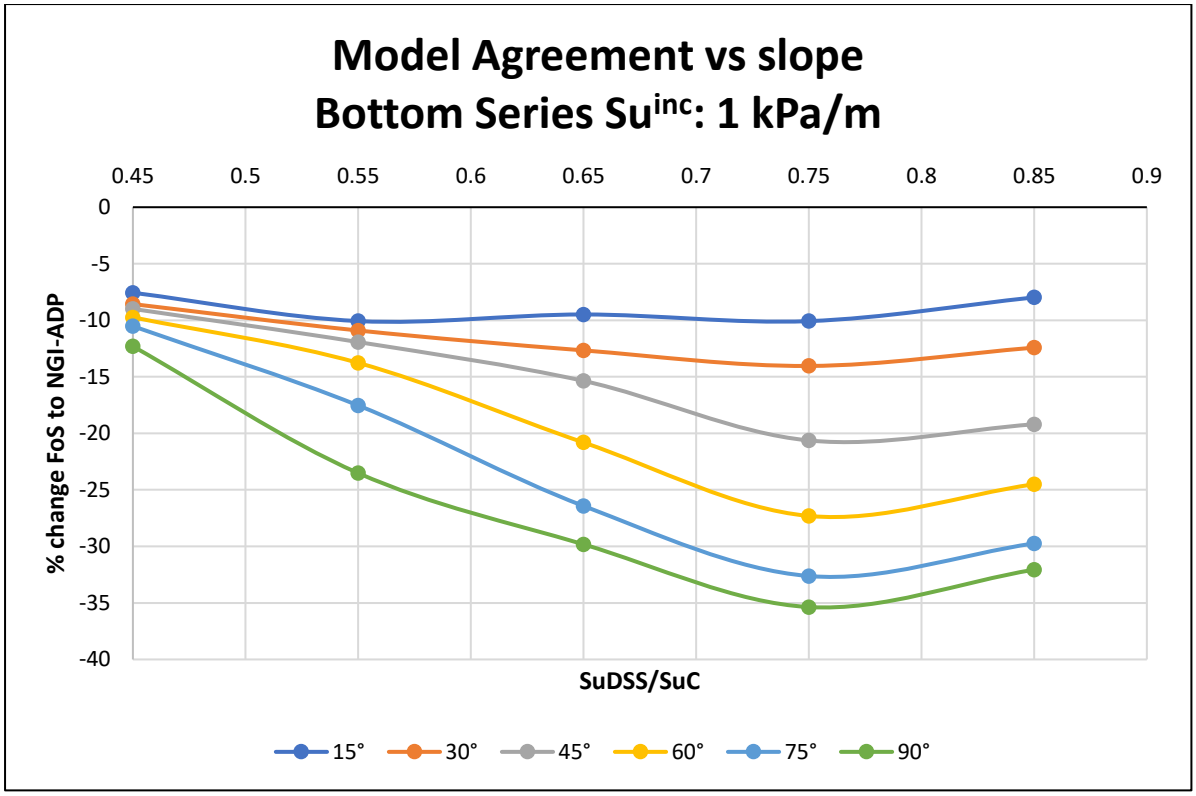

Figure 37. Model agreement vs slope angle for the bottom boundary anisotropic strength ratios.

Figure 37 shows the effect of slope angle on the calculated FoS for the Bottom range of anisotropy. The trends visible in this figure are consistent with those previously presented. The AUS soil model generates lower FoS solution in all illustrated scenarios. Increasing slope angle is directly related to underestimation of the FoS by the AUS soil model relative to the NGI-ADP model. For slopes 30° and steeper, the increasing magnitude of the s_{uDSS} and s_{ue} anisotropy factors results in greater difference, or a lower FoS solution by the AUS model. The AUS soil model is shown to generate a FoS up to 35% lower than the solution generated by the NGI-ADP model. It should be noted that the data points for $^{s_{uDSS}}/_{s_{uC}} = 0{,}45$ correspond to $s_{uE} = 0$, which is not expected in real soil behavior. However, as this is admissible in both soil programs, it was included. This anisotropic strength ratio shows the highest agreement between the two models along the lower boundary of admissible anisotropic strengths, but, does not necessarily generate reliable solutions given that complete lack of shear strength in extension is unrealistic. Quick clays are of course characterized by a nearly complete absence of shear strength when deformed, but the reader is reminded that neither soil model incorporates strain softening behavior.

The FoS in the case of the 15° slope with increasing shear strength with depth of 1 kPa/m can be seen in Figure 38. It is quickly noted that the for the NGI-ADP model, transitioning from the top boundary to bottom boundary gives higher FoS solutions, while for the AUS model this gives lower FoS values.

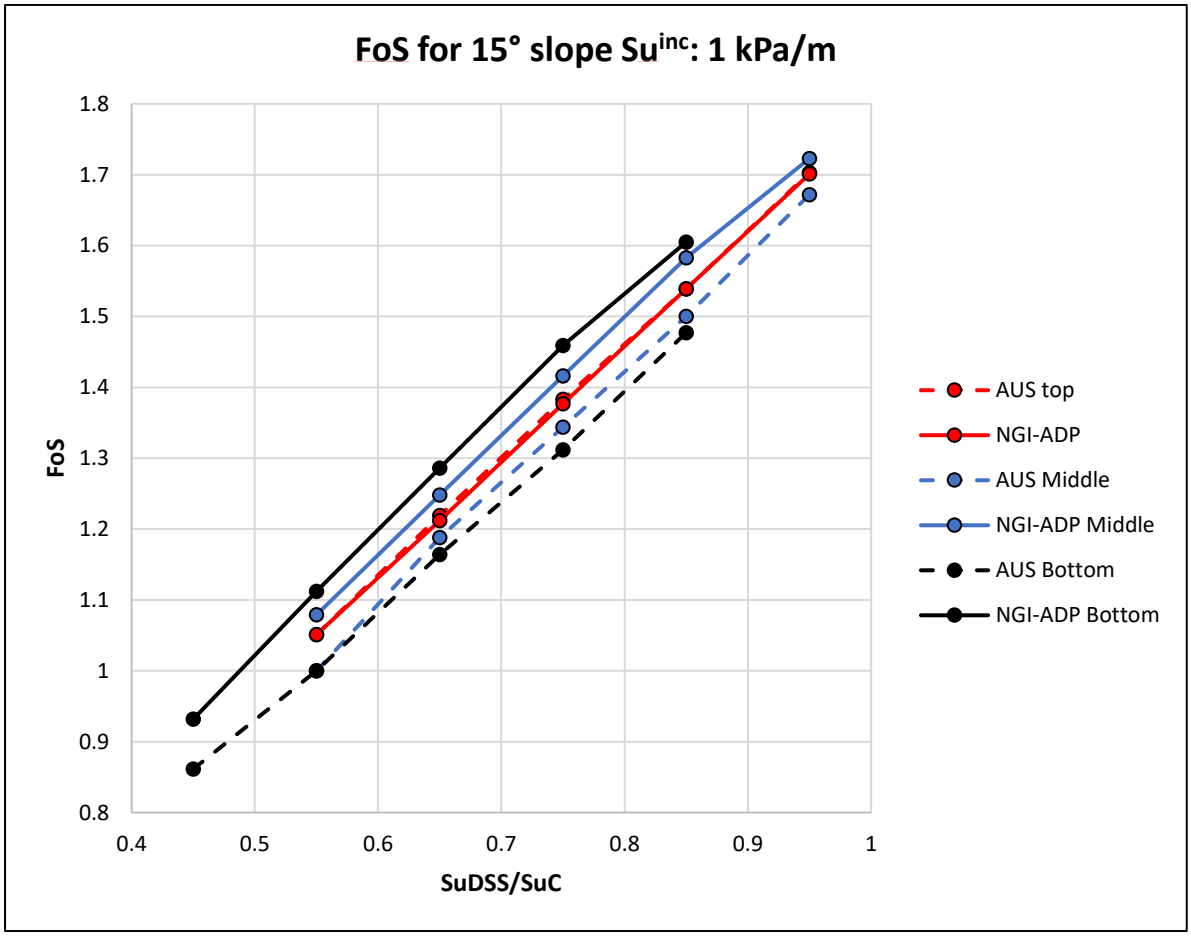

Figure 38. Factor of Safety solution for 15° slope.

The case of the vertical slope can be seen in Figure 39. As a consequence of the chosen shear strength parameters used in this study, several simulations of the slope resulted in FoS less than 1.0, indicating failure. To verify the validity of these results, undrained shear strength was increased to 70 kPa + 3 kPa/m for the case of the vertical slope to give solutions with FoS ≥1. These results are shown in Figure 40 and Figure 41.

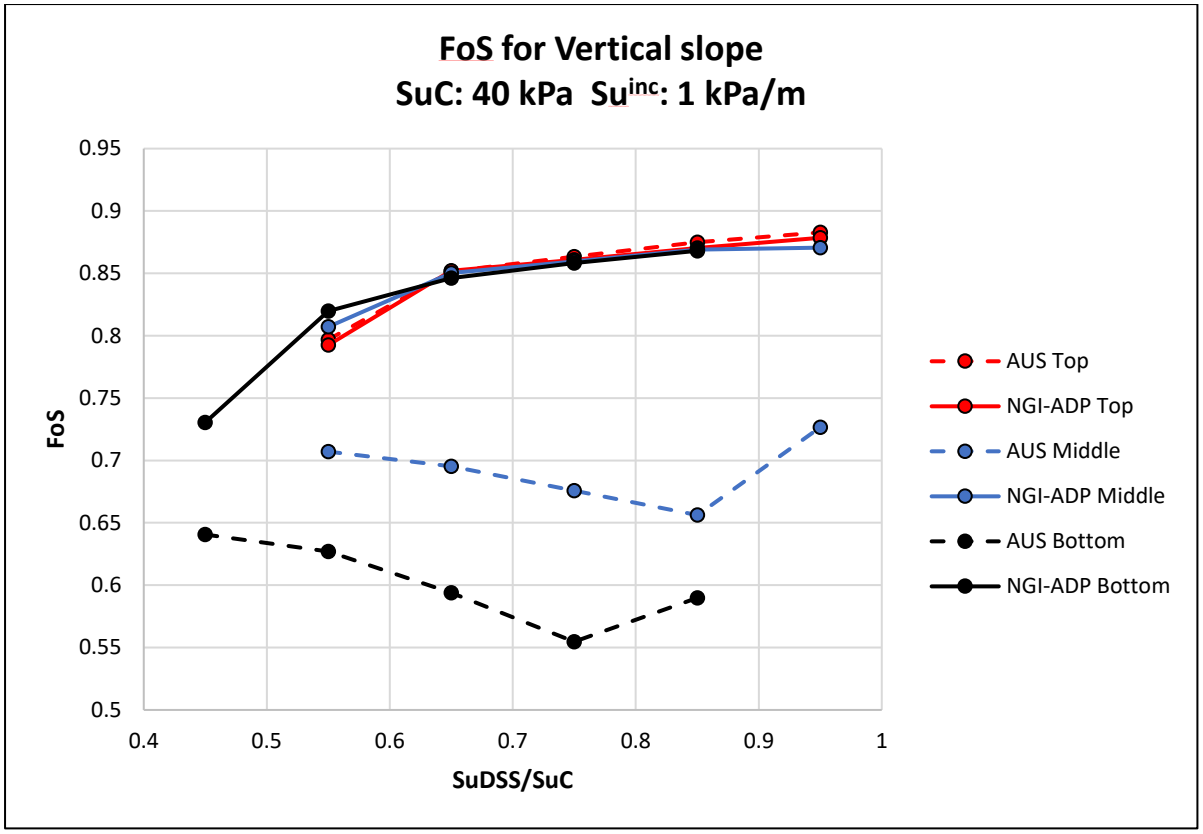

Figure 39. Factor of Safety solution for vertical slope.

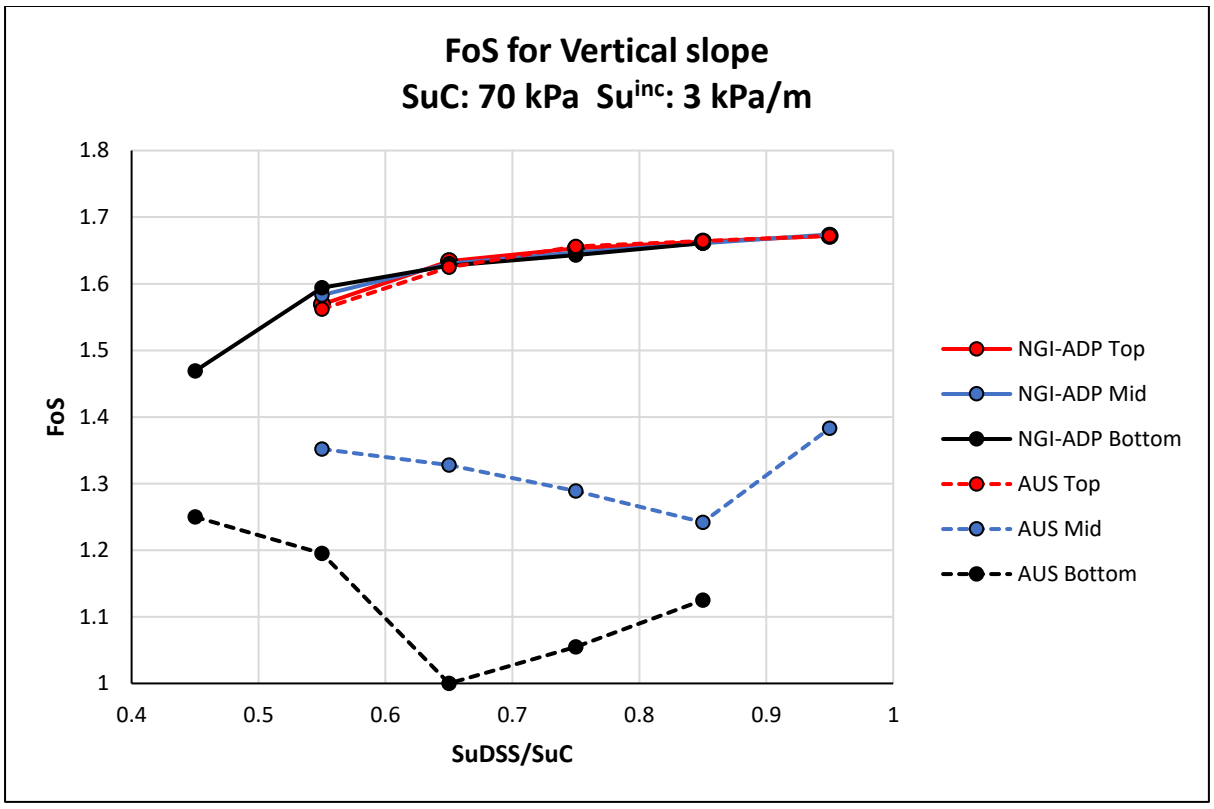

Figure 40. FoS for vertical slope with Su= 70 kPa + 3 kPa/m.

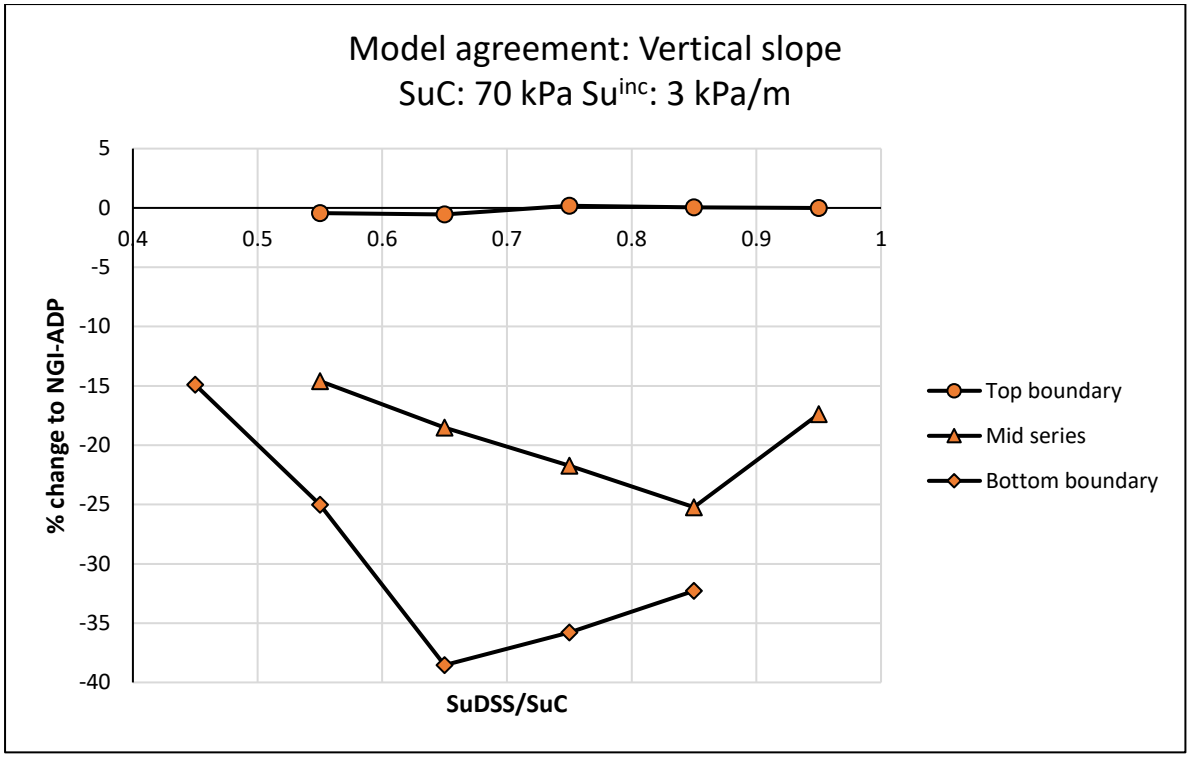

Figure 41. Model agreement for vertical slope with Su=70 kPa + 3 kPa/m.

Shear mechanisms

Shear mechanisms were visually controlled. The failure mechanisms are consistent with the changes in anisotropic shear strength. Drastically reducing the strength in extension results in deeper bearing capacity failures, while having higher anisotropic strength gives the more classic toe failures with increasing shear strength with depth. While some differences in the slip surfaces can be seen in the two models, the general shape is similar. Shear strain was not normalized as the geometry of the failure surface was the primary focus, thus, the scaled colorations are not consistent from figure to figure.

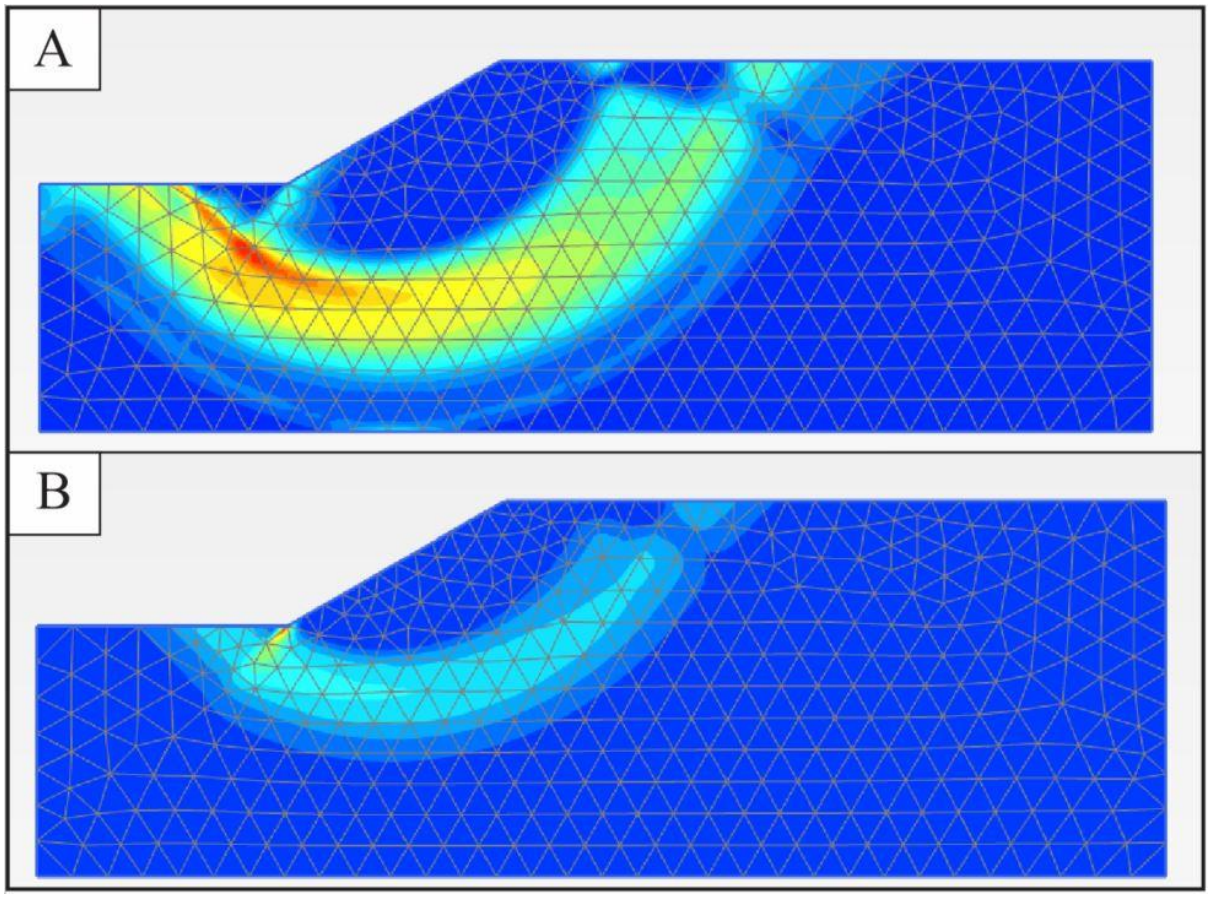

Figure 42. Total deviatoric strain for 30° slope with $s_u = 40\ kPa + 1 * z\ (\frac{kPa}{m})$ *for (A).* $s_{uDSS} = 0{,}55$ *and* $s_{uE} = 0{,}1$ *and (B).* $s_{uDSS} = 0{,}85$ *and* $s_{uE} = 0{,}8$ *for the NGI-ADP model.*

Shown in Figure 42 and Figure 43 is the deeper failure mechanism when $s_{uDSS} = 0{,}55$ and $s_{uE} = 0{,}1$ compared to the shallower failure mechanism with increasing strength, when $s_{uDSS} = 0{,}85$ and $s_{uE} = 0{,}8$.

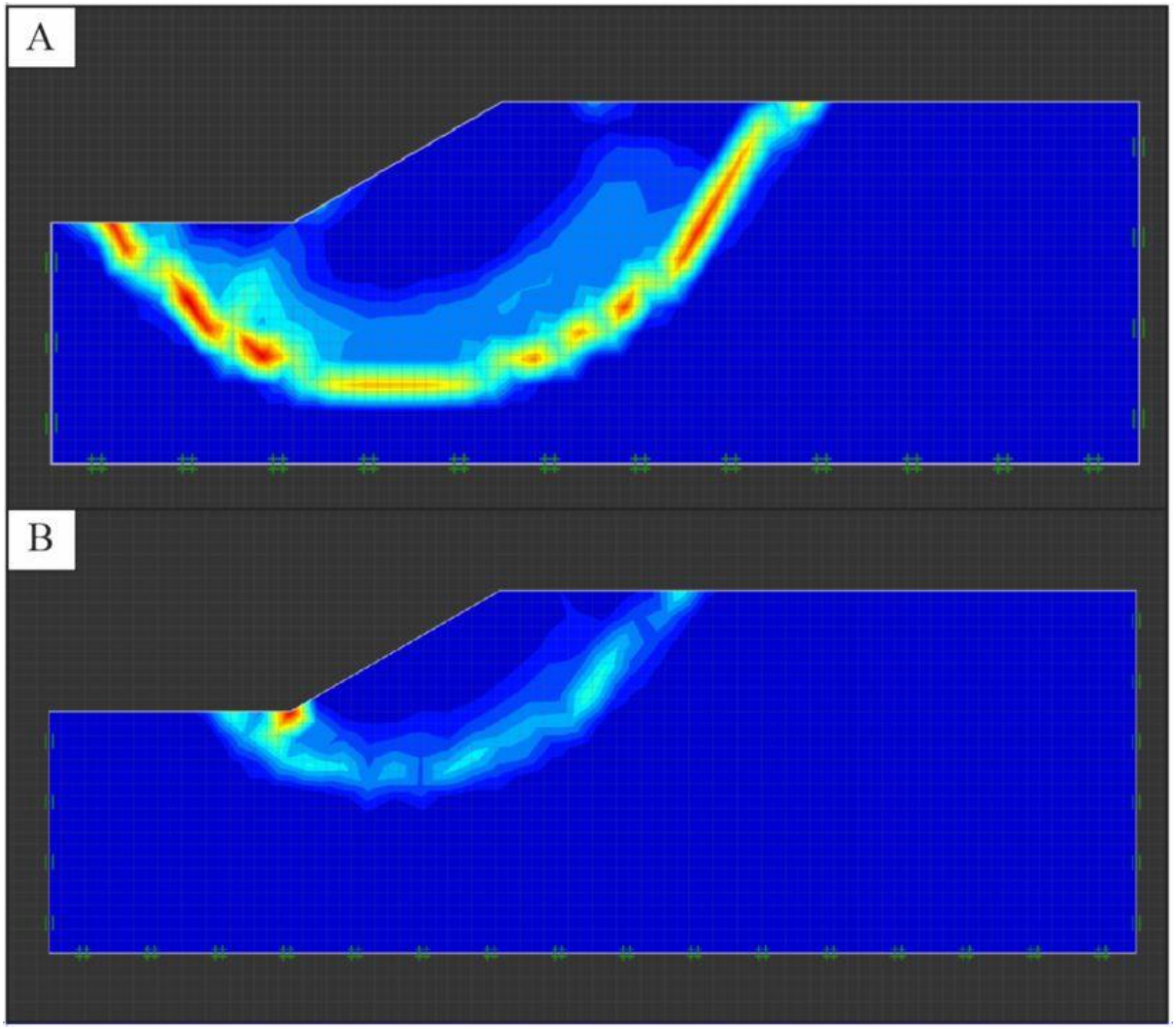

Figure 43. AUS total deviatoric strain for 30° slope with $s_u = 40\ kPa + 1 * z\ (\frac{kPa}{m})$ *for (A).* $s_{uDSS} = 0{,}55$ *and* $s_{uE} = 0{,}1$ *and (B).* $s_{uDSS} = 0{,}85$ *and* $s_{uE} = 0{,}8$.

As shown by the figures, the failure mechanisms illustrated by the two programs are similar, though the much broader shear band given by the NGI-ADP model makes quantitative analysis of the failure geometries somewhat inappropriate. An interesting phenomenon that occurred in both models is the development of significant strain in the toe point even when the failure mechanism does not pass directly through the toe.

The deepening of the failure mechanism with low s_{uDSS} and s_{uE} strengths is more greatly pronounced with steeper slopes and becomes extremely relevant for the case of the vertical slope, as seen in Figure 44 and Figure 45. However, it should be noted that while sufficient strength in s_{uDSS} and s_{uE} results in toe failure, a linear 45° failure surface as imagined in classical undrained total stress analysis is never reached, as some amount of curvature is present

both in the NGI-ADP and AUS models, though the AUS model appeared to more closely approach a linear failure. However, the resolution of the failure surface using the shear strain in the AUS model was very poor, as seen in the figures. A very large amount of strain develops at the toe of the slope.

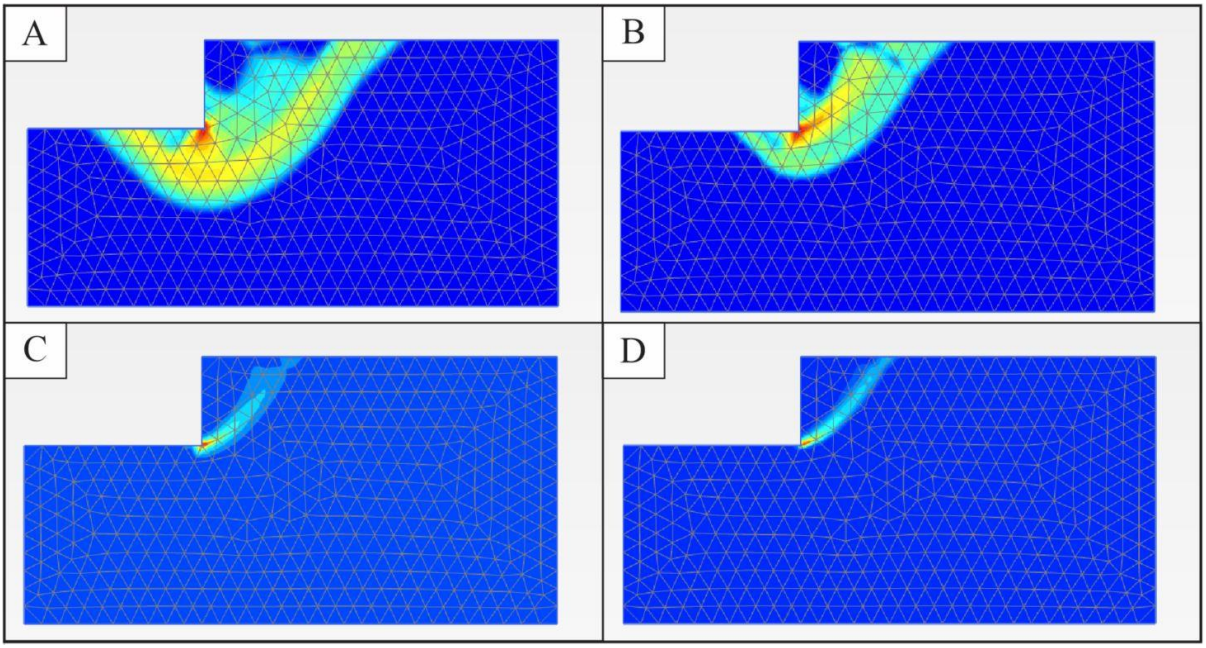

Figure 44. NGI-ADP strain envelopes for vertical slopes. (A). $s_{uDSS} = 0{,}55$ *and* $s_{uE} = 0{,}1$ *(B).* $s_{uDSS} = 0{,}65$ *and* $s_{uE} = 0{,}3$. *(C).* $s_{uDSS} = 0{,}65$ *and* $s_{uE} = 0{,}3765$. *(D).* $s_{uDSS} = 0{,}85$ *and* $s_{uE} = 0{,}8$

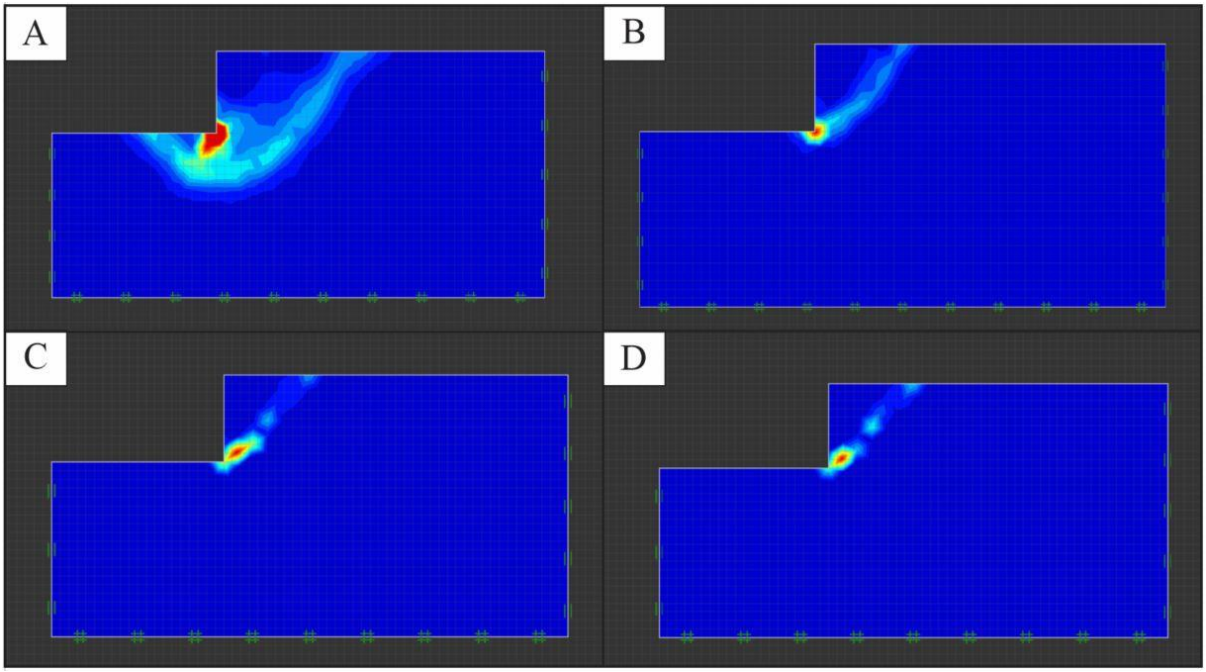

Figure 45. AUS strain envelopes for vertical slopes. (A). $s_{uDSS} = 0{,}55$ *and* $s_{uE} = 0{,}1$ *(B).* $s_{uDSS} = 0{,}65$ *and* $s_{uE} = 0{,}3$. *(C).* $s_{uDSS} = 0{,}65$ *and* $s_{uE} = 0{,}3765$. *(D).* $s_{uDSS} = 0{,}85$ *and* $s_{uE} = 0{,}8$

Chapter 8

Discussion

One of the first observations made is that along the upper boundary of the admissible anisotropic strength parameters for the AUS soil model, the two programs generate virtually the same FoS solution independent of slope angle. This indicates that for these cases, one would expect the two programs to be generating slip surfaces of equivalent geometry and anisotropic shear strength distribution along the slip surfaces. This follows simple intuitive reasoning: identical slip geometry, identical shear strengths, identical factor of safety.

When anisotropic shear strength parameters located below the upper AUS boundary are used, significant differences in the FoS solution develop between the two models. This difference, the lower FoS solution from AUS, becomes greater with increasing slope angle and as the s_{uDSS} and s_{uE} anisotropic strength factors approach the lower AUS boundary.

It is both useful to understand how both models behave by analyzing the FoS result and the percent change of the solution. Figure 46 and Figure 47 are useful to illustrate what is happening.

The encircled points can demonstrate important model behavior. In Figure 46, note the behavior of the NGI-ADP model by examining the three encircled points. In this method of presentation, the transition from 'Top' to 'Middle' to 'Bottom' really represents an increasing s_{uE} extension strength while the strength in direct simple shear s_{uDSS} is being held constant. These anisotropy values and ratios can be seen in the encircled points in Figure 47. In the NGI-ADP model, as the s_{uE} increases with a constant s_{uDSS}, the model generates a higher FoS, ergo a soil body with higher shear strength.

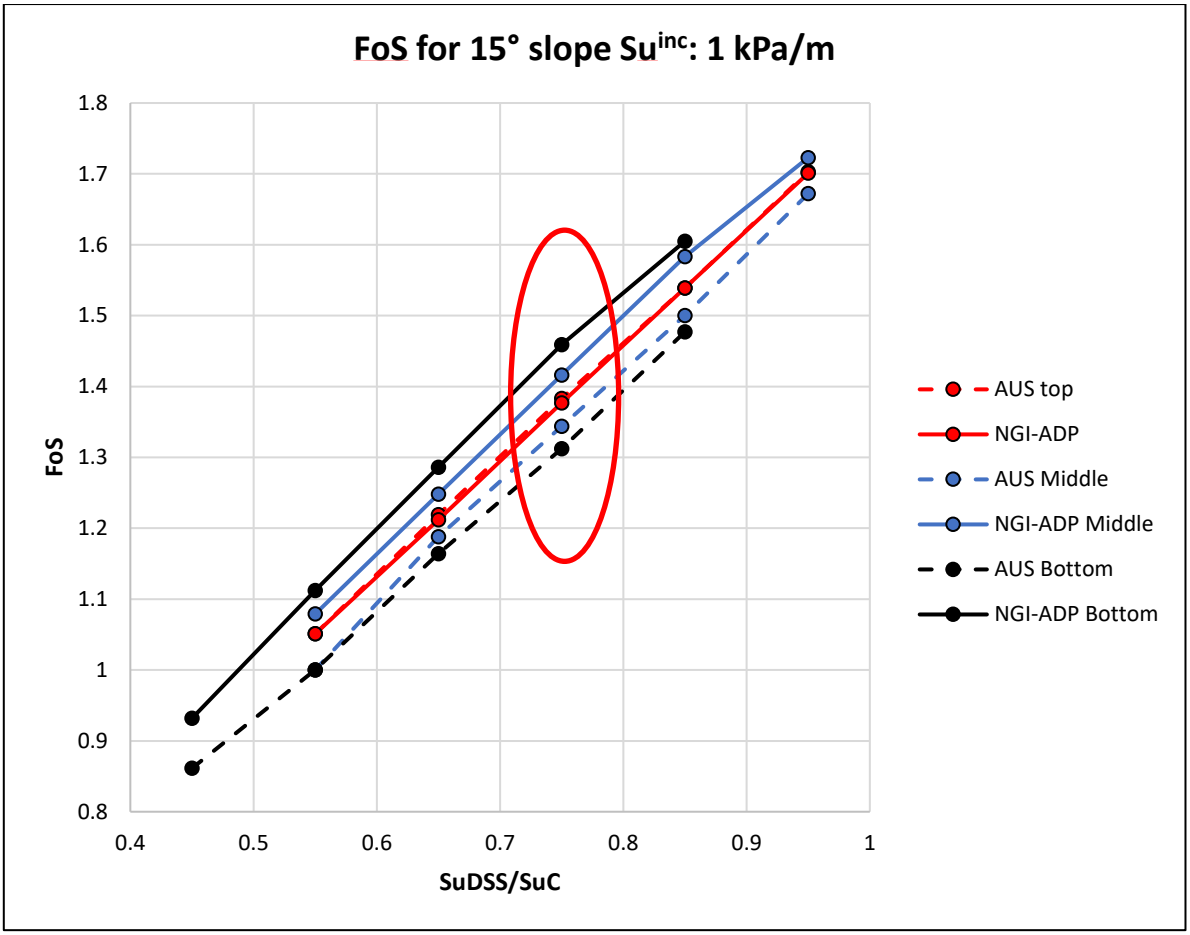

Figure 46. Factor of safety versus SuDSS/SuC for 15° slope. Red ellipse illustrates case of changing SuE when SuDSS is held constant.

Increasing s_{uE} when s_{uDSS} is constant for the AUS model gives lower FoS solutions. This seems counterintuitive at first glance, as the soil strength should be increasing, which would intuitively increase the FoS.

This phenomenon occurs consistently across the different simulations that were performed. This decrease in FoS from the AUS model also becomes more pronounced as slope angle increases, and it can be useful to examine the case of the vertical slope.

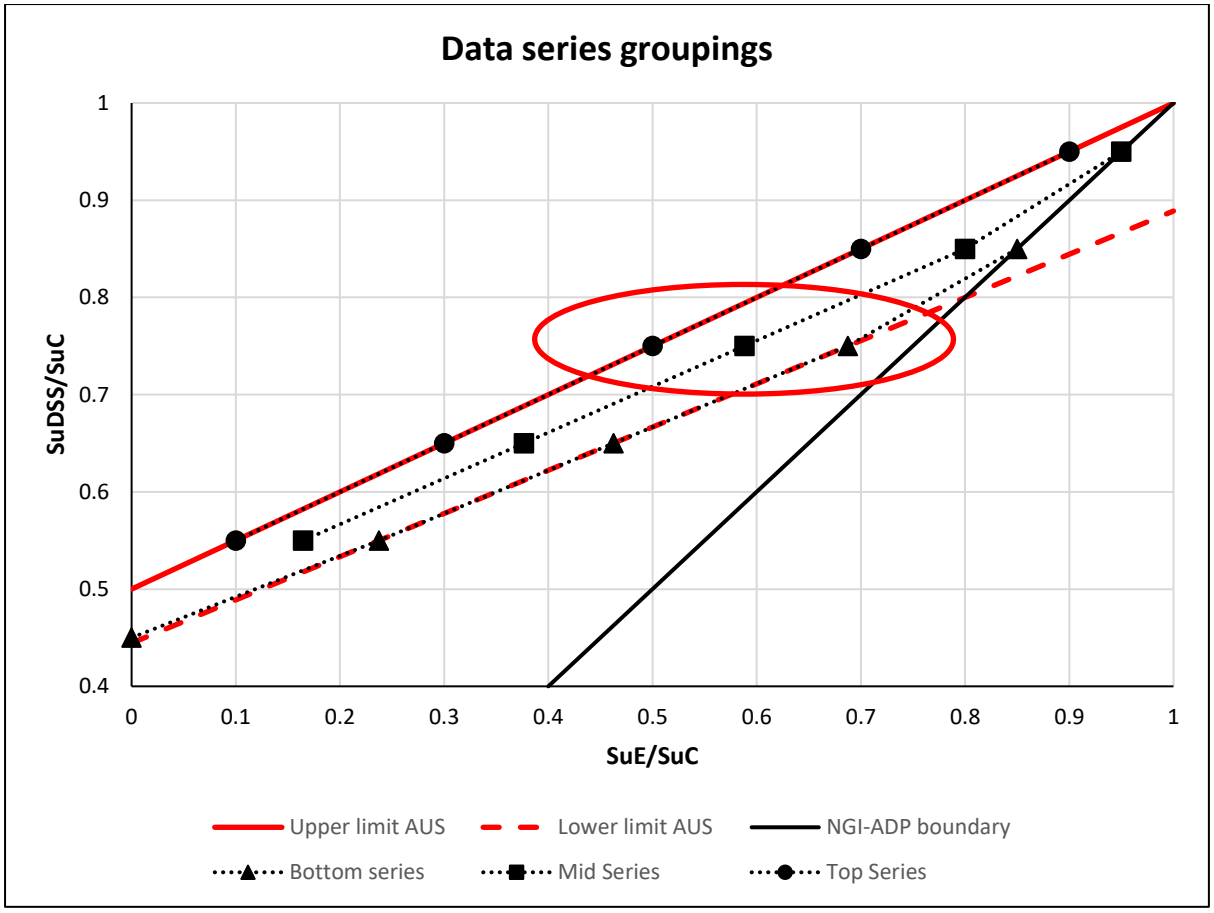

Figure 47. Focused anisotropy parameters encircled in red. Transitioning from Top Series to Bottom Series represents increasing SuE while keeping SuDSS constant.

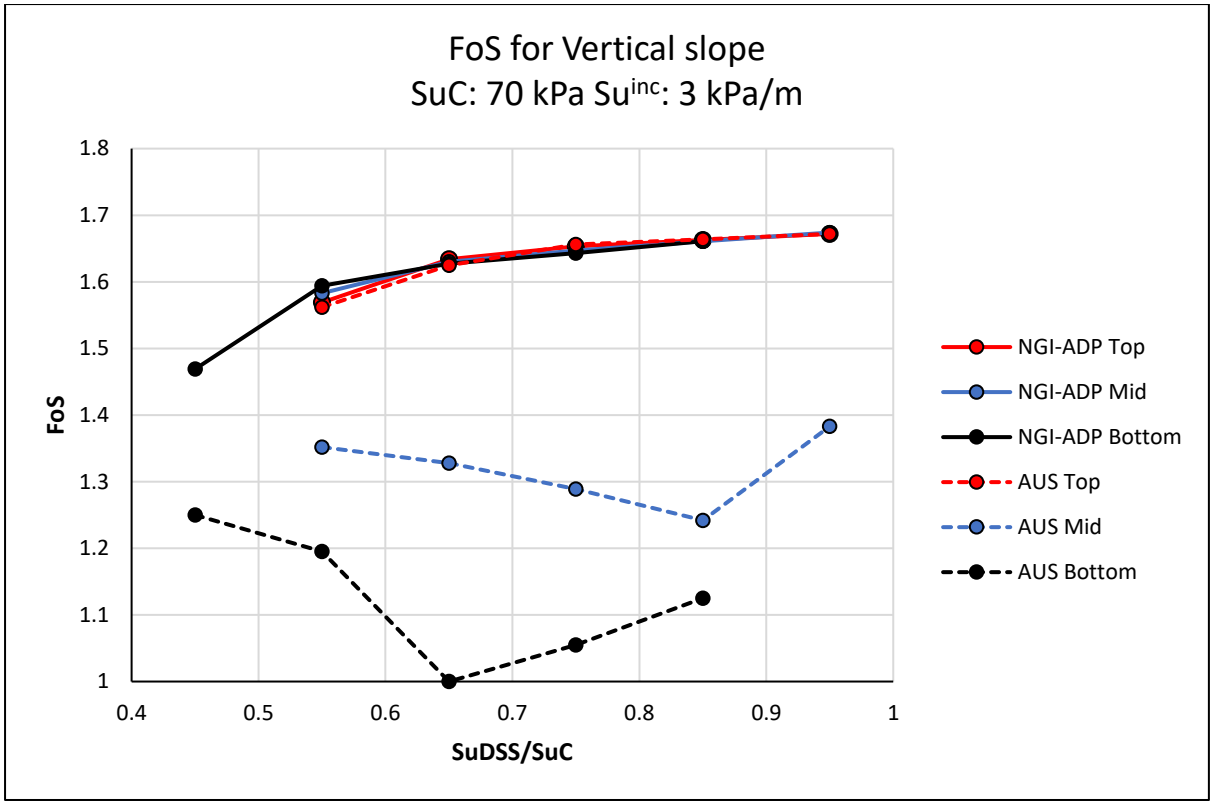

Figure 48. Factor of safety for vertical slope with Su= 70 kPa + 3 kPa/m.

Some of the results generated FoS solutions less than 1.0, meaning that the slope is unstable and should fail. Typically, resulting solutions less than 1.0 are not desirable for analytical comparison, as there can be uncertainty as to how these results are calculated. For most intents and purposes, any safety factor less than 1.0 is equivalent in the sense that the slope will fail, so a slope with a safety factor of 0.8 is no more stable than a slope with a safety factor of 0.5. However, in the strength reduction analysis used in this study, these values are still useful. In the strength reduction analysis, soil strength is altered until equilibrium is reached. Therefore, a FoS less than 1.0 actually represents the degree to which the soil strength must be improved to reach equilibrium. The lower FoS given by the AUS soil model shows that it models the soil as having lower strength.

In order to verify these results, undrained soil strength was increased in the case of the vertical slope to result in a FoS $\geq$ 1.0 for all anisotropic strength ratios in both models. The results are shown in Figure 48. As shown earlier in Figure 41, these results support earlier observations and verify the percent difference in FoS between the two models, approaching up to 40% for the case of the vertical slope along the lower anisotropic strength ratio boundary.

Figure 48 also illustrates another important concept. The reader will note that the results generated by the NGI-ADP model are very closely grouped together. This is implying that for this situation, changing amounts of anisotropic strength ratios have little to no impact on the shear strength of the soil and the FoS of the slope in the NGI-ADP model. When considering the classical approach to a vertical slope for undrained failure, it is anticipated that the slope failure will be a complete Active Rankine failure mechanism. This then means that one would expect all or nearly all of the soil along the failure zone to experience active strength conditions, meaning that changes to the soil strength in the extension and direct shear regimes are not expected to have an impact on the soil strength.

When examining the results of the AUS soil model in this scenario, it is very clear that the soil strength is being negatively impacted by increasing the strength in extension when the strength in direct shear is constant. However, as previously discussed, considering that for the vertical slope the entirety of the failure zone is expected to be in the active regime, one would not expect the changing of anisotropic strength to impact the FoS or soil strength. It must then be determined as to why the AUS soil model generates lower FoS solutions in these circumstances. If it is concluded that the decreasing FoS is not due to lower soil strengths in the passive and shear zones, then the soil strength in the active zone must be decreasing. This is slightly confusing as the specified shear strength in compression is fixed and has not been changed, however, there must be made a very important distinction between strength in the triaxial compression regime and that of active plane strain soil strength. The two models approach this distinction in two very different ways.

In the NGI-ADP model, a rounding ratio S_{uC}/S_{uA} is applied can be manipulated and set by the user. This ratio is then independent of any other soil parameters used in the soil model. Such an input parameter does not exist in the AUS model. Rather, perhaps as a consequence of employing a flexible yield criterion, the relationship between active plane strain strength and triaxial compression strength varies considerably based on the anisotropic shear strength parameters.

The failure criterion of the AUS model in plane strain is written:

$$F = \sqrt{(\sigma_z - \sigma_x + ak)^2 + 4\tau_{zx}^2} - \frac{4\rho}{1+\rho}k \tag{8.1}$$

For the Active and Passive states in plane strain, $\tau_{zx} = 0$. Changing compressive stresses to positive, it is possible to substitute for $-2t = \sigma_z - \sigma_x$, where t is the undrained shear strength in Active or Passive plane strain. This manipulation results in:

$$t = \frac{s_{uC}}{1+\rho}\left[\rho - \frac{s_{uE}}{s_{uC}} \pm \frac{2\rho}{1+\rho}\left(1 + \frac{s_{uE}}{s_{uC}}\right)\right] \tag{8.2}$$

Plotting this equation in Figure 49 clearly shows that the changing ratio ρ which relates the direct simple shear strength to the strength in extension and compression changes the ratios of Active plane strain strength to triaxial compressive strength and Passive plane strain strength to triaxial extension strength.

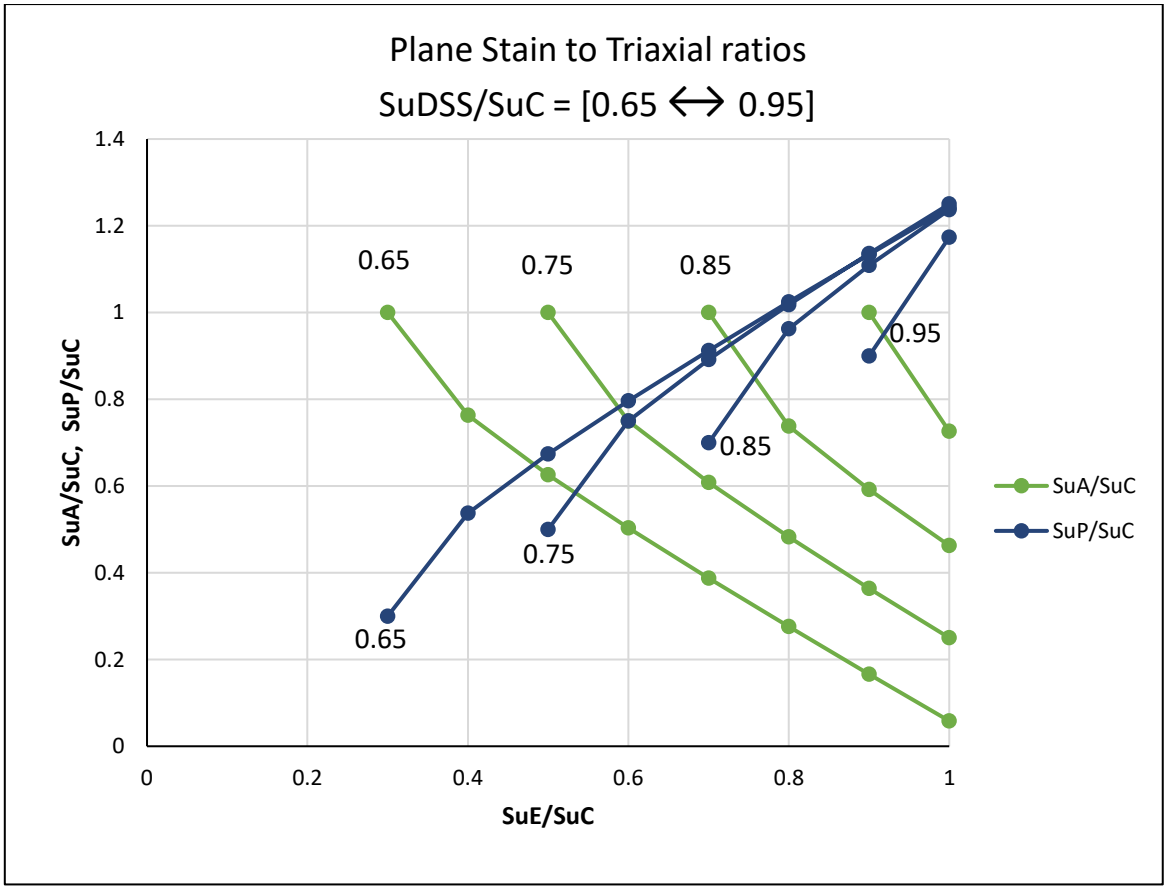

Figure 49. Influence of anisotropic strength ratios on the ratios between triaxial and plane strain strengths. Data labels show value of SuDSS/SuC for given data line.

Figure 50 shows the behavior of ${}^{s_{uA}}/_{s_{uC}}$ and ${}^{s_{uP}}/_{s_{uC}}$ for the upper and lower bounds of s_{uDSS}. Along the upper ${}^{s_{uDSS}}/_{(s_{uE}+s_{uC})} = 0{,}5$ boundary, the model generates identical solutions to the NGI-ADP model which uses a constant ${}^{s_{uC}}/_{s_{uA}} = 0{,}99$. Note that along this boundary the ${}^{s_{uP}}/_{s_{uC}}$ ratio is nearly identical to the input ${}^{s_{uE}}/_{s_{uC}}$.

However, along the lower ${}^{s_{uDSS}}/_{(s_{uE}+s_{uC})} = 4/9$ boundary, the ${}^{s_{uA}}/_{s_{uC}}$ ratio is significantly lower and decreases with increasing s_{uE}. Indeed, when ${}^{s_{uE}}/_{s_{uC}} = 0{,}8$, ${}^{s_{uA}}/_{s_{uC}} = 0{,}6$, representing a reduction in the strength in active plane strain of 40%, which is consistent with the results in the vertical slope. Perhaps as a measure of compensation for this effect, the ${}^{s_{uP}}/_{s_{uC}}$ ratio is elevated and increases beyond 1.0 for ${}^{s_{uE}}/_{s_{uC}}$ values greater than 0.8.

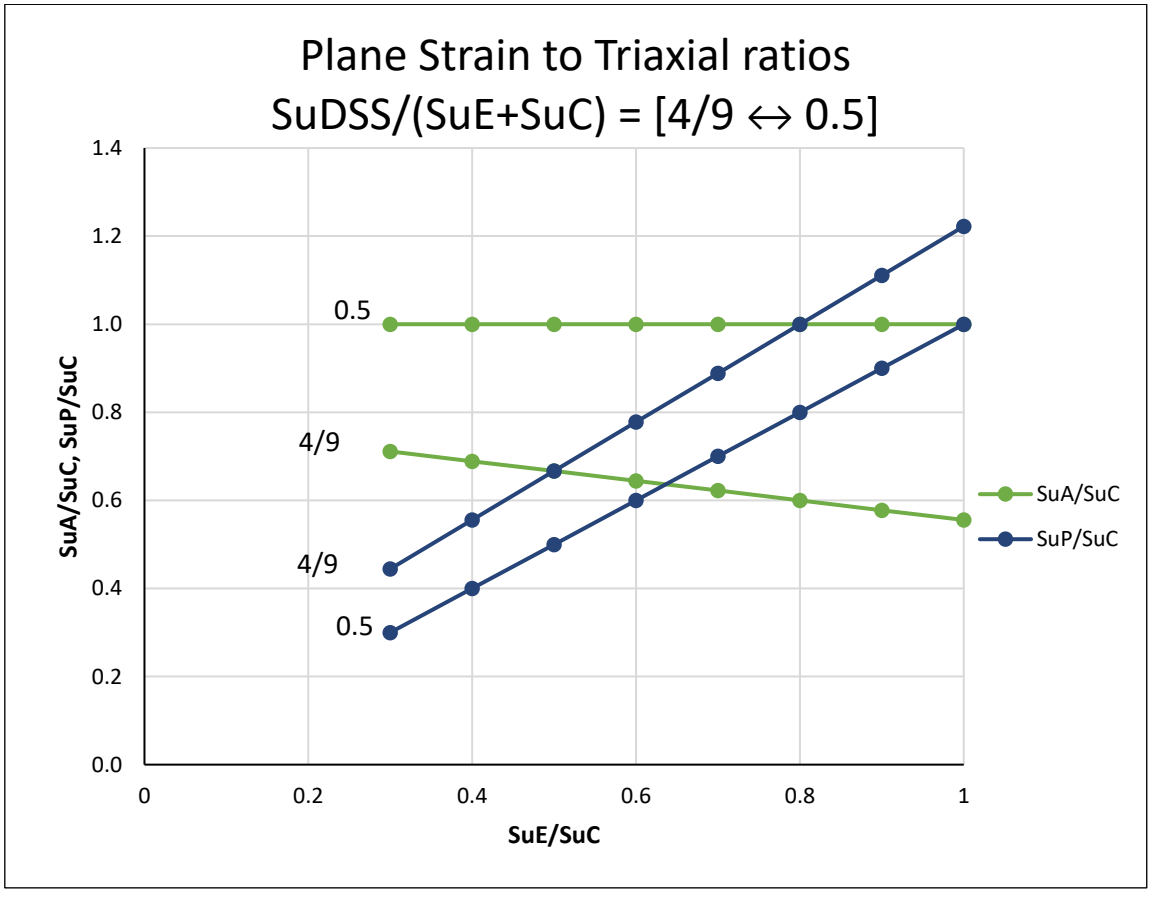

Figure 50. Plane strain to triaxial strength ratios for the upper and lower boundaries of SuDSS for the AUS soil model.

This can readily explain why larger differences in FoS are observed in steeper slopes. As the slope angle increases, less of the failure surface is in the passive or direct shear regimes. In other words, a greater proportion of the failure surface is in the active regime, and this reduction of active strength has a larger effect as there is less 'reinforced' soil in passive strength to counterbalance this effect.

Another observation is that the $^{s_{uA}}/_{s_{uC}}$ ratio decreases as $^{s_{uE}}/_{s_{uC}}$ increases for the case of $^{s_{uDSS}}/_{(s_{uE}+s_{uC})} = 4/9$. This is consistent with results showing that for a given $^{s_{uDSS}}/_{(s_{uE}+s_{uC})}$ ratio, increasing the magnitudes of the anisotropic shear strengths results in larger differences between the two models due to a lower FoS solution from the AUS model.

The simulations performed in this thesis are limited in their mode of failure to curved failures in homogenous clay. It is well known that slope failure geometries are variable in nature due to the governing soil conditions. Soils may fail in a near-circular shear zone, or a linear planar failure, or some geometry in between. As such, the influence the anisotropic strengths varies significantly with the geometry of the slide. For instance, a classical circular slip surface will have a relatively even contribution of the active, passive and direct shear strengths. On the other hand, a more elongated slip surface would result in a greater influence of the direct strength, as a larger proportion of the slip surface would be failing in direct shear as seen in Figure 51. With less influence of the active strength, the two models might be in better agreement in such an instance. Thus is it vital to understand that the observations made in the analysis of this thesis are limited to simplified slope failure cases and cannot be applied to any situation before first understanding the fundamental differences.

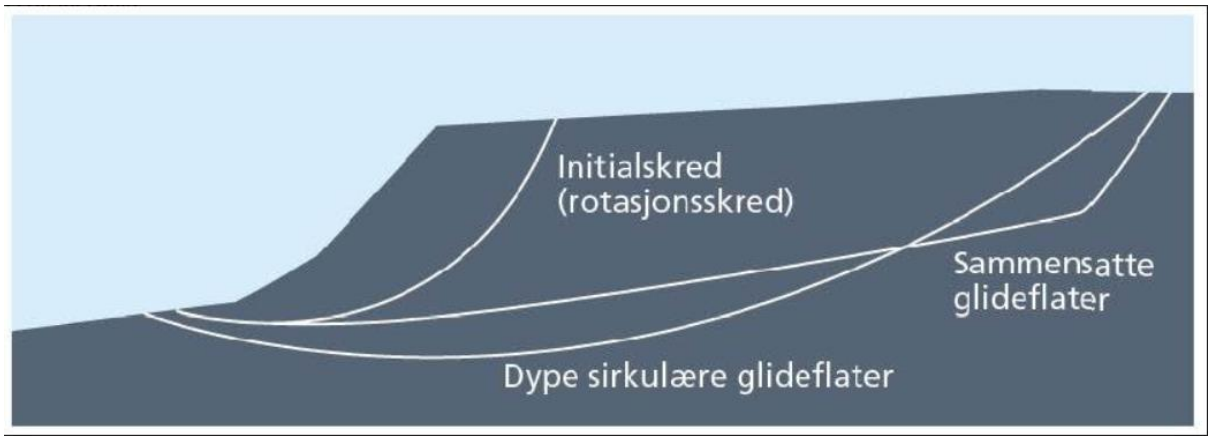

Figure 51. Different geometries of slope failure. From Schanche & Haugen (2014).

One of the complicating factors is that direct simple shear tests are not always performed. In a situation in which only triaxial tests are performed, estimation of the direct shear strength will have significant implications in the FoS generated by the two models. Several empirical relationships exist for estimating the direct strength from index test parameters, such as water content, but these empirical relationships only provide a best guess. Additionally, the data obtained by Karlsrud & Martinez (2013) show anisotropy values outside the admissible ranges of the AUS model. The study further illustrates that the sample quality can have significant effects on the measured anisotropic strength ratios. When choosing a model, these factors must be carefully considered. The NGI-ADP model may be necessary in some cases merely to accommodate the measured anisotropic strength ratios if these do not fall within the acceptable ranges of the AUS model.

Model Accuracy

It is not obvious that one model necessarily gives more accurate solutions. Both models incorporate curve-fitting approximations to fit the data as reasonably as possible while remaining simple and uncongested of a large amount of cumbersome input parameters. As such, both models may be prone to oversimplifications that decrease accuracy. What is clear is that the models give statistically identical solutions for a specific anisotropic strength ratio, at which the failure criterion in 3D stress space is a Tresca hexagon. As this anisotropic strength ratio changes, corresponding to a transition from Tresca to Rankine triangle yield surface for the AUS model, the difference in solution from the two models increases.

The NGI-ADP model incorporates a Tresca yield criterion for all anisotropic strength ratios. This choice of yield criterion, while simple and easy to incorporate, likely gives false solutions in some quadrants. It may be conservative in some areas and unconservative in others. This can be easily observed in Figure 52 in which the NGI-ADP yield criterion is compared with the curved ADPX3 yield criterion as described by Aamodt (2019).

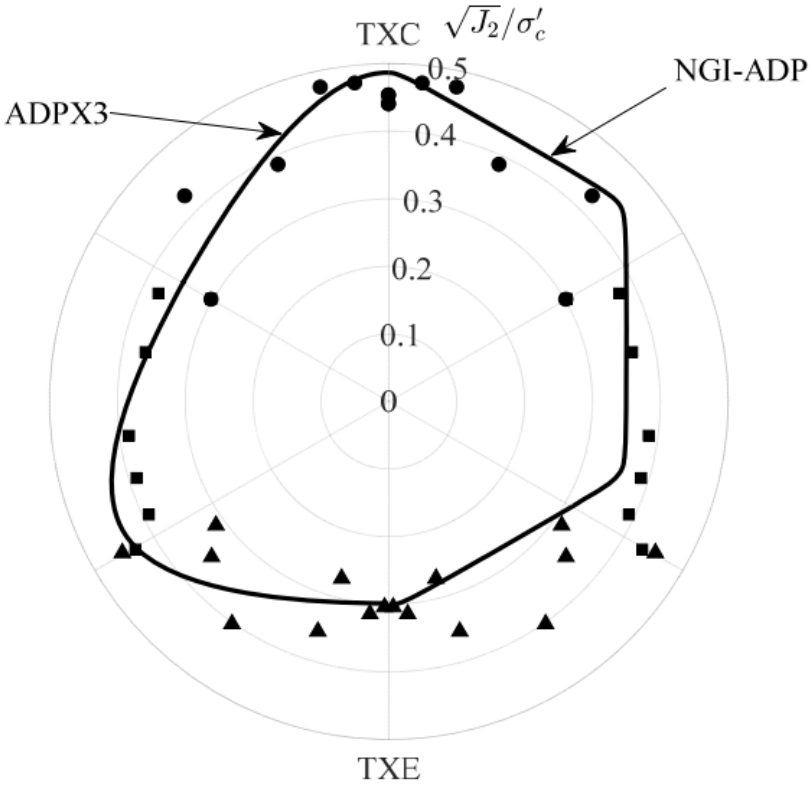

Figure 52. True triaxial data from San Francisco bay mud by Kirkgard and Lade (1993) plotted in the pi plane with the NGI-ADP failure criterion and newly proposed ADPX3 failure criterion. From Aamodt et. al. (2021).

In an attempt to generate better fit to true triaxial data and minimize false solutions, the creators of the AUS model employ a variable yield surface that is controlled by the anisotropic strength ratios. This is advantageous as it allows the soil model to remain simple and operational requiring only the undrained anisotropic shear strengths. At some geometry between the Tresca and Mohr-Coulomb hexagonal yield surfaces, this potentially generates a much better fit to experimental data. However, the shrinking of the yield surface into a straight-edged triangle may significantly underestimate soil strength and is in much worse agreement with the rounded yield surface shown above. While changing the shape of the yield surface based on the anisotropic strength ratios allows the soil model to remain simple, this results in a drastic change in predicted soil strength over a small change in anisotropic strength ratio, and this may not accurately reflect real soil behavior. While this model provides excellent fit to experimental data from undrained true triaxial tests on normally consolidated Edgar Plastic Kaolinite performed by Lade (1990), it has previously been shown that anisotropic strength ratios for Norwegian clays collected by high-quality block samples (Karlsrud & Hernandez-Martinez, 2013) extend beyond the admissible input boundaries of the AUS soil model. Additionally,

while water content may be used to approximate anisotropic strength in Norwegian clays, it has been shown that anisotropic strength ratio is influenced by many complicated factors. Therefore, while this method of fit may give excellent agreement for some clays, it may not be appropriate in all instances. Additionally, the manner in which the AUS model is formulated results in the decrease of Active plane strain shear strength as the yield criterion becomes more triangular due to the changing anisotropic strength ratio. This results in the model generating lower FoS solutions in instances when the soil strength has actually been increased. This particular effect is more influential for higher slope angles, as the subsequently reinforced Passive plane strain shear strength has less of a counterbalancing effect. This particular manner of attempting to mathematically reconcile strength anisotropy into the soil model may not be the optimal representation of real soil behavior.

It can be confidently stated that the AUS soil model gives a more conservative solution. This is not necessarily a negative implication, as conservative assumptions are most often used in geotechnical engineering and in many cases it is better to underestimate soil strength than to overestimate soil strength. However, it is important to understand the reasoning for the differences between the two models. Should one model be used to verify the solution from another model, these differences must be accounted for.

While major focus continues to be rightfully focused on improving soil modelling capabilities to provide the most accurate representation possible, the accuracy of soil model simulations is ultimately dependent on the trustworthiness of soil data collected from experimental data. Heterogeneity and uncertainty in soil conditions will always be present, and as discussed in Karlsrud & Hernandez-Martinez (2013), sampling techniques can have major impacts on laboratory data quality. For these reasons, it is vital to never rely fully on results from a given soil test or soil model simulation, but to instead utilize the entirety of one’s competence and knowledge as a geotechnical engineer.

Chapter 9

Conclusions and Further Work

9.1 Conclusions

This study was conducted to explore the similarities and differences between the NGI-ADP soil model and AUS soil model for the case of slope stability in idealized simple slopes in undrained, homogenous clays. Of primary interest was determining if the two models would generate similar or dissimilar solutions, and under what soil conditions this would occur. The findings show that:

- When Adaptive Meshing is not used, and adequate mesh density is applied, simple soil models in PLAXIS and Optum soil modeling programs generate identical solutions, meaning that they can be directly compared without compensating for mesh effects.
- The NGI-ADP and AUS soil models generate statistically identical solutions when $s_{uDSS}/(s_{uE} + s_{uC}) = 0{,}5$.
- When $s_{uDSS}/(s_{uE} + s_{uC}) < 0{,}5$ the AUS soil model generates lower FoS solutions relative to the NGI-ADP model.
- $s_{uDSS}/(s_{uE} + s_{uC})$ approaching $4/9$, results in lower FoS solutions generated by the AUS soil model and greater difference between the two models.
- When s_{uDSS} and s_{uC} are kept constant, increasing s_{uE} will result in higher FoS solutions for the NGI-ADP model, and lower solutions for the AUS model.
- Difference between the two models increases as slope angle increases.
- For a given $s_{uDSS}/(s_{uE} + s_{uC})$ ratio, model agreement decreases as the magnitudes of the anisotropic shear factors s_{uDSS} and s_{uE} increase. In steep slopes, increasing these

factors along a constant ratio may result in the AUS model generating subsequently lower FoS solutions.

- Differences in FoS up to 35% are demonstrated in the case of the vertical slope. This magnitude coincides with the decrease in Active plane strain strength in the AUS model, which depending on anisotropic strengths and relative magnitudes can reduce Active plane strain strength as much as $^{S_{uA}}/_{S_{uC}} = 0{,}6$.

- Both models use curve-fitting simplifications and are designed for use with minimal input data, which may lead to unconservative or overly conservative estimations dependent on soil strength parameters.

9.2 Future Work

This thesis explored the apparent similarities and differences between the NGI-ADP and AUS soil models for the case of undrained slope stability analysis in idealized simple slopes with homogenous anisotropic soils. While relevant, this is limited to a specific scenario and does not comprehensively describe the implications of choice of soil model for other or more complex geotechnical problems. More comprehensive comparisons of the two models should be undertaken to more thoroughly describe the similarities and differences between these two models. As more soil models are improved, developed, and made commercially available, it becomes vital to thoroughly understand the capabilities and limitations of these new models, and the implications of choosing to use these. Failing to do so could result in misinterpretation of data in an instance in which parties lack in-depth understanding of soil models.

References

Aamodt, M.T. 2019. *An effective Stress Based Model for Undrained Slope Stability Analyses in Anisotropic Clay*. M.Sc. Master Thesis, Norwegian University of Science and Technology (NTNU), Geotechnical Division.

Aamodt, M.T., Grimstad, G., & Nordal, S. 2021. Effect of Strength Anisotropy on the Stability of Natural Slopes. *NGM 2020 Helsinki 18th-19th January 2021*.

Arthur, J. R. F., Chua, K. S., & Dunstan, T. 1977. Induced anisotropy in a sand. *Geotechnique*, *27*(1), 13-30.

Billington, E.W. 1988. Generalized isotropic yield criterion for incompressible materials. *Acta Mechanica*; **72**:1–20.

Berre, T. & Bjerrum, L. 1973. Shear strength of normally consolidated clays. *The 8th International Conference on Soil Mechanics and Foundation Engineering, Moscow.*

Bjerrum, L., & Landva, A. 1966. Direct simple-shear tests on a Norwegian quick clay. *Geotechnique*, *16*(1), 1-20.

Brinkgreve, R. B., K. S. . S. W. M. 2017. *PLAXIS 2D Manuals*. CRC Press, Inc.

Cook, R.D. & Young, W.C. 1999. *Advanced Mechanics of Materials*, United States of America, Prentice-Hall, inc.

Coulomb, C. 1773. Application des rigles de maximus et minimis a quelques problemes de statique relatifs a Larchitecture. Memoires de savants etrangers de L.

El-Nasrallah, S. N. 1976. *Shear strength of a cohesionless soil under plane strain and triaxial conditions*. Doctoral dissertation. McMaster University.

Gens, A., Hutchinson, J. N., & Cavounidis, S. 1988. Three-dimensional analysis of slides in cohesive soils. Geotechnique, 38(1), 1-23.

Grimstad, G. Andresen, L. & Jostad, H.P. 2012. NGI-ADP: Anisotropic shear strength model for clay. *International Journal for numerical and analytical methods in Geomechanics*, Vol. 36, 483-497.

Grimstad, G. & Benz, T. 2018. Implementation of Soil Models, PhD course BA8304. Norwegian University of Science and Technology (NTNU), Geotechnical Division.

Grimstad, G., Rønningen, J.A. & Nordal, S. 2018. Application of a generalized continuous Mohr-Coulomb criterion. Proceedings of the 9th European Conference on Numerical Methods in Geotechnical Engineering (NUMGE 2018), June 25-27, 2018 Porto, Portugal. CRC Press.

Isachsen, M. 2012. *Effekt av anisotropi på udrenert skjærstyrke i naturlige skråninger*. M.Sc. Master Thesis, Norwegian University of Science and Technology (NTNU), Geotechnical Division.

Jordbakke, T. 2017. *Effect of initially inclined principle stress directions on undrained shear strength for anisotropic clay*. M.Sc. Master Thesis, Norwegian University of Science and Technology (NTNU), Geotechnical Division.

Kirkgard, M.M. & Lade, P.V. 1993. Anisotropic three-dimensional behavior of a normally consolidated clay. *Canadian Geotechnical Journal*, 30, 848-858.

Krabbenhøft, K. (2020, January 17). Webinar: Introduction to OPTUM G3 with Optum CE co-founder Prof Kristian Krabbenhoft [PowerPoint video presentation]. Optum Computational Engineering. YouTube. https://www.youtube.com/watch?v=E2DjfRgECPM&t=444s

Krabbenhøft, K., Galindo-Torres, S.A., Zhang, X. & Krabbenhøft, J. 2019. AUS: Anisotropic undrained shear strength model for clays. *International Journal for Numerical and Analytical Methods in Geomechanics*. *43*(17), 2652-2666.

Krabbenhøft, K., Lymain, A.V., & Krabbenhøft, J. 2016. OptumG2: Theory. www.optumce.com

Ladd, C. C. 1991. Stability evaluation during staged construction. *Journal of geotechnical engineering*, *117*(4), 540-615.

Ladd CC, Foott R, Ishihara K, Schlosser F, Poulos HG. 1977. Stress-deformation and strength characteristics. *State-of the-art Report, Proceedings of the Ninth*

International Conference on Soil Mechanics and Foundation Engineering, Tokyo, Japan; 421–494.

Lade, P.V. 1978. Cubical Triaxial Apparatus for Soil Testing. *Geotechnical Testing Journal*, Vol 1, 93-101.

Lade, P. V. 1990. Single-hardening model with application to NC clay. *Journal of geotechnical engineering*, *116*(3), 394-414.

Lade, P.V. & Duncan, J.M. 1973. Cubical triaxial tests on cohesionless soil. *Journal of Soil Mechanics and Foundations*, Vol. 99, 793-812.

Lade, P.V. & Musante, H.M. 1978. Three-Dimensional Behavior of Remolded Clay. *Journal of the Geotechnical Engineering Division*, Vol. 104, 193-209.

Lambe, T.W. 1958. The Structure of Compacted Clay. *Journal of the Soil Mechanics and Foundations Division*, Vol. 84, 1-34.

Lunne, T. & Andersen, K. H. 2007. Soft Clay Shear Strength Parameters For Deepwater Geotechnical Design. *Offshore Site Investigation And Geotechnics, Confronting New Challenges and Sharing Knowledge.* London, UK: Society of Underwater Technology.

Matsuoka, H. & Nakai, T. 1974. Stress-Deformation And Strength Characteristics Of Soil Under Three Different Principal Stresses. *Proceedings of the Japan Society of Civil Engineers***,** 59-70.

Nordal, S. 2018. Soil Modeling, PhD course BA8304. Norwegian University of Science and Technology (NTNU), Geotechnical Division.

Nordal, S. 2019. Geotechnical Engineering Advanced Course. Norwegian University of Science and Technology (NTNU), Geotechnical Division.

Schanche, S. S., & Haugen, E. D. 2014. Sikkerhet mot kvikkleireskred Vurdering av områdestabilitet ved arealplanlegging og utbygging i områder med kvikkleire og andre jordarter med sprøbruddegenskaper (NVE-rapport 2014: 7). *Hentet fra http://publikasjoner. nve. no/veileder/2014/veileder2014_07. pdf*.

Optum CE (n.d.) About: Optum CE-Delivering the Next Generation FE Tools. https://optumce.com/about/

Optum G2 (2019), Finite Element Program for Geotechnical Analysis, Optum Computational Engineering, www.optumce.com.

Potts, D. & Zdravkovic, L. 1999. Some Pitfalls when using Modified Cam Clay. Proceedings of the Workshop on Soil and Structure Interaction (COST C7), Thessaloniki, Greece, 1-14.

Prashant, P. & Penumadu, D. 2005. A laboratory study of normally consolidated kaolin clay. *Canadian Geotechnical Journal,* Vol. 42**,** 27-37.

Rabstad, K. 2011. *Slope stability in natural slopes with vertical or principal stress induced undrained shear strength anisotropy.* M.Sc. Master Thesis, Norwegian University of Science and Technology (NTNU), Geotechnical Division.

Roscoe, K.H. & Burland, J.B. 1968. On the generalized stress-strain behaviour of wet clay. In: Engineering Plasticity, Cambridge: 535-609.

Sandven, R., Senneset, K., Emdal, A., Nordal, S., Janbu, N., Grande, L. & Amundsen, H. A. 2015. Geotechnics, Field and Laboratory Investigations. Norwegian University of Science and Technology (NTNU), Geotechnical Division.

Shibata, T. & Karube, D. 1965. Influence of the variation of the intermediate principal stress on the mechanical properties of normally consolidated clays. *Proceedings of the Sixth International Conference in Soil Mechanics and Foundation Engineering.* Montreal.

Steigerwald, L. 2020. Initial exploration of the Optum 3D software for analysing slope stability in three dimensions for undrained analysis. Specialization Project Report, Norwegian University of Science and Technology.

Terzaghi, K. 1942. *Theoretical Soil Mechanics,* New York, John Wiley and Sons.

Won, J. Y. 2013, September. Anisotropic strength ratio and plasticity index of natural clays. In *Proceedings of the 18th international conference on soil mechanics and geotechnical engineering* (pp. 445-448).

Appendix A

List of Abbreviations

LEM Limit Equilibrium method

FEM Finite element method

SRM Strength reduction method

FoS Factor of Safety

DSC Directional Shear Cell

Appendix B

Table 3. Parameter study for direction comparison of PLAXIS and Optum soil modelling programs.

Parameters in PLAXIS – Optum comparison	
Slope height H	15, 20, 25 m
Unit weight γ	18, 20 22 kN/m3
Slope angle β	26.56°, 45°, 90°
Undrained shear strength s_u	20, 30 kPa
Shear strength increase with depth s_u^{inc}	1, 2, 3 kPa/m
Number of elements	
Element type	Upper Bound, Lower Bound, Gaussian

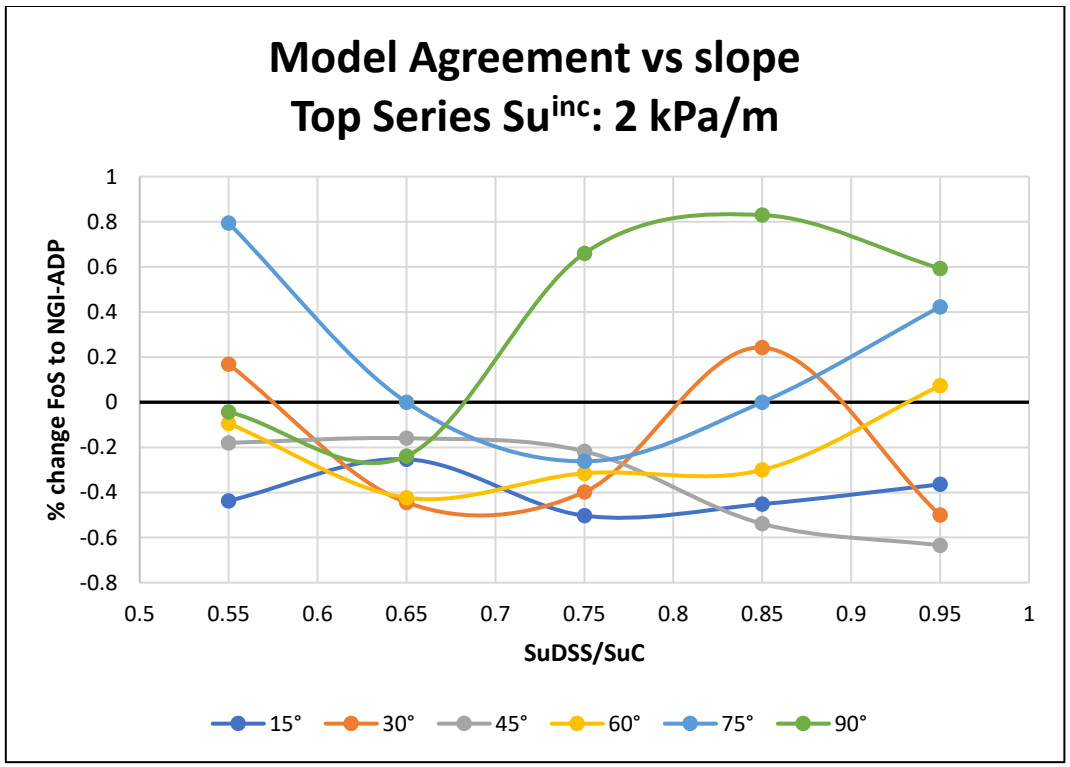

Figure B- 1. Model agreement along top of anisotropic strength ratio boundary vs slope with increasing shear strength with depth 2 kPa/m.

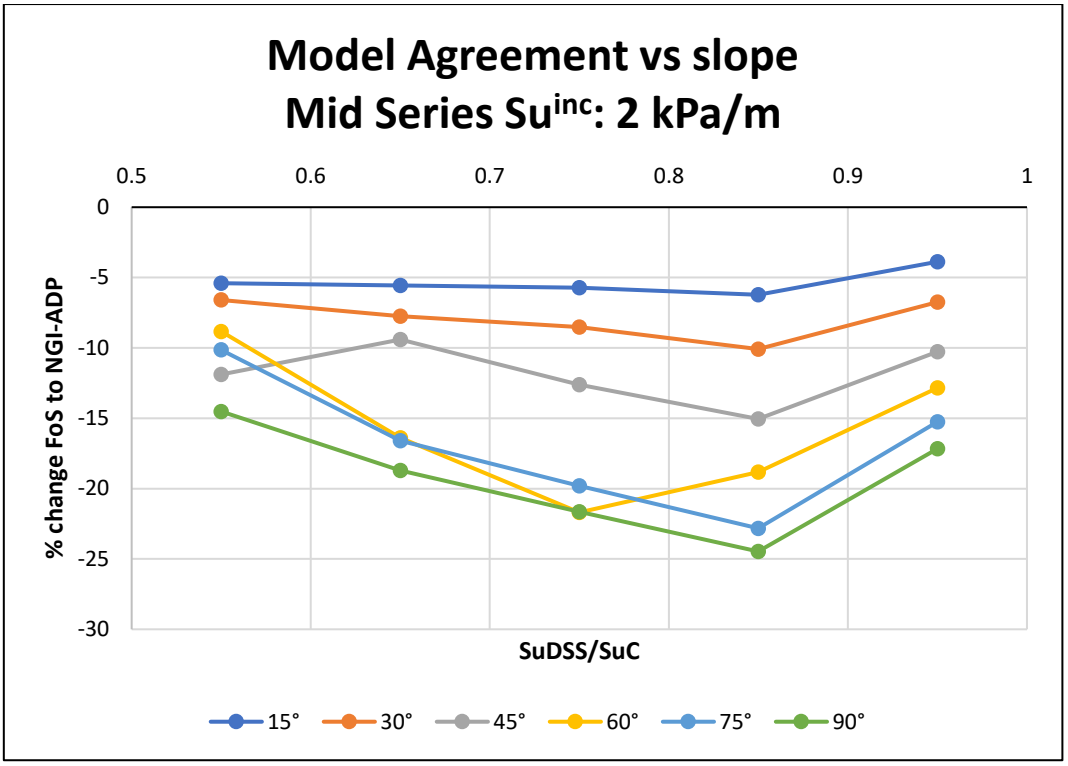

Figure B- 2. Model agreement vs slope for the mid anisotropic series with Su = 40+2kPa/m.

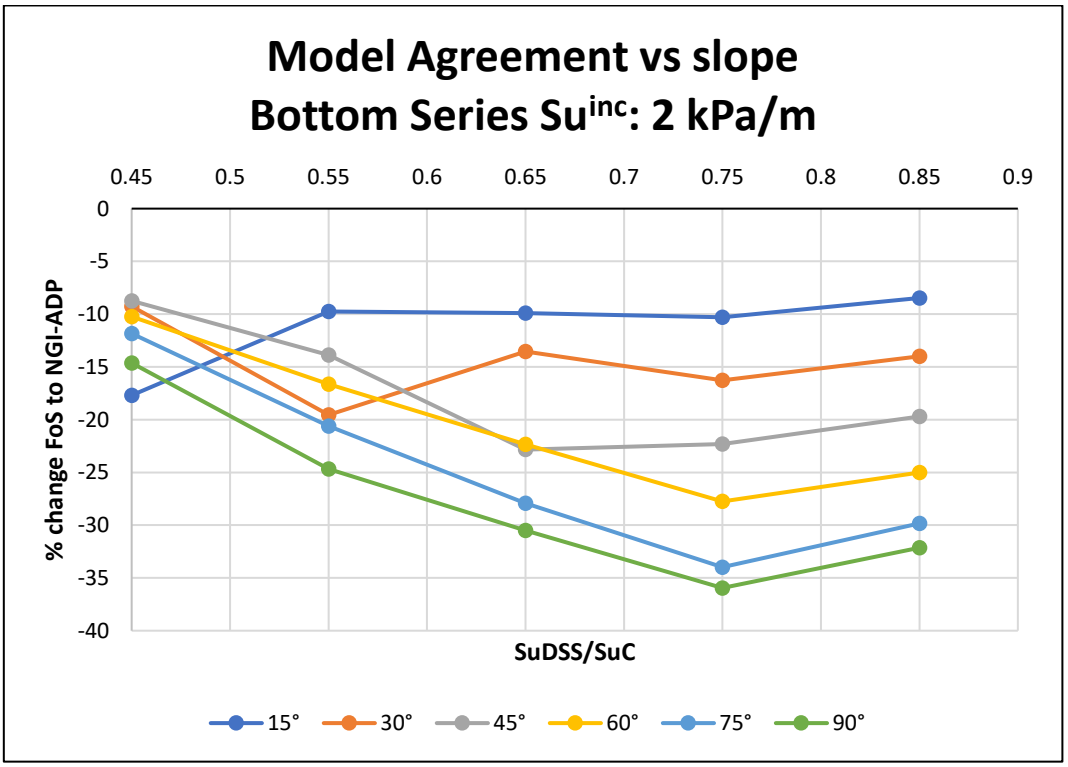

Figure B- 3. Model agreement vs slope for the bottom anisotropic series with Su = 40+2kPa/m.

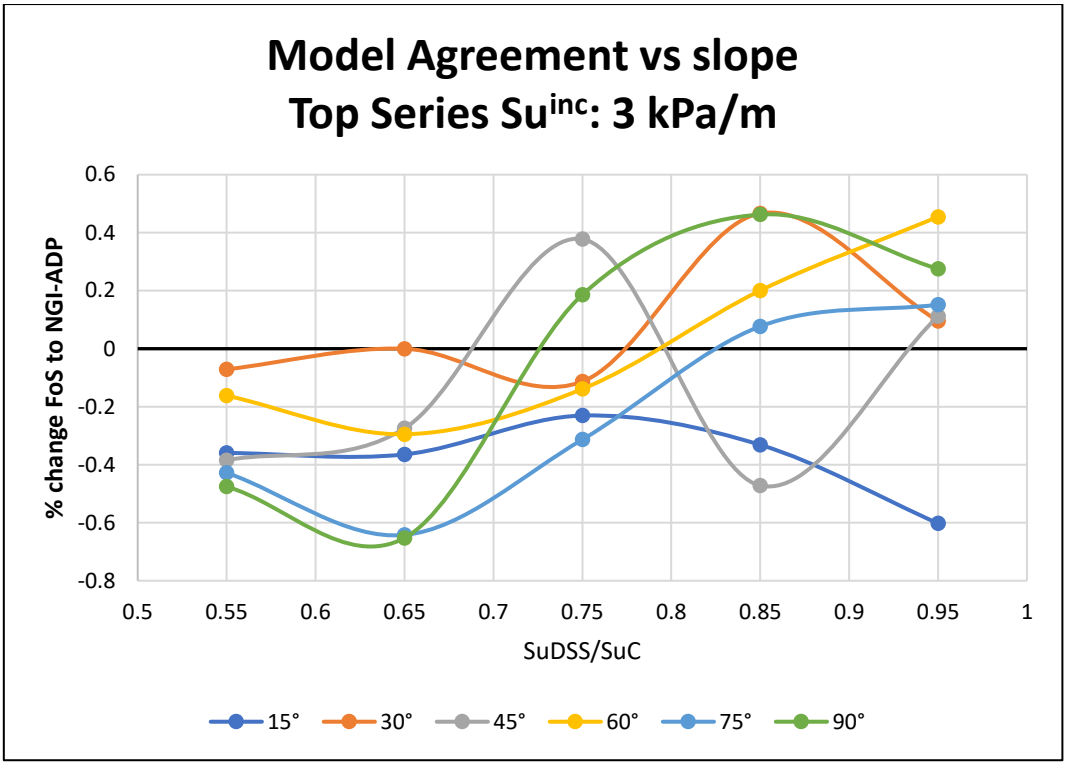

Figure B- 4. Model agreement vs slope for the top anisotropic series with Su = 40+3kPa/m.

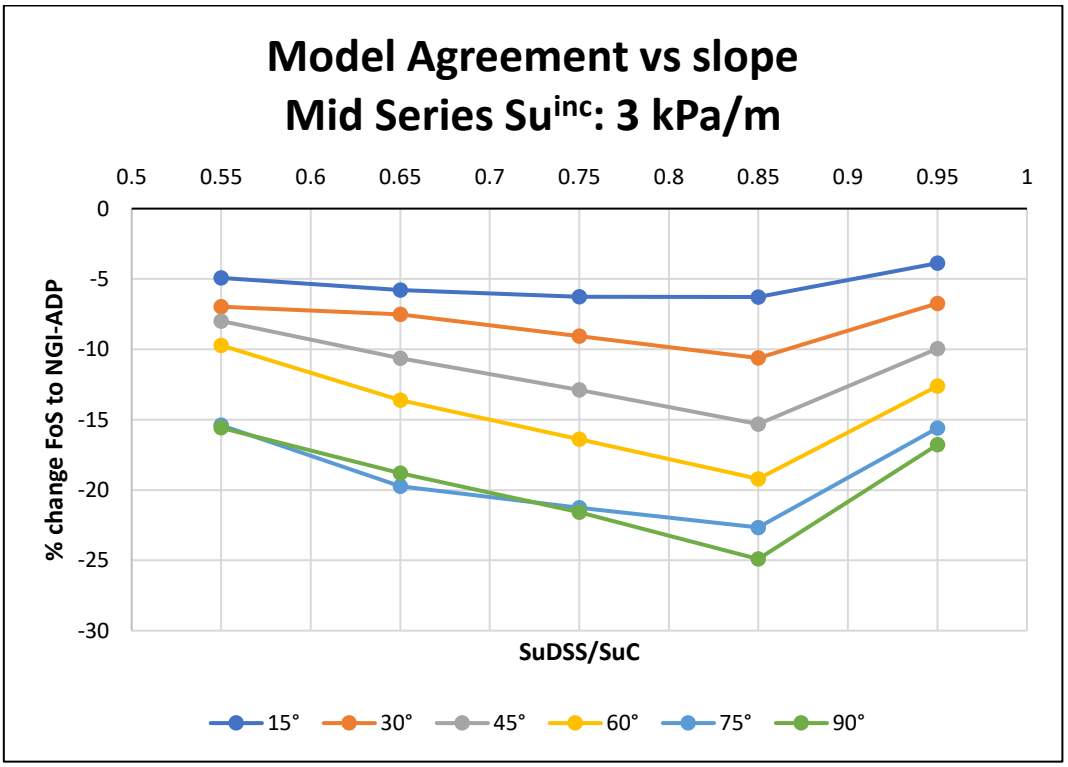

Figure B- 5. Model agreement vs slope for the mid anisotropic series with Su = 40+3kPa/m.

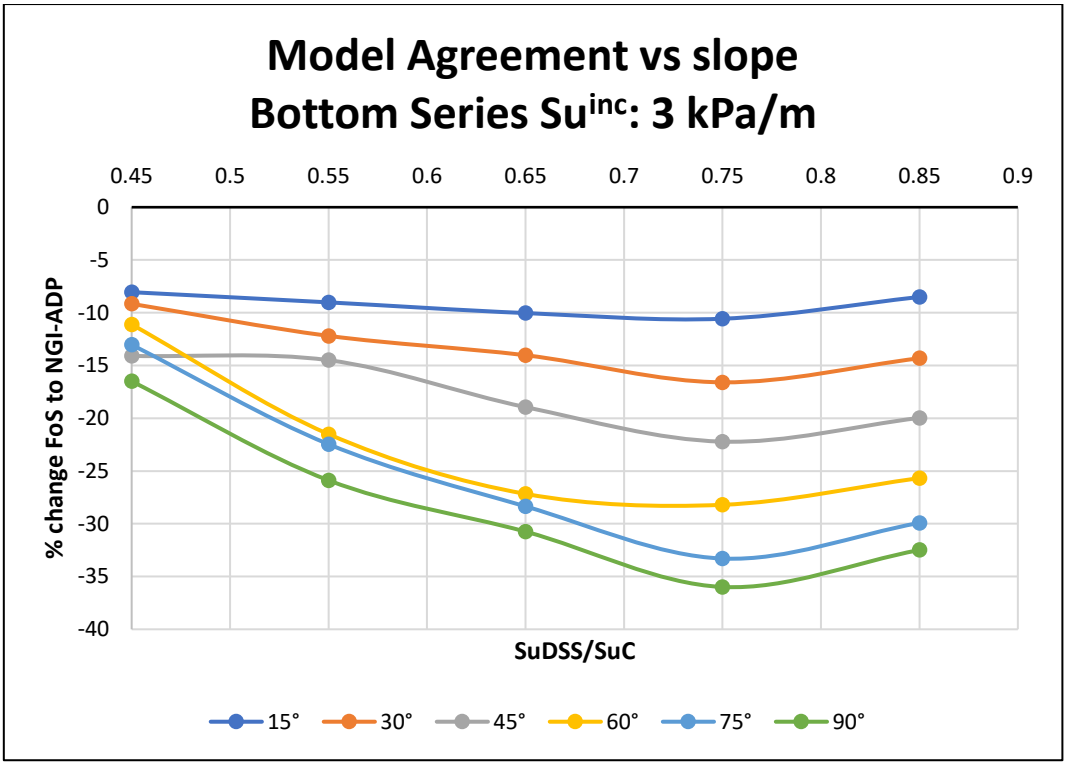

Figure B- 6. Model agreement vs slope for the bottom anisotropic series with Su = 40+3kPa/m.

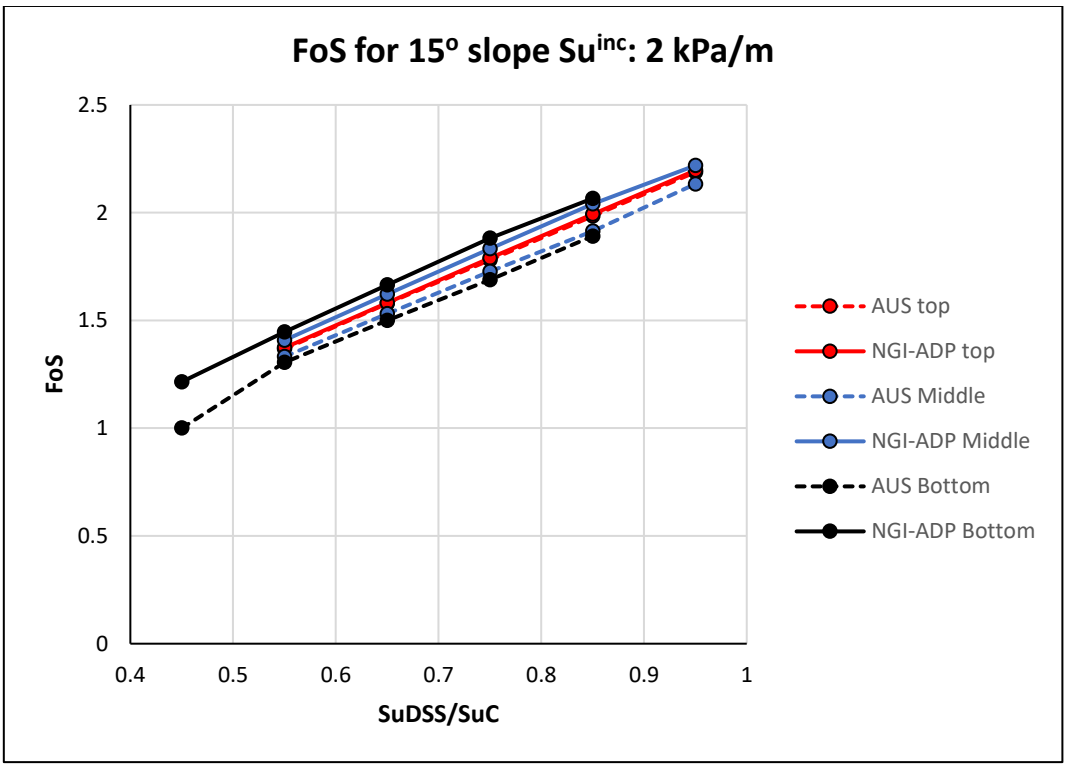

Figure B- 7.

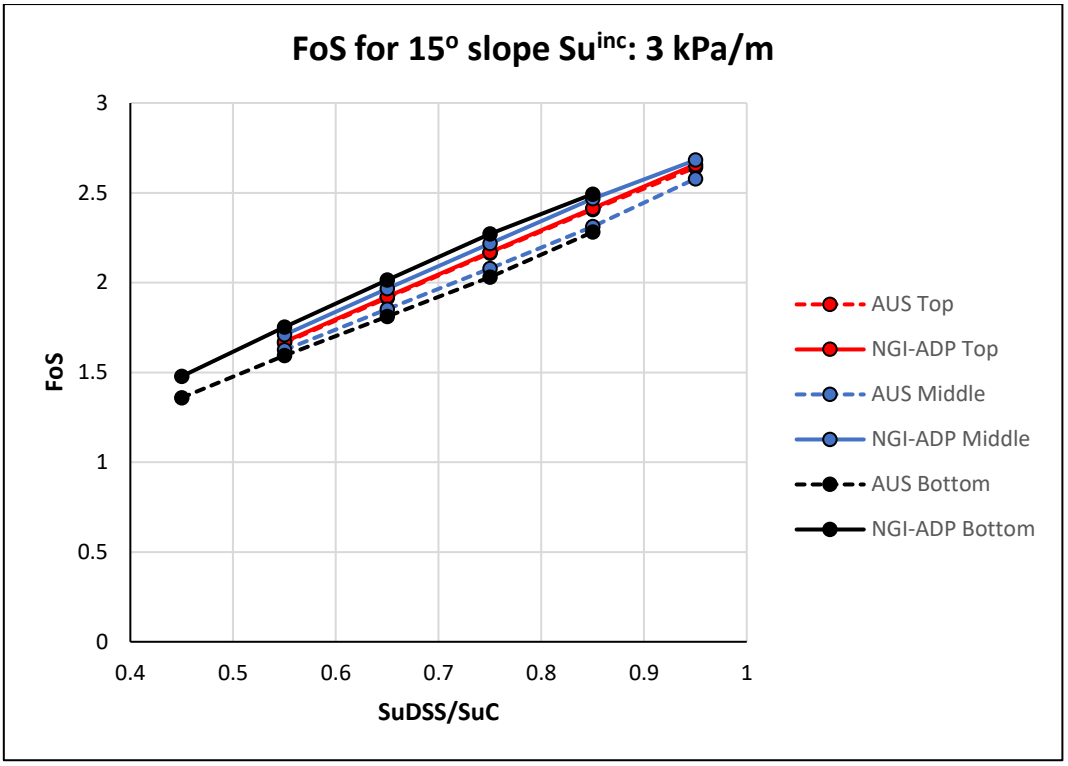

Figure B- 8.

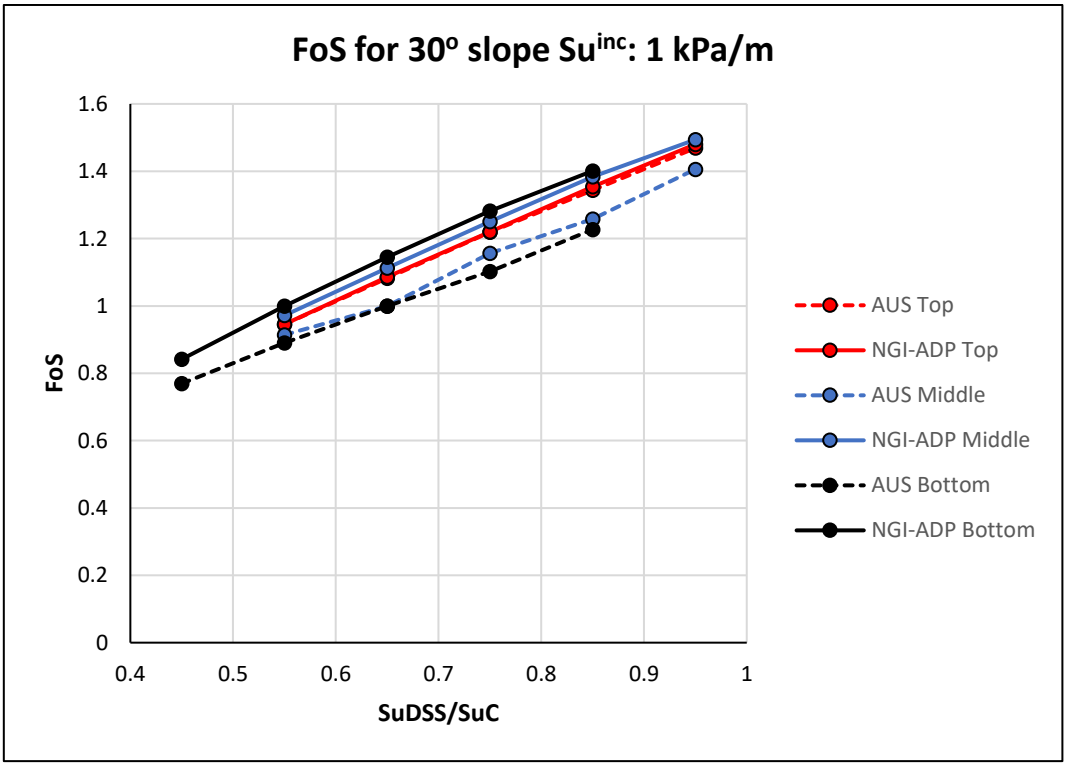

Figure B- 9.

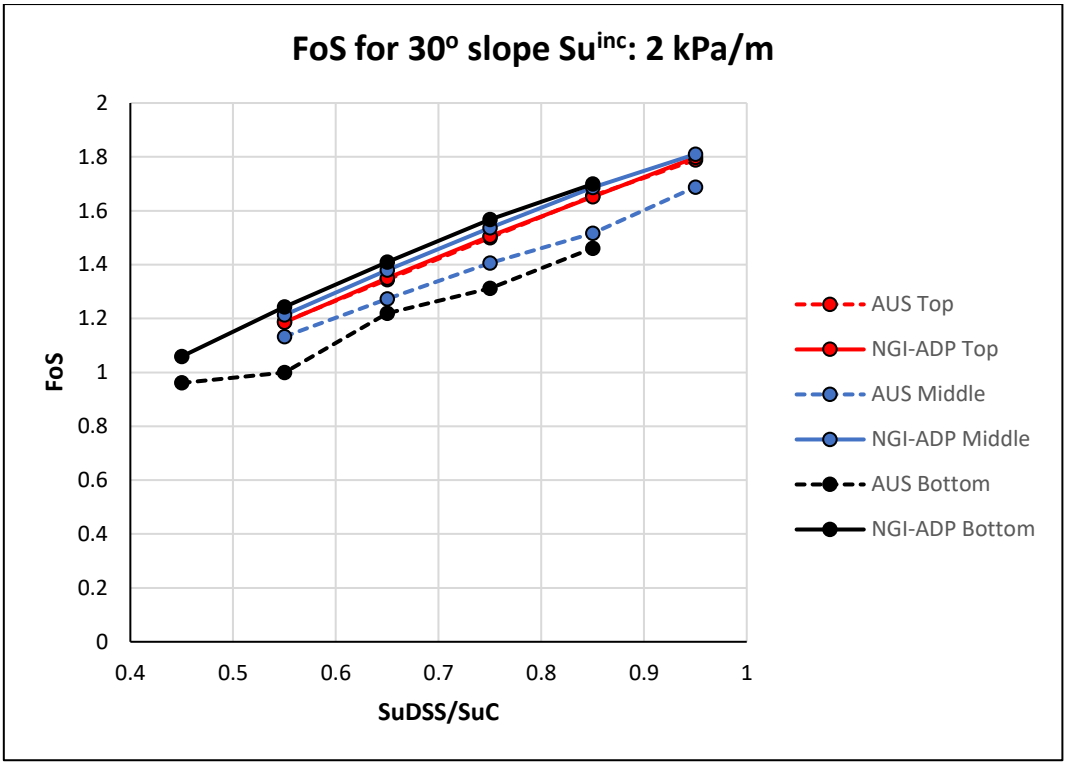

Figure B- 10.

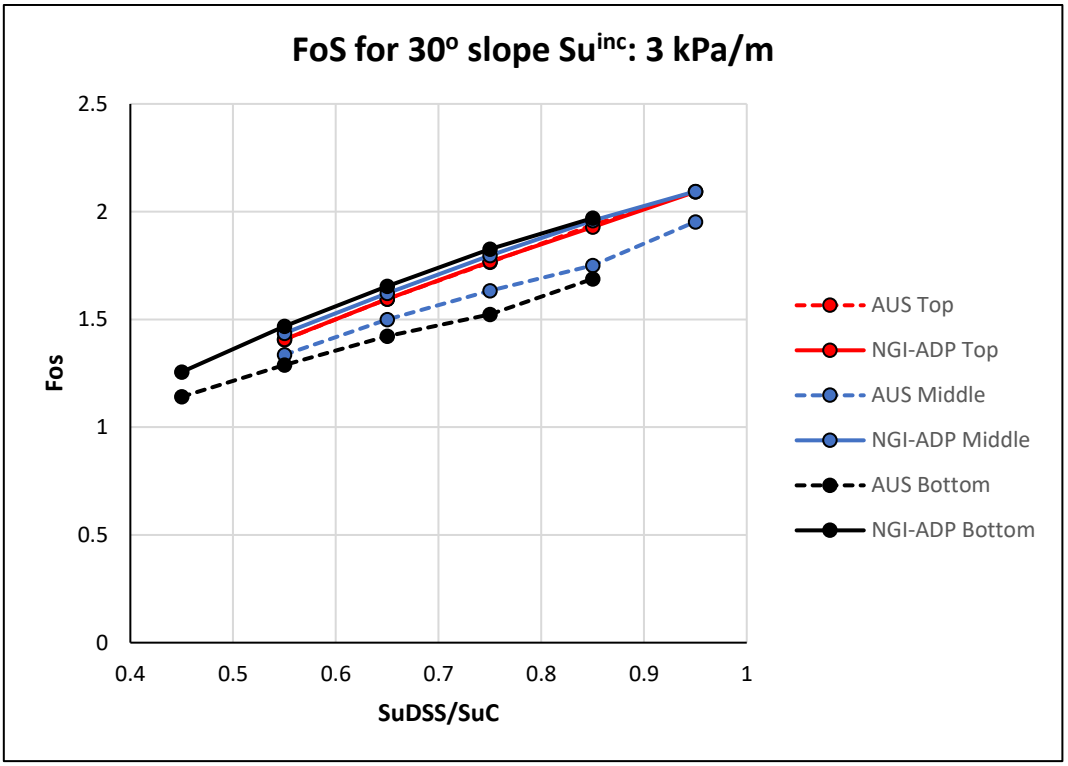

Figure B- 11.

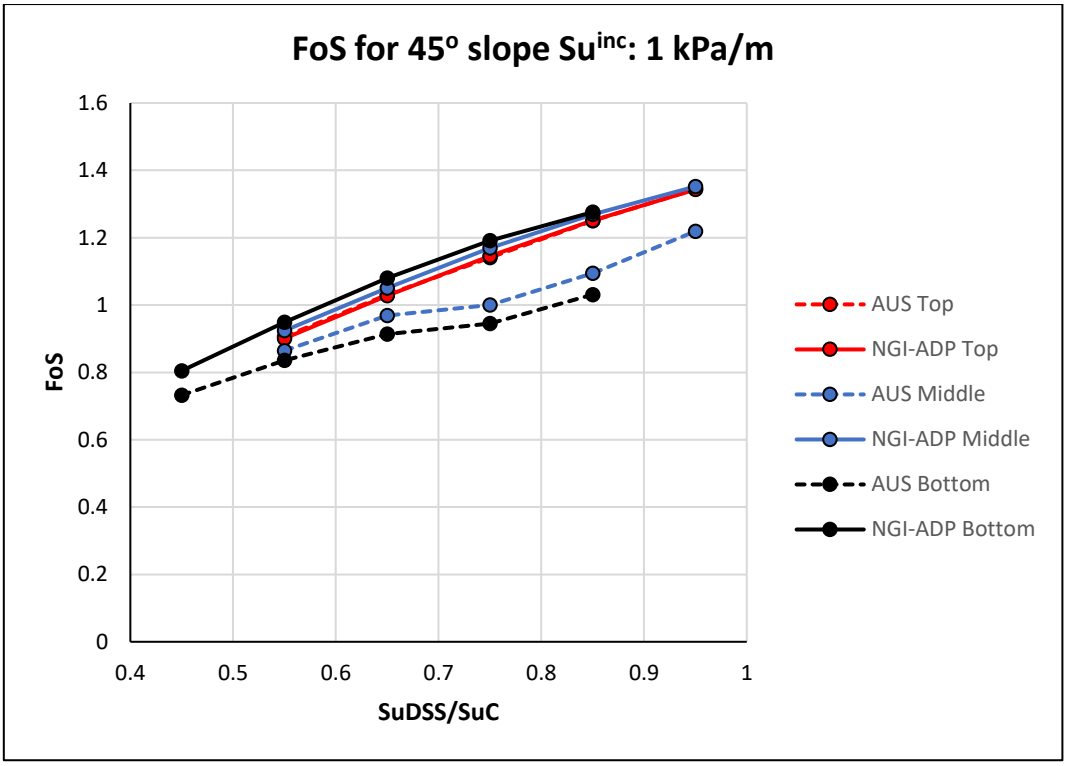

Figure B- 12.

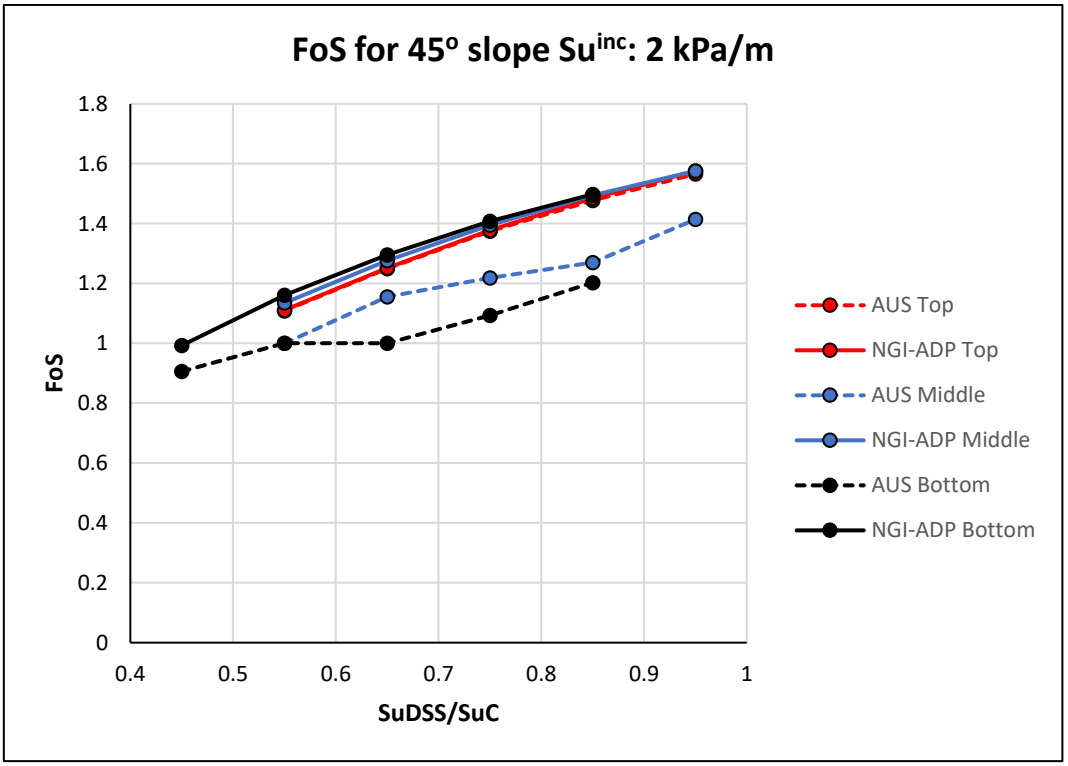

Figure B- 13.

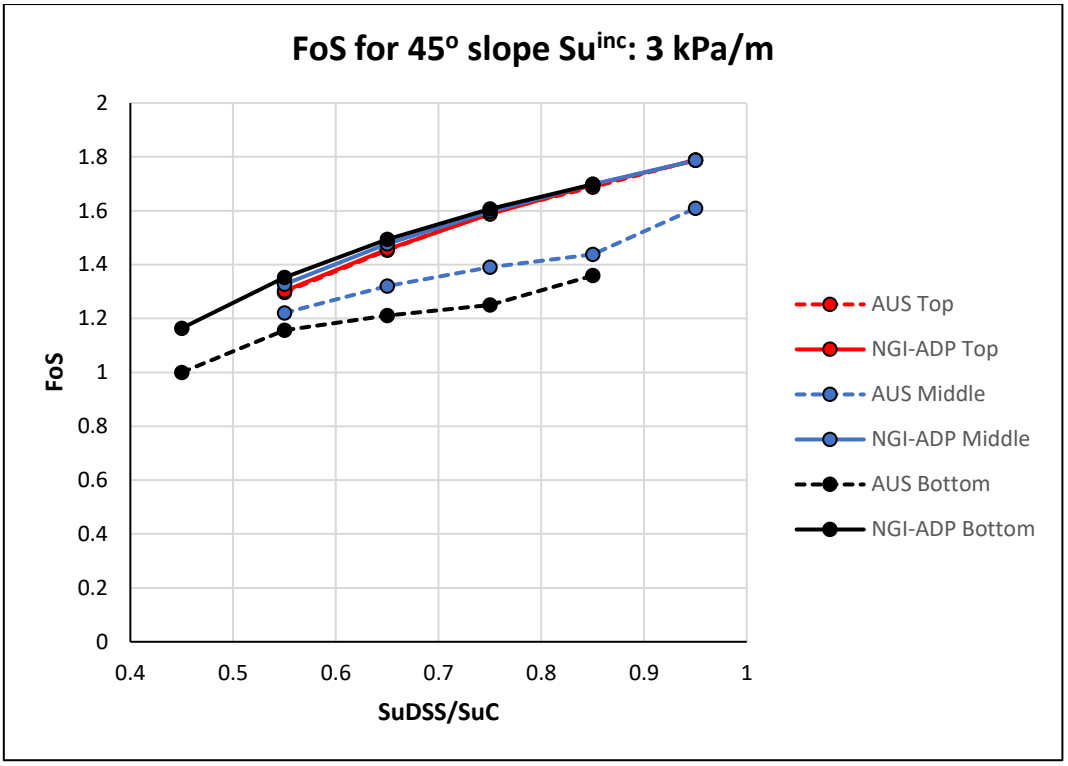

Figure B- 14.

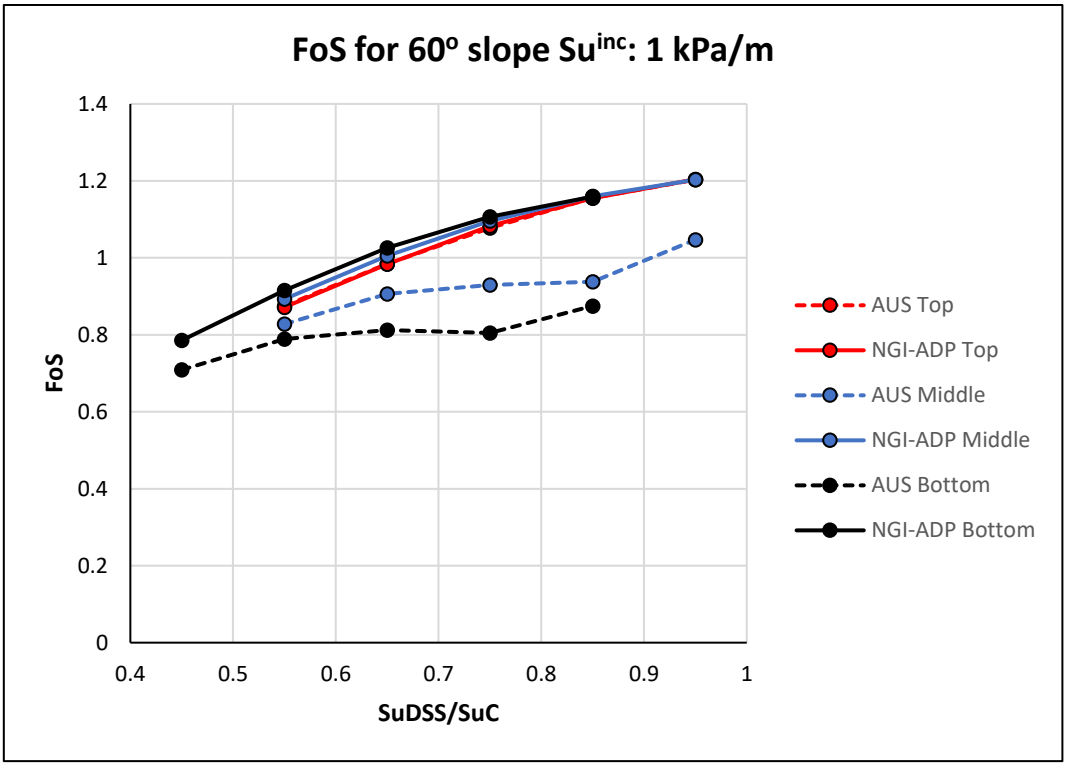

Figure B- 15.

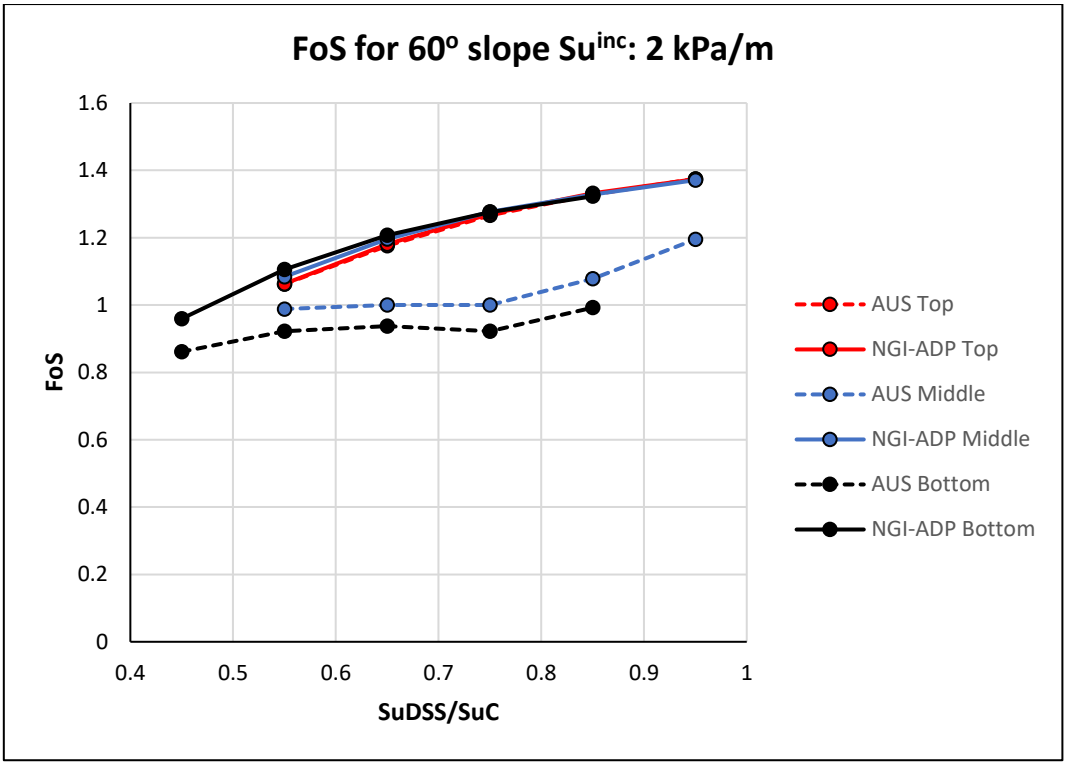

Figure B- 16.

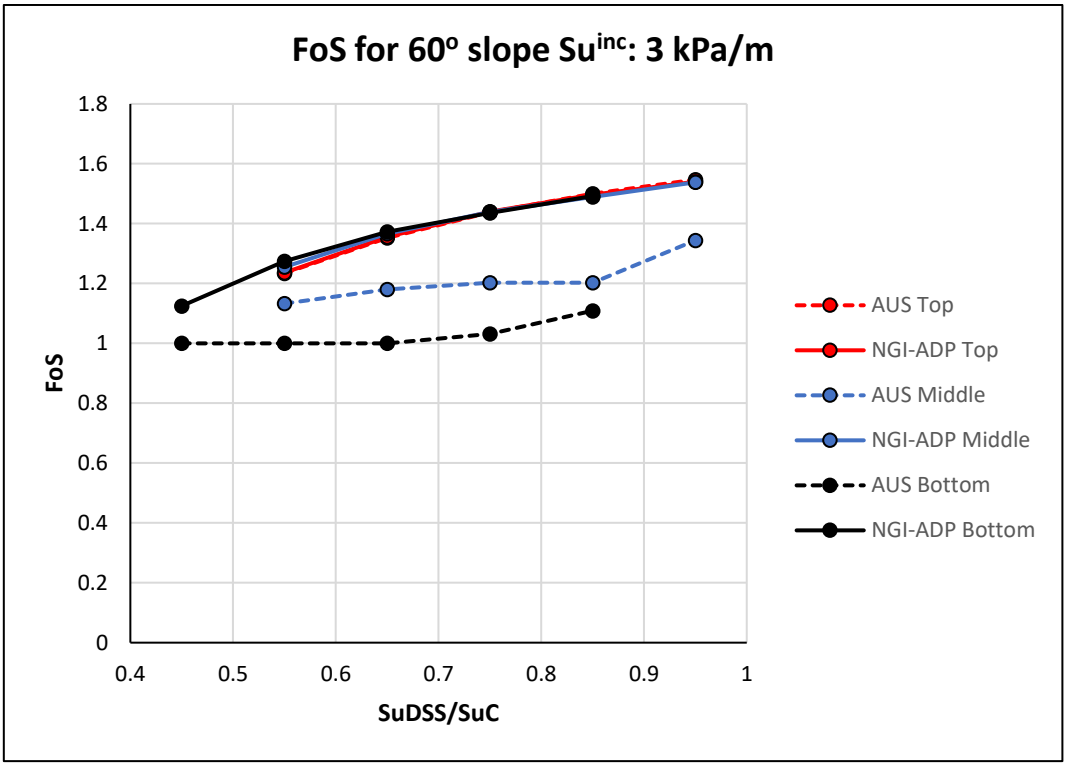

Figure B- 17.

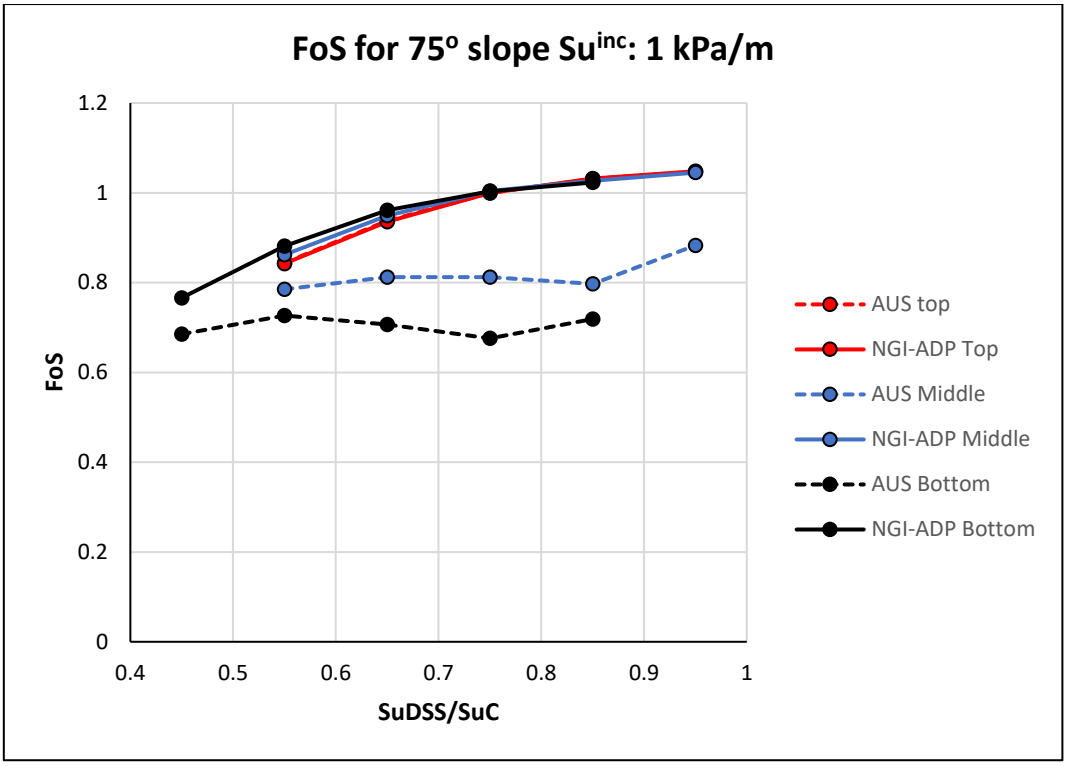

Figure B- 18.

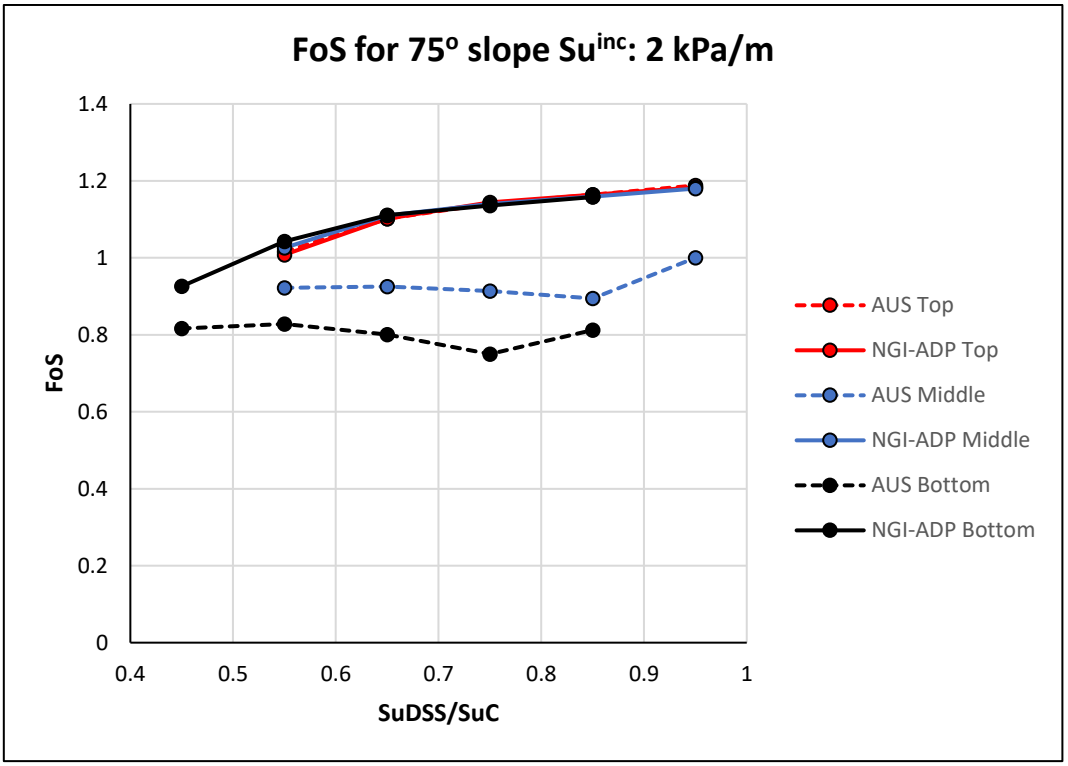

Figure B- 19.

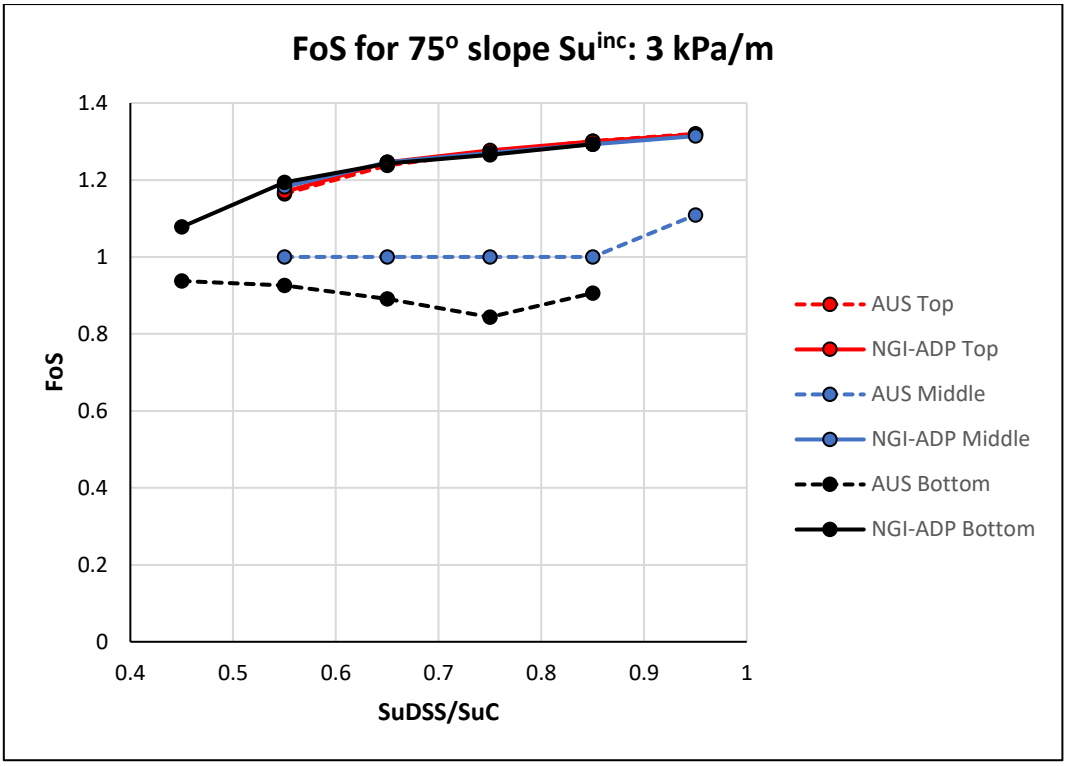

Figure B- 20.

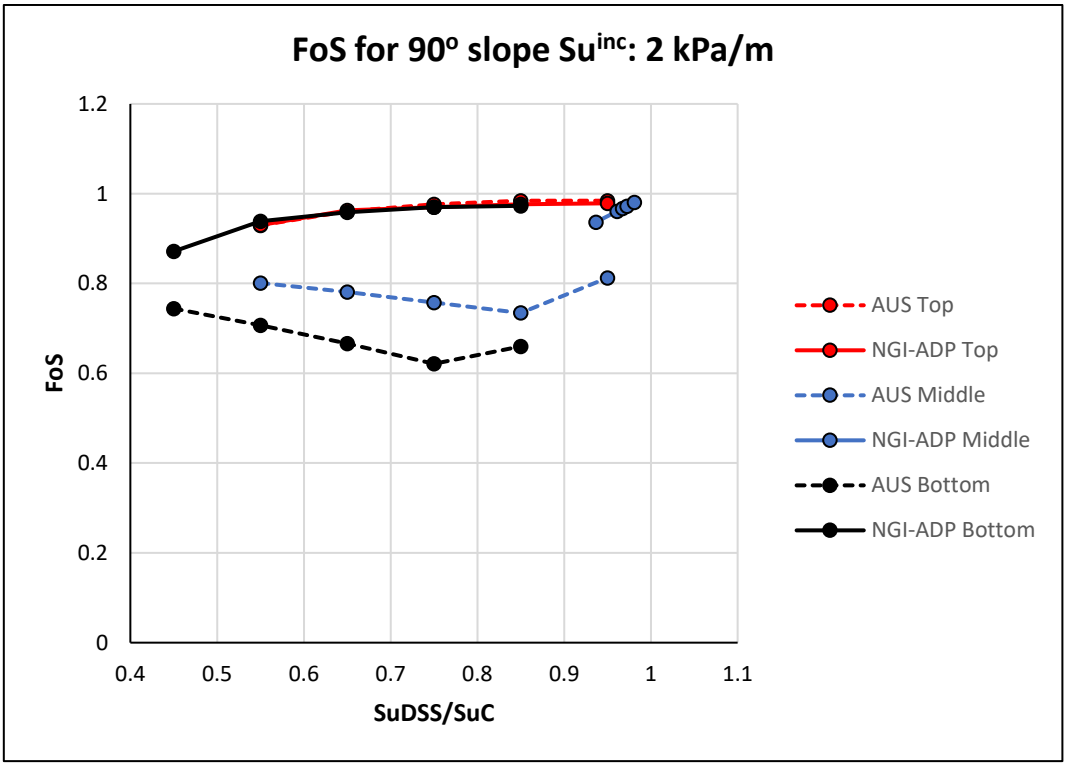

Figure B- 21.

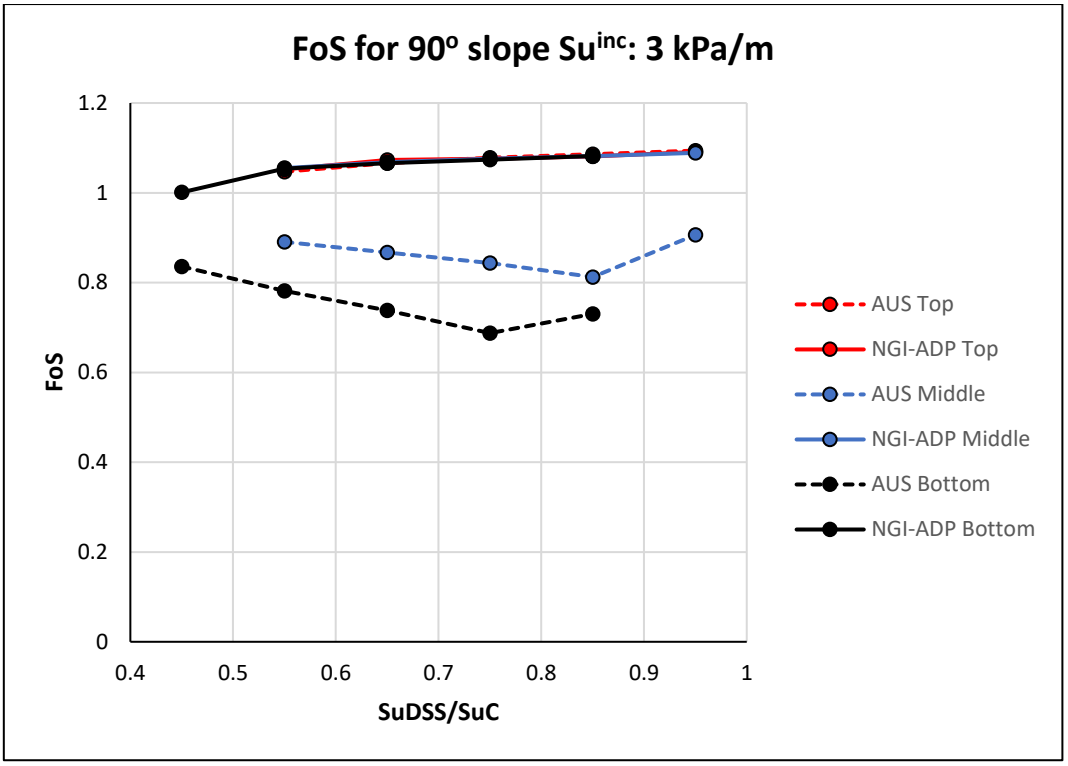
FoS for 90º slope Su^inc: 3 kPa/m
1.2
1
0.8
0.6
0.4
0.2
0
FoS
0.4
0.5
0.6
0.7
0.8
0.9
1
SuDSS/SuC
AUS Top
NGI-ADP Top
AUS Middle
NGI-ADP Middle
AUS Bottom
NGI-ADP Bottom

Figure B- 22.

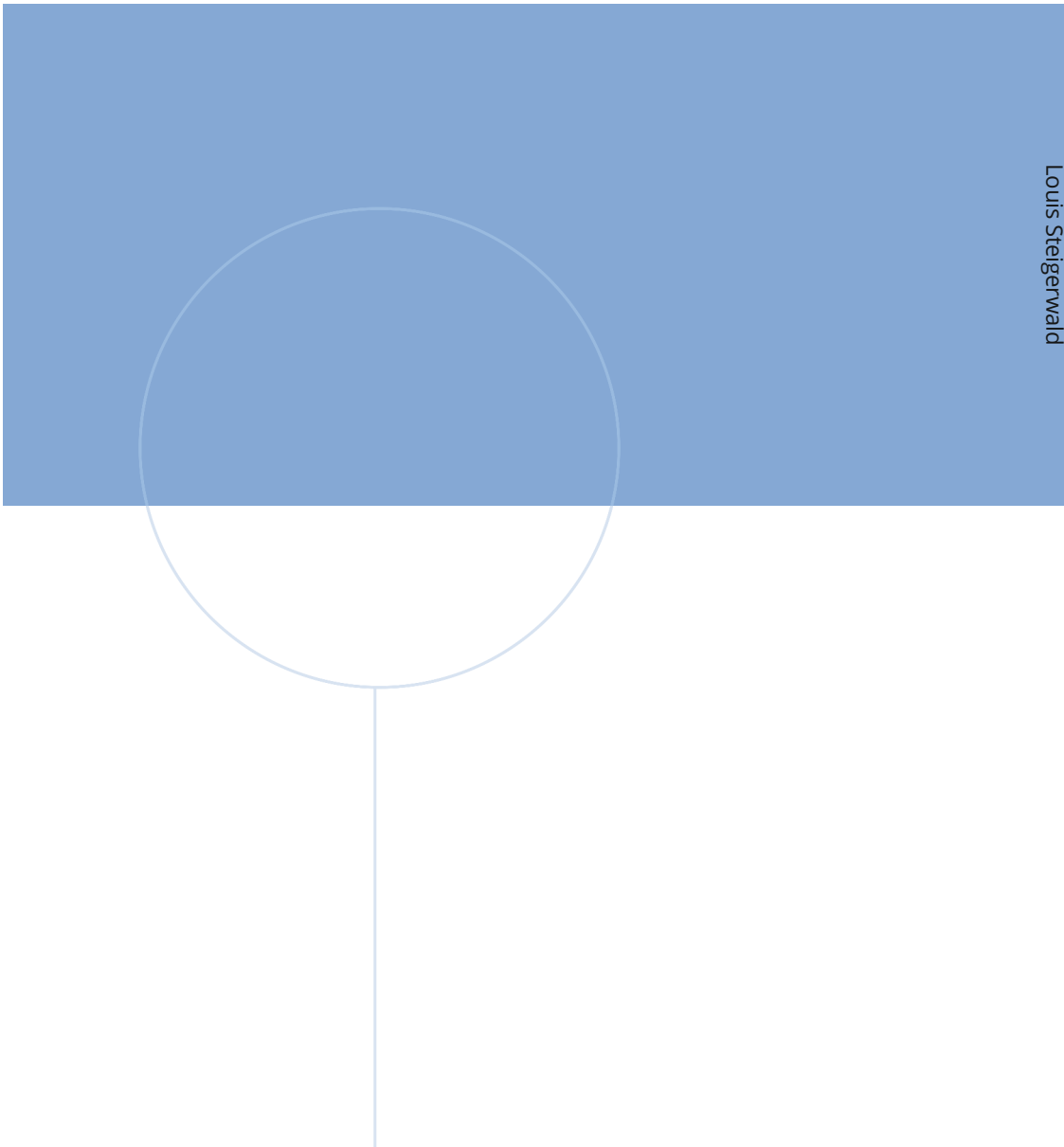

Louis Steigerwald

NTNU
Norwegian University of
Science and Technology